JOURNAL OF APPLIED PHYSICS

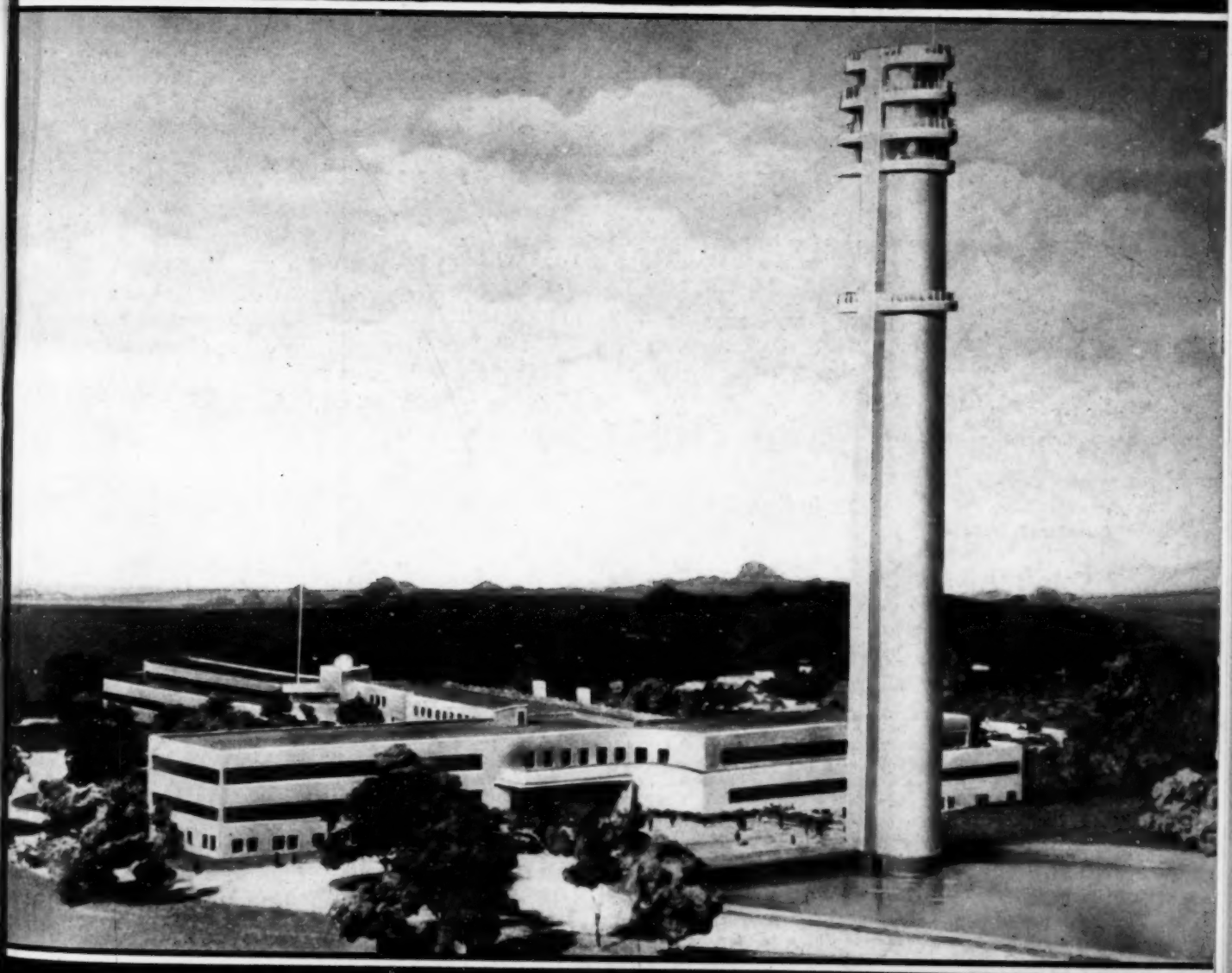

JOURNAL OF APPLIED PHYSICS

Vol. 17, No. 9 SEPTEMBER, 1946

In This Issue

Internal Friction and Plastic Extension of Zinc Single Crystals
THOMAS A. READ AND E. P. T. TYNDALL 713

Design of Broad Band I.F. Amplifier. Part II RICHARD F. BAUM 721

Numerical Solution of Laplace's Equation in Composite Rectangular Areas MAX M. FROCHT 730

Erratum: Correction of Diffraction Amplitudes for Lorentz and Polarization Factors M. J. BUERGER AND GILBERT E. KLEIN 743

Thermoluminescence and Conductivity of Phosphors
ROBERT C. HERMAN AND CHARLES F. MEYER 743

Oscillation Conditions in Single Tuned Amplifiers
WILLIAM R. FAUST AND HUGO M. BECK 749

Letter to the Editor:

Evaporation of Antimony LOUIS HARRIS 757

In Every Issue

Calendar of Meetings 756

Here and There 757

Index to Advertisers xxxiv

BOARD OF EDITORS

ELMER HUTCHISSON, *Editor*

Associate Editors

R. BOWLING BARNES
OTTO BEECK
W. F. BUSSE
S. H. CALDWELL
CLARK GOODMAN
SELIG HECHT
W. JAMES LYONS
PAUL E. SABINE
FREDERICK SEITZ
J. R. TOWNSEND

Publication of the American Institute of Physics

ADMINISTRATIVE STAFF

HENRY A. BARTON, *Director*

MARGARET S. GRIFFIN *Publications Manager*

THEODORE VORBURGER, *Business Manager*

JOHN T. TATE, *Adviser on Publications*

GOVERNING BOARD

PAUL E. KLOPSTEG, *Chairman*

WALLACE WATERFALL, *Secretary*

GEORGE B. PEGRAM *Treasurer*

R. B. DOW
L. A. DUBRIDGE
W. F. FAIR, JR.
FLOYD A. FIRESTONE
HARVEY FLETCHER
R. C. GIBBS
K. S. GIBSON
W. H. MARKWOOD, JR.
A. H. PFUND
JOHN T. TATE
L. W. TAYLOR
A. G. WORTHING

The JOURNAL OF APPLIED PHYSICS, published monthly at Prince and Lemon Sts., Lancaster, Pa., is devoted to physics in its role as the science basic to other natural sciences and to the arts and industries. Previous to 1937 this publication was known as PHYSICS. The JOURNAL OF APPLIED PHYSICS publishes editorials, news of physicists, and reviews, as well as technical papers of applied physics.

Manuscripts should be submitted to Elmer Hutchisson, Editor, Case School of Applied Science, Cleveland 6, Ohio.

Subscriptions and orders for back numbers should be addressed to Prince and Lemon Streets, Lancaster, Pa. or to the American Institute of Physics, 57 East 55 Street, New York 22, N. Y.

Subscription Price	U.S. AND CANADA	ELSEWHERE
To members of scientific societies	$5.00	$5.70
To all others	7.00	7.70

Back Number Prices

Complete set: Vol. 1, July, 1931–Vol. 16, 1945—$101.50
Yearly back number rate: $7.70
Single copies: $0.70 each.

Changes of address and proofs should be addressed to the Publications Manager.

Advertising rates supplied on request. Orders, advertising copy, and cuts should be sent to the American Institute of Physics.

Entered as second class matter January 22, 1937, at the Post Office at Lancaster, Pennsylvania, under the Act of March 3, 1879. Accepted for mailing at the special rate of postage provided for in the Act of February 28, 1925, authorized May 2, 1932.

Copyright 1946, by the American Institute of Physics.

Journal
of
Applied Physics

Volume 17, Number 9 September, 1946

Internal Friction and Plastic Extension of Zinc Single Crystals

THOMAS A. READ*
Westinghouse Research Laboratories, East Pittsburgh, Pennsylvania

AND

E. P. T. TYNDALL
Department of Physics, State University of Iowa, Iowa City, Iowa

(Received April 29, 1946)

This paper presents data on the internal friction of four single crystals of zinc while oscillating longitudinally, and a description of various slow speed tension tests on a fifth crystal within and beyond the elastic limit. In the first named measurements the behavior of the crystals bears little resemblance to that of crystals of zinc of greater purity prepared by another method, which has previously been reported (see reference 1). The most outstanding feature is that the decrement, although higher at the lowest stress amplitude than for the previous ones, shows very little rise with increasing stress amplitude, even up to stresses far beyond the statically-determined elastic limit. The difference in behavior seems to be caused by the difference in purity of the zincs. An optically mosaic structure, such as that described by Schilling (see reference 4), does not appear to be responsible. In the slow speed tension tests the zinc crystal, after a period of self-annealing at room temperature, has a Hooke's law region up to about 70 g/mm² (R.S.S. = 28 g/mm²) and at greater stress shows transient and steady creep. Under some circumstances the transient creep is in two parts, a slow starting creep followed by much more rapid creep. The crystal, when measured following a permanent strain, shows creep at loads well below the previous elastic limit and has a large amount of hysteresis. Self-annealing occurs during rest periods and the initial elastic limit is gradually regained while the hysteresis disappears.

INTRODUCTION

THE only previous work on the internal friction of zinc single crystals is that described by one of the authors in a previous paper.[1] The specimens used in this earlier investigation were grown from spectrographically pure zinc (99.999 percent Zn) by the Bridgman method in Pyrex glass tubes coated with graphite. The damping behavior of these crystals was very complicated, but may be briefly summarized by saying that after a one- or two-day anneal at room temperature their internal friction was very low (decrement about 1×10^{-5}) at small amplitudes of vibration, but increased with increasing amplitude. This increase was very rapid for crystals whose hexagonal axis made an angle of from 15 to 75 degrees with the axis of the rod. For example, the decrement of a crystal for which this angle was 74.5° was 1.7×10^{-5} at a stress amplitude of .15 g/mm², and 144×10^{-5} at a stress amplitude of 22.2 g/mm². Both these figures for the stress refer to the values at displacement nodes. The corresponding values of the strain amplitude are 1.2×10^{-8} and 176×10^{-8}.

* Westinghouse Research Fellow. Now at the Ordnance Laboratory, Frankford Arsenal, Philadelphia, Pennsylvania.

[1] T. A. Read, Phys. Rev. 58, 371 (1940).

The objects of the investigation described in the present paper were to compare the internal friction of zinc single crystals grown by another method with that of the Bridgman crystals, and to study the relation between internal friction and behavior in slow tension tests.

SPECIMEN MATERIAL

The zinc crystals used in the present investigation were grown from "Bunker Hill" zinc, a commercial zinc whose total impurity content is about 0.01 percent. It is to be noted that this purity is somewhat less than that of the spectrographically pure zinc used in the earlier investigation referred to above. At the conclusion of the work a spectrographic analysis was made on four of the crystals and on a small ingot cast from the original material. It revealed that crystals Nos. 2 and 4 were identical with the original material but that Nos. 3 and 5 contained excess amounts of lead and tin,[2] which had apparently been introduced accidentally by the use of a "seed" crystal contaminated with these metals. The effect of the difference in purity between the two pairs of crystals was very marked as may be seen below.

TABLE I. Description of crystals.

Designation	Orientation	R.S.S. factor	Remarks
2	15°	0.25	O.M.
3	72°	0.29	G.C. Pb, Sn
4	70°	0.32	G.C.
5	81°	0.17	O.M. Pb, Sn
6	63°	0.41	G.C.

O.M.: Optically mosaic.
G.C.: Good crystal.
Pb, Sn: Lead and tin impurities.

These crystals were grown by the modified Kapitza method described by Cinnamon.[3] The molds were made of well-baked transite with trapezoidal grooves, 0.25 cm² in cross section for crystals Nos. 2–5 and 0.5 cm² for crystal No. 6. The surface of specimens grown this way is somewhat rougher than that of crystals grown in glass molds. This is caused by the wrinkling of a very thin surface film of oxide when the metal contracts in freezing. The method is believed, however, to be more likely to produce more nearly perfect crystals because of lack of constraint on the growing crystal. Two of the crystals were, however, purposely grown of the "optical mosaic" type.[4,5]

The specimens are described in Table I. The orientation is given as the angle between the hexagonal axis and the specimen length. The third column gives the factor by which a longitudinal stress must be multiplied to obtain the resolved shear stress in the basal (glide) plane. Further resolution into the glide direction would require an additional factor which must, however, always lie between 1.0 and 0.866. Any deviation of this from 1.0 has been neglected in the following.

The decision as to the presence of an optically mosaic structure was made on the basis of examination of the portions of the crystal adjacent to the specimen, and of the specimen itself after the completion of the measurements.

After growth the first four crystals were cut to approximately the proper length for one half-wave of longitudinal vibration with a jeweler's hack saw run automatically and so arranged that the blade pressed very lightly against the crystal. They were then packed in Vaseline in brass tubes which were in turn packed in cotton in a sturdy box. This box was mailed from Iowa City to East Pittsburgh. The authors feel that the care taken in this handling of the specimens sufficed to insure that their internal friction was not affected thereby. The results of the measurement are consistent with this view with one exception, as noted below. In East Pittsburgh the crystals were cut to exact length with a jeweler's saw after being waxed in two V-blocks with beeswax and rosin. One end of each crystal was ground flat by holding the crystal lightly in a V-block and grinding it on a cast iron surface plate. This same method of preparation was employed in the previous work.[1] Crystal No. 6 was mounted in the measuring apparatus as grown. The crystal was 15 cm long and measurements were made on a central 9 cm length.

[2] In crystals Nos. 2 and 4 and the ingot Sn was either not detected or less than 0.001 percent, while Pb was either not detected or less than 0.002 percent. In Nos. 3 and 5 Pb was about 0.01 percent, and Sn 0.1 percent (No. 3) and 0.03 percent (No. 5).

[3] C. A. Cinnamon, Rev. Sci. Inst. **5**, 187 (1934).

[4] H. K. Schilling, Physics **6**, 111 (1935).

[5] Electrical and thermal resistivities of optically mosaic crystals differ in an erratic way from those lacking this structure. W. J. Poppy, Phys. Rev. **46**, 815 (1934) and C. A. Cinnamon, Phys. Rev. **46**, 215 (1934).

INTERNAL FRICTION

The internal friction of these crystals was measured for longitudinal vibration at a frequency of 33.5 kilocycles per second by the composite piezoelectric oscillator method. The apparatus used was similar to that previously described.[1] The dependence of the internal friction of the specimen crystals on the amplitude of vibration was obtained by measuring the impedance of the composite piezoelectric oscillator as a function of the voltage impressed on electrodes attached to the quartz and of frequency in the neighborhood of the resonant frequency. It can be readily shown that the stress amplitude σ at a displacement node in the specimen is given by the formula

$$\sigma = \frac{2E\mathcal{E}(10)^{\frac{1}{2}}K}{R_0 V} \times 10^3 \text{ dynes/cm}^2, \qquad (1)$$

where E = Young's modulus in dynes/cm² of the specimen in the direction of its length.

$\mathcal{E}$ = r.m.s. voltage applied to electrodes.

K = proportionality constant between equivalent inductance of composite piezoelectric oscillator and its mass in henrys per gram.

R_0 = resistance at resonance in ohms for given value of $\mathcal{E}$.

V = velocity, in cm/sec., of sound in the specimen in the direction of its length.

The formula (1) was given in reference 1 in a somewhat less convenient form.

For all of the measurements the specimens were suspended in a vacuum and maintained at a temperature of 23°C.

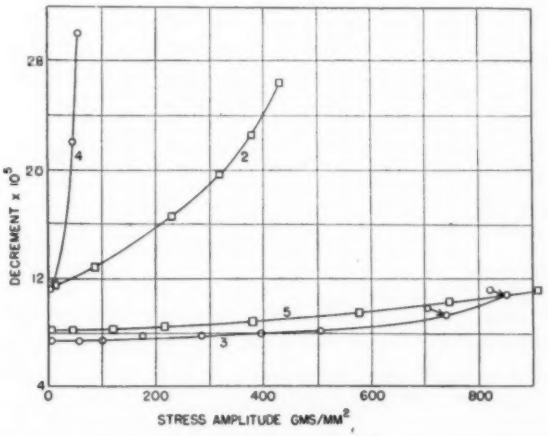

FIG. 1. The internal friction of the four crystals investigated as a function of the stress amplitude at a displacement node. The arrows indicate a change with time at constant driving voltage. The crystal number is indicated on each curve.

A convenient measure of internal friction is the decrement, defined as the ratio of the energy dissipated in the specimen in a cycle of vibration to twice the total energy stored in the vibration of the specimen.

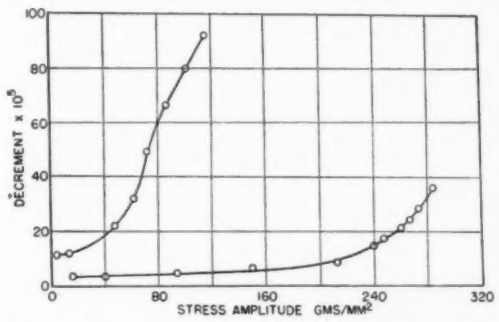

FIG. 2. The lower curve gives the internal friction of crystal number 4 after a one hour anneal at 330°C. The upper curve, repeated from Fig. 1, shows the original internal friction.

The dependence of the internal friction of each of the four specimens on the amplitude of vibration is given in Fig. 1. These data, obtained without any annealing or other treatment except as described above, are remarkable for five reasons. First, the recovery period of a day or two after mounting, during which the previously measured crystals[1] exhibited a decrease in internal friction by a factor of from 10 to 100, was completely absent for these crystals, although exactly the same technique of affixing the specimens to the quartz rod was used. Second, the internal friction of the two crystals of lesser purity is only slightly greater at stress amplitudes of several hundred g/mm² than at very small amplitudes of vibration. Third, there is no marked difference between the behavior of the crystals of the same purity which have an optically mosaic structure and those which do not (compare Nos. 2 and 4 and Nos. 3 and 5). Fourth, these crystals have considerably higher internal friction at small amplitudes of vibration than did the zinc crystals described in reference 1. Fifth, the change of the internal friction with time, at constant driving force, which occurs at the largest amplitudes is a *decrease*. This change is indicated by the arrows.

Data were obtained on three methods of

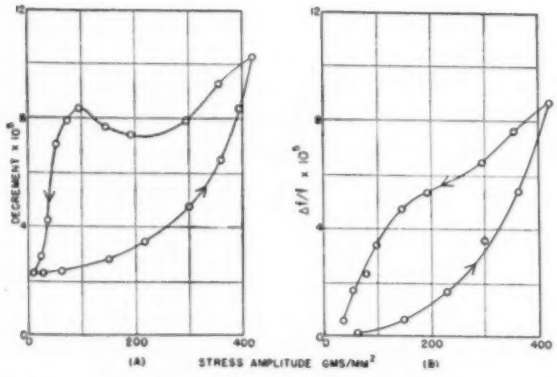

FIG. 3. (a) The internal friction of crystal number 3 as a function both of increasing and decreasing amplitude of vibration. The sequence of the measurements is indicated by the arrows. (b) The changes in the natural frequency of longitudinal vibration of crystal specimen number 3 which are observed simultaneously with the decrement values plotted in Fig. 3(a).

changing the internal friction of these crystals, *viz.*, etching, annealing, and cold-working.

Etching one of these crystals does not appreciably affect the dependence of internal friction on amplitude, but does produce a lowering of the curve as a whole. For example, a three-minute immersion of crystal No. 3 in 30 percent HCl decreased the small-amplitude decrement from 7.6×10^{-5} to 4.0×10^{-5}. This treatment decreased the weight of this crystal by 0.05 percent. Subsequent electrolytic etching of this crystal lowered the small-amplitude decrement further to 2.3×10^{-5}. The corresponding loss in weight was 3.8 percent. It may be concluded that the greater part of the original internal friction of this crystal at small amplitudes was a surface effect rather than a property of the material.

As shown in Fig. 1 (and in Fig. 2, where a more extensive curve is plotted), the internal friction of crystal number 4 was considerably higher and rose more rapidly with increasing amplitude than for the other crystals. For this reason this crystal was selected for an investigation of the effect of a heat treatment; it was suspected that this crystal may have been strained by the handling described above. The change in the internal friction which was produced by an anneal of one hour at 330°C is shown in Fig. 2, with the lower curve depicting the results obtained after the anneal. Of the four crystals described in this paper, this particular crystal exhibited the greatest similarity in properties to the crystals reported on in reference 1. For example, the internal friction of this crystal always increased with time when any change was observed at constant amplitude of vibration.

Cold-working raises the internal friction of these zinc crystals, except in certain cases in which the cold-work is introduced by the internal friction measurement itself. This exception has been mentioned in connection with Fig. 1. The more typical case, in which the cold-working associated with the internal friction measurement raises the internal friction is exemplified by Fig. 3 (a). In this figure is plotted a sequence of measurements on crystal No. 3, beginning at a very small amplitude of vibration, proceeding in steps to a stress amplitude of 420 g/mm², and then decreasing in steps to the initial amplitude of vibration. This curve is similar in shape to one given in reference 1, except that here the internal friction actually rises to a maximum as the amplitude of vibration is decreased. A period of only twenty minutes elapsed during the measurements. After approximately 24 hours the lower branch of the curve may be reproduced. The internal friction of the crystal shows a more rapid rise than that shown in Fig. 1 because shortly before making the measurements for Fig. 3 this crystal was cold-worked statically in the manner described below.

As is described at greater length in reference 1, there is in general associated with the change in the decrement produced by a change of the amplitude of vibration a change in the natural frequency of longitudinal vibration of the specimen rod. This change in the resonant frequency is, in many cases, related in a simple way to the change in internal friction. In the instances cited there a plot of successive values of the change in natural frequency against the corresponding values of the decrement for a series of amplitudes of vibration produced a straight line. That this simple relation does not exist for crystal number 3 under the present conditions of measurement is demonstrated by a comparison of Fig. 3 (a) with Fig. 3 (b) which gives the changes (decreases) in the natural frequency of this crystal which were observed simultaneously with the decrement changes plotted in Fig. 3 (a). It is, however, important to note that a maximum slope of the frequency change curve given in

Fig. 3 (b) occurs at the same amplitude of vibration as the maximum of the internal friction curve of Fig. 3 (a).

The effect on the internal friction of the cold-work introduced by a static load is shown by the difference between the lower and upper curves of Fig. 4, which were taken, respectively, immediately before and after subjecting crystal No. 3 to a compressive stress of 1.8 g/mm² for one minute. The greater part of this increase in internal friction disappeared in the course of two or three days. These data suggest that a previously applied static load which acts for an appreciable time is more effective in causing the decrement to show the rapid rise with increasing stress amplitude (i.e., the specimen acts less elastically) than is a much greater stress which is rapidly alternated. The slow speed tension tests described below seem to afford some clue to this behavior.

SLOW SPEED TENSION TESTS

Various slow speed tension tests were made on crystal No. 6 with the apparatus which has been described briefly elsewhere.[6] The tests consisted in observing the elongation under load for various conditions of the crystal, which were determined by the nature of the preceding runs, periods of rest between runs, etc. Creep curves under steady loads of various values were also obtained. Representative experiments are described in detail below.

The first run taken on the crystal immediately after mounting it in the apparatus showed slight hysteresis and a lower elastic limit[7] than was

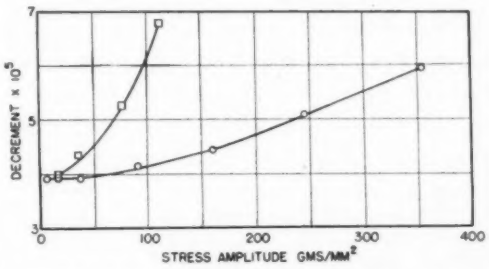

FIG. 4. The increase in the internal friction of specimen number 3 produced by a static compressive stress of 1.8 g/mm² applied for one minute. Note that this static stress is much smaller than the stress amplitude in the internal friction measurements.

[6] I. H. Swift and E. P. T. Tyndall, Phys. Rev. 61, 359 (1942).

[7] At a stress of 43 g/mm².

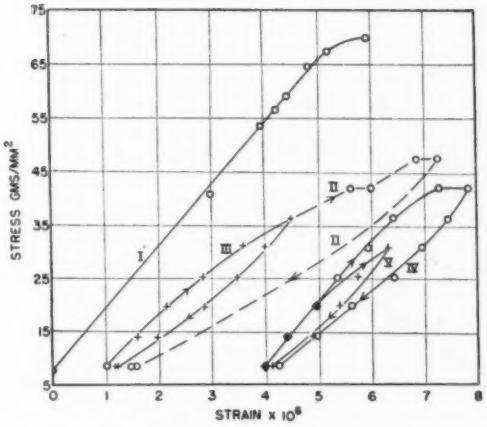

FIG. 5. Crystal No. 6: curve I, in the elastic state. The last load produced a permanent set of $\Delta l/l = 2\times10^{-4}$ (not shown on curve). Curves II, III, crystal in inelastic state. Curve IV, after two days rest. Curve V, hysteresis loop produced by small plastic strain at end of curve IV.

expected. A slight permanent set ($\Delta l/l = 1.5 \times 10^{-6}$) was given the crystal at this time. It was therefore allowed to rest under the minimum load (equivalent to a stress of about 7 g/mm²) for two weeks. It was then found to be in an "elastic state" (see later) and the Young's modulus was carefully measured, using the photoelectric multiplying device[6] and, for safety, with the maximum load kept below the previously found elastic limit. After a total period of 42 days in which the crystal had either rested or been subjected to only small loads, the load was gradually increased. The data obtained are shown in curve I, Fig. 5. It will be seen that the proportional region goes to a stress of 67.2 g/mm². The next load (stress = 69.9 g/mm²) caused creep to an "off-scale" deflection and the specimen was hurriedly unloaded. The creep, however, was observed to occur rather slowly at first and then with increasing rapidity. In fact the point plotted at 69.9 g/mm² corresponds to the scale reading a second or two after completing the loading.[8] This phenomenon of slow creep followed by much more rapid creep was observed many times in subsequent experiments. The duration of the slow creep is far too long to be accounted for by the inertia of the load or of the moving parts of the observing apparatus. The permanent set left after unloading was

[8] The loading is done by running mercury into a container hung from the lower end of the crystal. About 20 seconds elapsed between the 67.7 and 69.9 g/mm² readings.

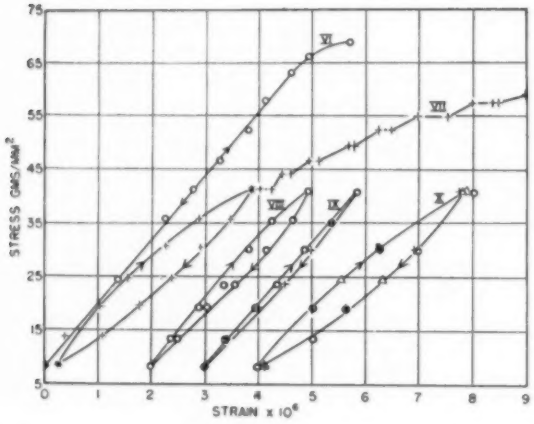

FIG. 6. Crystal No. 6: curve VI, crystal in elastic state after ten days rest. Permanent set at end of curve VI, $\Delta l/l = 1.7 \times 10^{-4}$ (not shown). Curve VII hysteresis loop and creep, immediately following curve VI. Curves VIII and IX, one and three days after curve VII. Curve X, typical hysteresis loops of crystal in inelastic state.

$\Delta l/l = 2 \times 10^{-4}$. The data shown in curve II were taken next.[9] This curve shows creep at two values of stress (41.4 and 46.9 g/mm²) which were previously within the elastic or proportional region. The time interval between the two points plotted at 41.4 g/mm² is 3 minutes; at 46.9, it is 2 minutes. On unloading there is a slight recovery in 1 minute as shown by the two points at the minimum stress. Curve III followed immediately, a well-defined and definite hysteresis loop. While at each load one point only is plotted, it should be mentioned that, if given time, noticeable creep will occur at the higher stress points on the increasing stress branch. On the descending branch, however, no observable creep occurs. After curve III was completed, the crystal was loaded to 50 g/mm² and various observations of creep made. It was then left under the minimum load for 22 hours, following which curve IV resulted. The first, straight part of the curve is, within the accuracy of observation, identical in slope to the "elastic" curve (I). Definite creep occurs, however, at the highest stress shown (2 minutes interval between the two readings), and the following run, curve V, again shows hysteresis. This hysteresis is not as much as it is in curve III and the average slope is nearer that of the elastic curve.

The results depicted in Fig. 6 are very similar to those just described. Curve VI is an elastic curve taken after the crystal had had quite a few runs taken on it but had then rested for 10 days. Points were taken on this curve for both increasing and decreasing loads below 60 g/mm², and no observable hysteresis was found. At the highest stress shown the results described in connection with curve I were duplicated. The permanent set after unloading was $\Delta l/l = 1.7 \times 10^{-4}$. The lower part (hysteresis loop) of curve VII was taken next, and then the complete curve with repetition of the upper branch. In this curve the time intervals between successive points at the same stress are 1 minute, except for 2 minutes at 40.2 g/mm². After taking the upper part of curve VII and returning to the minimum load, the lower part (hysteresis loop) was duplicated. Curves VIII and IX were taken one and three days, respectively, after the data for curve VII, with no other runs intervening. The gradual recovery of the crystal is obvious. In both these curves the ascending branch is almost straight and parallel to the "elastic" curve (VI). Curve X shows three successive runs on a hysteresis loop like that of curve VII with points indicated by circles (○), crosses (+), and triangles (△), and taken in that order. These sets of observations agree within the experimental accuracy and a definite cyclic state seems to be indicated.

Creep data of the same type as that shown by the succession of points at each stress in curve VII, are represented in a different way in Fig. 7. These data were taken when the crystal was in a strained condition which was produced by starting with the crystal in an elastic state and then going beyond the elastic limit to a permanent set of $\Delta l/l = 0.8 \times 10^{-4}$. For each curve, except XI, the strain at the point marked A is arbitrarily plotted as zero although it is really the strain reached at the end of the preceding run (curve of next lower number). At A the increment to the load commenced and was completed several seconds before taking the reading at B, which is 20 seconds after A. The pronounced "toe" on curve XV shows the initial slowness

[9] The first point on curve II and on the other curves is plotted at the correct stress value but the strain is set arbitrarily in order to separate or compare certain curves. Thus II and III are set together with the same initial strain whereas in fact III started from the last point observed in II. Curves IV and V are similarly arranged.

of the transient creep, to which attention has been directed previously.

From the foregoing one may conclude that a zinc crystal of this orientation,[10] when sufficiently rested (self-annealed), has an elastic limit which is very well defined by the simultaneous occurrence of the end of the Hooke's law region and the point at which marked and rapid creep occurs. This limit is of the type previously reported for lead crystals[6] but the subsequent behavior of the zinc is very different from that of lead when the limit is passed and creep occurs. The zinc is now in an inelastic state in which Hooke's law fails both for increasing and decreasing stress and in which marked hysteresis occurs. It must be emphasized that the hysteresis loop cannot be wholly accounted for by assuming creep while the load on the specimen is being increased since one should then find, at the end of the cycle, a permanent set equal to the accumulated deviation from the elastic curve. This inelastic state gradually disappears with the self-annealing of the zinc. Before complete recovery the material may return to almost the original elastic state, with no or very little hysteresis, but with an elastic limit markedly lower than in the completely recovered state. Something like seven or eight days rest at room temperature seem to be needed for the limit to rise to the value of curves I and VI.

During the whole set of experiments on crystal No. 6 the total accumulated permanent set was only $\Delta l/l = 11 \times 10^{-4}$, or about 0.1 percent. The specimen showed no strain nor slip bands on its surface. A careful measurement of Young's modulus after an appropriate rest interval yielded $E = 11.6 \times 10^{11}$ dynes per cm². This is about 3 percent lower than the initial value of 12.0×10^{11} dynes/cm², corresponding to the crystal in the state of curve I, Fig. 5.[11]

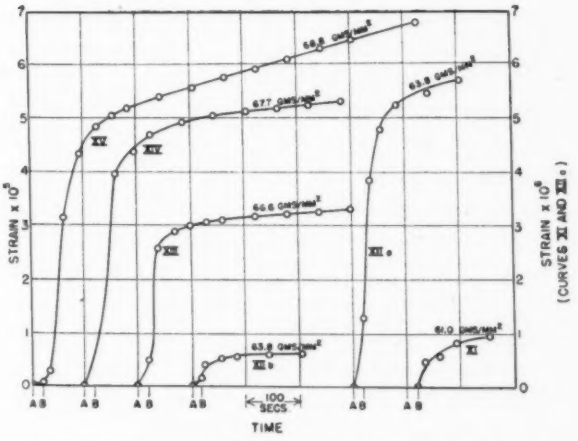

FIG. 7. Crystal No. 6: creep under successively greater loads. At A the load is that shown on the curve of next lower number. Between A and B the load is raised to the value shown on the curve and thereafter kept constant. The loading is complete several seconds before B. The interval AB is twenty seconds. Time increases from left to right with the lowest point on each curve at $t=0$. The initial strain for each curve is arbitrarily set equal to zero.

DISCUSSION

Some of the hitherto puzzling phenomena observed in connection with internal friction of zinc crystals may receive provisional and qualitative explanations in terms of the slow speed observations. If a zinc crystal may be put into the inelastic state by accidental strains incurred during handling, mounting for measurement, etc., then such a crystal would be expected to have a high decrement (as measured at the minimum stress amplitude). With some rest this decrement should decrease, but it might still rise with increasing stress amplitude until rested sufficiently for a complete return to the elastic state. When this state is reached the decrement at low stress amplitudes should be a minimum and the decrement curve should stay substantially level until at least the static elastic limit is reached. Indeed this point might be exceeded somewhat since it is the maximum stress amplitude which is plotted and this exists in only a very small portion of the crystal with less stress elsewhere. It is, however, rather obvious that in these experiments the decrement does not show any marked rise until the elastic limit has been greatly exceeded. Thus for crystal No. 4 (after the anneal, Fig. 2) a noticeable rise starts at about 230 g/mm² which is twice the elastic

[10] More recent work at the University of Iowa has confirmed the behavior described above for crystals of orientations above 45° but has shown that crystals of orientation lower than 45° act somewhat differently.

[11] The critical reader will note that the slope of this curve does not correspond to the stated value of Young's modulus. This is because the curves were all plotted with the stress computed from a provisional value of cross section. The cross section was only obtained accurately at the conclusion of the work by cutting out and weighing the actual 9-cm length on which observations were made. It did not seem worth while to correct all the curves since the error in stress is small and is the same for all the curves.

limit to be expected[12] from the observations on crystal No. 6, of the same purity. For crystal No. 2 (Fig. 1) the decrement has only doubled when the stress is four times the elastic limit. It has not, however, been definitely shown that an inelastic state can be set up in a crystal of such low orientation[10] by the means employed for the higher orientation crystals. Crystals Nos. 3 and 5 show level decrements to very much higher stresses. On account of their greater impurity the elastic limit may well be much higher than for crystal No. 6. No statement can therefore be made as to how much the elastic limit is exceeded in these crystals.

The observation that the decrement may remain fairly constant well beyond the static elastic limit seems to be connected with the initial slow rate of transient creep previously mentioned. With a rapidly alternating stress it seems likely that sufficient plastic deformation to cause an appreciable hysteresis loop, and a corresponding increase in the decrement, does not have time to occur. If the presence of dislocations is essential for creep and if the rate of creep depends on the number present,[13] then both the rapid and slow speed experiments seem to point to the necessity of supposing that some sort of incubation period exists for generation of the many more dislocations needed to give either a rapid rise in decrement or the greatly increased rate of creep shown by the steep parts of the curves of Fig. 7.

If, however, the rate of creep depends on the rate of generation of dislocations it must be assumed that these are generated only at a low rate for the first small time interval following an increase in stress.

The difference found here between the two pairs of crystals of different purity may explain the behavior of the very pure crystals of reference 1. Such pure material may have so low an elastic limit that it is just about reached when the stress amplitude is the lowest at which the measurements can be made. On this hypothesis the crystals would be in the inelastic state when mounting in the apparatus was completed, since strains due to handling would be unavoidable. The decrements observed immediately would be high, but would decline with time as the crystals annealed and approached the elastic state. The decrements could not be expected to stay level over any considerable range of stress amplitude, however.

Miller's[14] experiments bear out some such supposition as to the very low elastic limit of very pure zinc since he obtained creep with a resolved shear stress equal to about one-third of that at the elastic limit of crystal No. 6. His creep rate (averaged for the first 80 hours) is roughly one-tenth of the steady creep rate taken from the last part of curve XV in Fig. 7. Such a rate would be well within observation with the present apparatus and definitely does not occur for a well-annealed zinc crystal of 99.99 percent purity. Of course if Miller's crystal was in the inelastic state, due to handling, etc., both the rate of creep and the stress at which it occurred seem possible without assuming a vanishingly low elastic limit. The change to a much faster rate of creep, however, after the strain had reached 5×10^{-4} seems to point to the onset of an inelastic state at this time rather than to its being present earlier.

Attempts to compare creep rates and internal friction have been made by Seitz and Read.[15] If the mean transient creep rate taken from the steep parts of the curves of Fig. 7 is used, with a corresponding stress of 65 g/mm^2, a decrement of about 10^{-5} results. While this is of the right order of magnitude, the result must be regarded with some suspicion if there is any validity in the preceding speculations, in which it has been assumed that in the region of level decrement this rapid transient creep does not occur.

The writers are indebted to Mr. George Kuck for making the spectrographic analyses.

[12] Computed on the basis of the same resolved shear stress.

[13] F. Seitz and T. A. Read, J. App. Phys. 12, 470 (1941). See in particular pp. 471 and 478.

[14] See Fig. 40, reference 12.

[15] Reference 12, Eqs. (4) and (5).

Design of Broad Band I. F. Amplifier. Part II

RICHARD F. BAUM
Raytheon Manufacturing Company, Waltham, Massachusetts
(Received May 13, 1946)

This paper is a continuation of a previous article on the design of broad band I.F. amplifiers of the stagger-tuned type. The analysis is extended to unrestricted band width. It is shown that an exact solution is possible for either an oscillatory or a monotonic response, with this result: 1. The necessary number of stages (t) for a given minimum attenuation in the cut-off region depends again only on the gain tolerance and the desired response. 2. Attentuation minima and maxima again appear at frequencies within the band, easily located and dependent only on the number of stages. 3. The amplifier consists of a number of pairs of circuits, which have the same figure of merit Q_n and tune at resonant frequencies f_{0n} disposed in geometric symmetry around the middle band frequency f_0 thus making f_{0n} equal to $\delta_n f_0$ and f_0/δ_n, respectively. Formulas for Q_n and δ_n are derived. The circuit impedances are calculated from a prescribed gain or from the maximum obtainable gain. A formula for the maximum gain band width product is given. A comparison is made between the performance of amplifiers with monotonic and oscillatory response. A practical example is worked out.

(A) INTRODUCTION

IN a previous paper on the design of broad band I. F. ampliers,[1] a method of calculating the circuit parameters was outlined, which leads to simple formulas both in the case of monotonic or oscillatory amplifier response. The formulas derived there give a very good insight into the influence and mutual dependence of the given and the calculated design quantities. This simplicity was achieved at the expense of bandwidth. It was necessary to introduce an approximation for the expression of the detuning ϵ. By replacing its exact value

$$\epsilon = f/f_0 - f_0/f$$

by its approximate value

$$\epsilon = 2(f-f_0)/f_0,$$

this approximation restricted the validity of all derived formulas to a band width not larger than say one-quarter the center frequency f_0.

It is obvious that a design procedure permitting the exact calculation without restriction of band width would be welcome. This problem was successfully solved by Wallman[2] for the case of a monotonic response curve. In this paper the calculation is extended to the oscillatory case, which is often preferred to the monotonic case for its higher gain band width product and steeper cut-off slope.

Any particular desired response curve is substantially described by 4 points. Two of them define a band width within which the gain does not vary more than a definite prescribed amount. This amount is small and makes the gain in this region essentially constant. The two other points prescribe a certain minimum attenuation which has to be reached at certain frequencies outside of the pass band. The amount of required attenuation at these points as well as the admitted gain variation are given quantities for any particular design problem. In some cases two points may coincide with the half-power points; but formulas which are not restricted to the use of the half-power points are obviously more general and convenient.

Wallman has shown that by arranging the circuits in pairs of same Q_n and with resonance frequencies f_{01} and f_{02} symmetrically disposed around the middle frequency f_0 so as to make $f_{01}=\delta_1 f_0$ and $f_{02}=f_0/\delta_1$ a monotonic response curve of the form $1+(Q\epsilon)^{2t}$ can be obtained, from which the individual Q_n and δ_n can be derived by factorization. In the present paper it shall be shown that the most general expression is a polynomial in ϵ of highest power $k_m=2t$, containing only even powers of ϵ. The same line of reasoning is applied as in the previous paper; the polynomial is identified with an expression derived from Tschebyscheff's polynomial, the roots of which have been calculated. They furnish the Q_n and δ_n for the oscillatory case.

The same designations are used, as in the first

[1] R. F. Baum, J. App. Phys. **17**, 519 (1946).
[2] H. Wallman, "Stagger tuned I. F. amplifiers," M.I.T. Report 524, February 1944.

paper, but some of the quantities will have to be defined in accordance with the more rigorous requirements of the present calculation. Because of the geometric symmetry, all corresponding frequencies will have the middle band frequency as their geometric mean, for instance the upper and lower band limits, the two points of prescribed attenuation outside the band, pairs of maximum or minimum gain, etc. The geometric symmetry of the response curve suggests further the introduction of a logarithmic frequency scale.

As the line of reasoning is very similar to that of the first paper, the deduction of formulas and the arrangement of paragraphs proceeds in the same sequence. In order to distinguish between the formulas of the first and second part the formulas of the second part have an additional index 2.

The introduction of a reference circuit, as in the first part, proves of only restricted value in the present case as no great simplification of formulas can be obtained.

(B) POSSIBLE ATTENUATION CURVES

With the same designations as in the first part, the gain of a single-tuned stage is:

$$G_n = g_n R_n/(1+jQ_n\epsilon_n) \qquad (2\text{-}1)$$

and its absolute value

$$|G_n| = g_n R_n/(1+Q_n^2\epsilon_n^2)^{\frac{1}{2}}. \qquad (2\text{-}2)$$

The exact expression for the detuning ϵ_n is

$$\epsilon_n = f/f_{0n} - f_{0n}/f. \qquad (2\text{-}3)$$

Again a reference circuit is introduced, which resonates at mid-band frequency f_0 and for which*

$$\epsilon = f/f_0 - f_0/f. \qquad (2\text{-}4)$$

A logarithmic coordinate system is to be used. The variables become

$$\beta_n = \lg (f/f_{0n}), \quad \beta = \lg (f/f_0), \qquad (2\text{-}5)$$

thus

$$\epsilon_n = 2 \sinh \beta_n, \quad \epsilon = 2 \sinh \beta. \qquad (2\text{-}6)$$

The resonance frequency f_{0n} of the nth circuit shall be determined by a factor δ_n:

$$f_{0n} = \delta_n f_0. \qquad (2\text{-}7)$$

Its logarithm is

$$\Delta\beta_n = \lg \delta_n, \qquad (2\text{-}8)$$

which makes

$$\epsilon_n = 2 \sinh (\beta - \Delta\beta_n). \qquad (2\text{-}9)$$

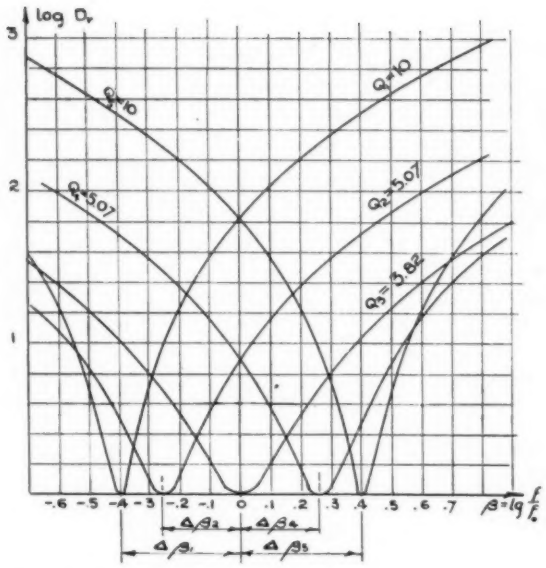

FIG. 1. Response curves of 5 stages. The center stage has the lowest Q and tunes at the geometric mean frequency f_0. The other stages are arranged in pairs of equal Q_n and with resonance points shifted the same distance above and below f_0 on a logarithmic frequency scale.

In the new coordinate system the origin corresponds to $f/f_0 = 1$, that is, to the mid-band frequency. The fact that the nth circuit resonates at $\delta_n f_0$ thus appears as a simple shift of its response curve by an amount of $\Delta\beta_n$ to the right (Fig. 1). The gain becomes

$$|G_n| = g_n R_n[1+Q_n^2 4 \sinh^2 (\beta - \Delta\beta_n)]^{-\frac{1}{2}}, \qquad (2\text{-}10)$$

which shows that the response curves are symmetric with respect to the point $\beta = \Delta\beta_n$.

The index $n=1$ again is given to the circuit resonating at the low frequency end of the band and the index $n=t$ to the circuit resonating at the upper end. The indices $n=2$ and $n=t-1$ are reserved for the two adjacent stages, etc.

The gain of t stages is

$$|G_n| = \prod_{n=1}^{n=t} g_n R_n[1+4Q_n^2 \sinh^2 (\beta - \Delta\beta_n)]^{-\frac{1}{2}}. \qquad (2\text{-}11)$$

At the mean frequency, β equals zero and the

* Quantities without index n refer to the reference circuit.

gain becomes:

$$|G_0| = \prod_{n=1}^{n=t} g_n R_n [1+4Q_n^2 \sinh^2 \Delta\beta_n]^{-\frac{1}{2}}. \quad (2\text{-}12)$$

If all stages should tune to the same frequency the gain would be:

$$|G_0^0| = \prod_{n=1}^{n=t} g_n R_n. \quad (2\text{-}13)$$

The loss in gain due to the displacement of the resonant frequencies is thus

$$l^2 = \prod_{n=1}^{n=t} [1+4Q_n^2 \sinh^2 \Delta\beta_n], \quad (2\text{-}14)$$

and the gain can again be written in the form

$$|G_0| = (1/l) \prod_{n=1}^{n=t} g_n R_n. \quad (2\text{-}15)$$

The part of (2-10) which is a function of frequency defines all possible response curves and is:

$$D_P = \epsilon^{2d} = \prod_{n=1}^{n=t} [1+4Q_n^2 \sinh^2 (\beta-\Delta\beta_n)], \quad (2\text{-}16)$$

where d is the voltage attenuation in Nepers.

Now the circuits may be arranged in pairs of the same Q_n and of resonance frequencies disposed in geometric symmetry to both sides of the mid-band frequency.* On a logarithmic scale this corresponds to a shift of $\Delta\beta_n$ in the positive sense for one circuit and in the negative sense for the other. The response of such a pair is:

$$\begin{aligned}
&[1+2jQ_n \sinh (\beta-\Delta\beta_n)] \\
&\qquad \times [1+2jQ_n \sinh (\beta+\Delta\beta_n)] \\
&= 1-2Q_n^2[\cosh (2\beta)-\cosh (2\Delta\beta_n)] \\
&\qquad + j4Q_n \sinh \beta \cosh \Delta\beta_n \\
&= [1+4Q_n^2 \sinh^2 \Delta\beta_n]-4Q_n^2 \sinh^2 \beta \\
&\qquad + j4Q_n \sinh \beta \cosh \Delta\beta_n \\
&= A-4Q_n^2 \sinh^2 \beta + j2BQ_n \sinh \beta.
\end{aligned}$$

Reintroducing ϵ from (2–6) the response of one pair becomes

$$D_P^1 = [A-Q_n^2\epsilon^2]^2 + Q_n^2\epsilon^2 B^2, \quad (2\text{-}17)$$

where A and B are constants.

* This idea and the corresponding proof is contained in Wallman's paper, reference 2.

This equation shows that the response curve of a pair of circuits is a polynomial of the fourth power of the variable ϵ, and containing only even powers of ϵ. The response of all stages is a polynomial obtained by multiplication of several such polynomials and can therefore possess only even powers of ϵ. Its highest power k_m will be $k_m = 2t$ or twice the number of circuits. This fact is obviously not altered by the addition of one single circuit resonating at mid-band frequency f_0, the response of which is quadratic in ϵ:

$$D_P = 1+Q^2\epsilon^2.$$

(C) THE REQUIRED RESPONSE CURVE

The result obtained checks closely with the one obtained in the first part of this paper, the only difference being that the variable ϵ now is defined by its exact value (2-4) instead of its approximate value according to Eq. (1-6). Thus the same reasoning may be applied to the present case as to the former:

It was shown that the required response curve could be represented in either of two forms:

$$D_r = |d_0| T_{2t}(\alpha) + (1+d_0) \quad (2\text{-}18)$$

for the oscillatory case, or

$$D_r^* = 1+2d_0\alpha^{2t} \quad (2\text{-}19)$$

for the monotonic case. In these expressions d_0 is the admissible gain variation within the pass band, and the variable α was defined by Eq. (1-20) with

$$\alpha = s/s_L = \epsilon/\epsilon_L. \quad (2\text{-}20)$$

This ϵ_L is that value which the variable ϵ takes at the ends of the band. This definition still applies to the present case although ϵ_L now is given by

$$\epsilon_L = f_L/f_0 - f_0/f_L, \quad (2\text{-}21)$$

where f_L is the upper frequency limit of the band. Setting

$$f_L = \delta_L f_0, \quad (2\text{-}22)$$

ϵ_L becomes

$$\epsilon_L = \delta_L - 1/\delta_L = 2 \sinh \beta_L, \quad (2\text{–}23)$$

where $\beta_L = \lg \delta_L$ and is the equivalent of ϵ_L on the logarithmic frequency scale.

The variable α thus becomes

$$\alpha = \epsilon/\epsilon_L = 2 \sinh \beta/\epsilon_L = \sinh \beta/\sinh \beta_L. \quad (2\text{-}24)$$

It was shown that the points of minimum attenuation within the band occur at points uniquely determined by the number t of stages employed and given (see Eq. (1-23)) by

$$\left.\begin{aligned} \alpha_n^{\min} &= \cos\left[(2m+1)\pi/2t\right] \\ m &= 0, 1, 2, \cdots (t-1) \\ &= n-1 \end{aligned}\right\}. \quad (2\text{-}25)$$

To this corresponds a certain detuning $\epsilon_n^{\min}$, a certain frequency $f_n^{\min}$, and a certain shift $\beta_n^{\min}$ on the logarithmic scale, given by

$$\alpha_n^{\min} = \epsilon_n^{\min}/\epsilon_L = 2 \sinh \beta_n^{\min}/\epsilon_L \quad (2\text{-}26)$$

and

$$\beta_n^{\min} = \lg\,(f_n^{\min}/f_0) = \lg\,\delta_n^{\min}. \quad (2\text{-}27)$$

Furthermore, it was shown that it is possible to calculate the complex roots α_{0n} of (2-18) and (2-19). Their real and imaginary parts were designated with αR_n and αI_n, respectively:

$$\alpha_{0n} = \alpha R_n + j\alpha I_n. \quad (2\text{-}28)$$

Their values were (Eq. (1-34) and (1-35)) for the oscillatory case [with added index n]:

$$\alpha R_n = \cosh\,(c/2t) \cos\left[(2m+1)\pi/2t\right], \quad (2\text{-}29)$$

$$\alpha I_n = \sinh\,(c/2t) \sin\left[(2m+1)\pi/2t\right], \quad (2\text{-}30)$$

where (Eq. (1-32)):

$$c = \cosh^{-1}\frac{1+d_0}{d_0},$$

and for the monotonic case (Eqs. (1-38) and (1-39))

$$\alpha R_n^* = \left[2d_0\right]^{-1/2t} \cos\left[(2m+1)\pi/2t\right], \quad (2\text{-}31)$$

$$\alpha I_n^* = \left[2d_0\right]^{-1/2t} \sin\left[(2m+1)\pi/2t\right]. \quad (2\text{-}32)$$

The roots corresponding to α_{0n} are, in the logarithmic coordinate system, given by β_{0n}:

$$\alpha_{0n} = \epsilon_{0n}/\epsilon_L = 2 \sinh \beta_{0n}/\epsilon_L. \quad (2\text{-}33)$$

Now as α_{0n} is complex, β_{0n} obviously is complex also:

$$\beta_{0n} = \beta R_n + j\beta I_n. \quad (2\text{-}34)$$

This introduced into (2-33) furnishes, after separation of real and imaginary components:

$$\alpha R_n = \frac{2}{\epsilon_L} \sinh \beta R_n \cos \beta I_n, \quad (2\text{-}35)$$

$$\alpha I_n = \frac{2}{\epsilon_L} \cosh \beta R_n \sin \beta I_n. \quad (2\text{-}36)$$

These two equations can easily be solved for βR_n and βI_n. The solution is

$$\cosh\,(2\beta R_n) = \frac{\sigma_n^2}{4} + \left[\left(\frac{\sigma_n^2}{4}\right)^2 + \frac{\tau_n^2}{2} + 1\right]^{\frac{1}{2}}, \quad (2\text{-}37)$$

$$\cos\,(2\beta I_n) = -\frac{\sigma_n^2}{4} + \left[\left(\frac{\sigma_n^2}{4}\right)^2 + \frac{\tau_n^2}{2} + 1\right]^{\frac{1}{2}}, \quad (2\text{-}38)$$

where

$$\sigma_n^2 = \epsilon_L^2(\alpha R_n^2 + \alpha I_n^2), \quad (2\text{-}39)$$

$$\tau_n^2 = \epsilon_L^2(\alpha R_n^2 - \alpha I_n^2). \quad (2\text{-}40)$$

By subtraction and by multiplication of (2-37) and (2-38) it is found that between βR_n and βI_n the following relations must exist:

$$\frac{\sigma_n^2}{4} = \sinh^2 \beta R_n + \sin^2 \beta I_n, \quad (2\text{-}41)$$

and

$$\frac{\tau_n^2}{2} + 1 = \cosh\,(2\beta R_n) \cos\,(2\beta I_n). \quad (2\text{-}42)$$

The quantity σ_n introduced here for convenience obtains significance in the calculation of the gain. βR_n is to furnish the resonance shifts $\Delta\beta_n$, and βI_n is to furnish the Q_n of the individual circuits.

Equations (2-35) to (2-42) apply as well to the monotonic as to the oscillatory case, depending upon which roots, (2-31), (2-32), or (2-29), (2-30), are introduced.

(D) CALCULATION OF CIRCUIT PARAMETERS

a. Selectivities and Resonant Frequencies

By equalizing the roots given by Eq. (2-16)

$$D_P = \prod_{n=1}^{n=t} \left[1 + 4Q_n^2 \sinh^2\,(\beta_{0n} - \Delta\beta_n)\right] = 0, \quad (2\text{-}43)$$

with the roots β_{0n} as calculated in the previous paragraph, all circuit parameters may be calculated. By setting each factor of (2-43) equal to zero, its root $\beta_{0n} = \beta R_n + j\beta I_n$ is found from:

$$\begin{aligned} 1 + 4Q_n^2 \sinh^2\,(\beta_{0n} - \Delta\beta_n) &= 0, \\ \sinh\,(\beta R_n + j\beta I_n - \Delta\beta_n) &= j/2Q_n. \end{aligned} \quad (2\text{-}44)$$

The right side of this equation is imaginary; thus on the left side the real component has to equal zero, or

$$\Delta\beta_n = \beta R_n. \quad (2\text{-}45)$$

This leaves

$$\sin\,\beta I_n = 1/2Q_n. \quad (2\text{-}46)$$

Equations (2-45) and (2-46) determine the simple relations between Q_n and $\Delta\beta_n$ (the selectivities and resonant frequencies) and the quantities β_{R_n} and β_{I_n}, as given by Eq. (2-37) and (2-38). Thus the problem is solved in principle. Whereas in the approximate case (treated in Part I) the Q_n and the resonant frequencies depended separately on the real or imaginary root components α_{R_n} and α_{I_n}, respectively, it is seen, that in the rigorous calculation they depend on both components in a rather involved manner. For this reason the result cannot be simply stated. Thus the importance of the approximate solution lies partly in the way it indicates in simple formulas the trend of the phenomena and the interconnection of the design parameters, whereas the final design can be based on the exact solution.

For both the oscillatory and the monotonic response, expressions (2-39) and (2-40) can be simplified:

In the oscillatory case with (2-29) and (2-30):

$$\sigma_n^2=\frac{\epsilon_L^2}{2}\{\cosh(c/t)+\cos[(2m+1)\pi/t]\},$$
$$=\epsilon_L^2\{\sinh^2(c/2t)+\cos^2[(2m+1)\pi/2t]\}, \quad (2\text{-}47)$$

$$\tau_n^2=\frac{\epsilon_L^2}{2}\{1+\cosh(c/t)\cos[(2m+1)\pi/t]\}, \quad (2\text{-}48)$$

in the monotonic case with (2-31) and (2-32):

$$\sigma_n^{*2}=\epsilon_L^2[2d_0]^{-1/t}, \quad (2\text{-}49)$$

$$\tau_n^{*2}=\epsilon_L^2[2d_0]^{-1/t}\cos[(2m+1)\pi/t]; \quad (2\text{-}50)$$

$$m=n-1=0,\ 1,\ 2,\ \cdots(t-1).$$

In the beginning the gain was written in terms of a reference circuit, which was supposed to resonate at mid-band frequency f_0 and has a Q_n equal Q (without index). This circuit requires the following solutions (from (2-45) and (2-46)):

$$\beta_{R_n}=\Delta\beta_n=0$$

and

$$\sin\beta_{I_n}=1/2Q$$

which are obtained by setting

$$(2m+1)\pi/2t=\pi/2.$$

This gives, in the oscillatory case (Eqs. (2-29), (2-30), (2-35), and (2-26)):

$$\alpha_R=0, \quad \alpha_T=\sinh(c/2t)=1/Q\epsilon_L, \quad (2\text{-}51)$$

and in the monotonic case (Eqs. (2-31), (2-32), (2-36), and (2-37)):

$$\alpha_R^*=0, \quad \alpha_T^*=[2d_0]^{-1/2t}=1/Q\epsilon_L. \quad (2\text{-}52)$$

These relations correspond exactly to formulas (1-45) and (1-49) of the first part. They obviously give a very simple relationship between the band width ϵ_L, the admissible gain variation α_0, and the Q of the reference circuit, which in the case of an uneven number of stages coincides with the middle stage. The corresponding value of σ becomes in both cases

$$\sigma=\sigma^*=1/Q. \quad (2\text{-}53)$$

From (2-49) furthermore (in the monotonic case):

$$\sigma_n^*=\sigma^*=1/Q \text{ constant for all stages.}$$

b. The Minimum Number of Circuits

Nothing has to be added to the corresponding chapter of Part I. All formulas derived there remain valid in the present case and this without restriction for the values of the quantity α_m appearing in formulas (1-57) to (1-64), the value of which is now defined by two frequencies, f_{m1} and f_{m2} ($f_{m1}\cdot f_{m2}=f_0^2$) at which the attenuation d should attain at least a prescribed minimum value d_m. Writing

$$\epsilon_m=f_{m1}/f_0-f_0/f_{m1}, \quad (2\text{-}54)$$

and

$$\epsilon_L=f_L/f_0-f_0/f_L$$

as in (2-20), α_m is given by

$$\alpha_m=\epsilon_m/\epsilon_L. \quad (2\text{-}55)$$

c. Impedances and Gain

The loss in gain due to the staggering of the resonance frequencies was (Eq. (2-14)):

$$l^2=\prod_{n=1}^{n=t}[1+4Q_n^2\sinh^2\Delta\beta_n]$$
$$=\prod_{n=1}^{n=t}4Q_n^2\left[\left(\frac{1}{2Q_n}\right)^2+\sinh^2\Delta\beta_n\right].$$

By introduction of Eqs. (2-45), (2-46), and (2-41)

this expression reduces to

$$l = \prod_{n=1}^{n=t} Q_n \sigma_n. \tag{2-56}$$

The product $\sigma_n Q_n$ of each circuit determines its loss in gain (or attenuation) at mid-band frequency. This loss, of course, is the same for each circuit of a circuit pair for reasons of symmetry, but is different for each pair.

The product given by Eq. (2-56) thus consists of a series of pairs of equal factors (squares). A single stage resonating at mid-band frequency obviously does not contribute to the gain loss, because, according to Eq. (2-53): $\sigma = 1/Q$.

In the case of monotonic response the product (2-56) is simplified because σ_n is the same (see Eq. (2-49)) for all circuit pairs:

$$l^* = \epsilon_L{}^t [2d_0]^{-\frac{1}{2}} \prod_{n=1}^{n=t} Q_n. \tag{2-57}$$

The expressions for the gain loss due to resonance staggering can be written also in terms of the Q of the reference circuit by introducing σ_n and Q from (2-51) or (2-52). They become

$$l = \prod_{n=1}^{n=t} \frac{Q_n}{Q} \left[1 + \frac{\cos^2 [(2m+1)\pi/2t]}{\sinh^2 (c/2t)} \right]^{\frac{1}{2}} \tag{2-58}$$

for the oscillatory case, and

$$l^* = \prod_{n=1}^{n=t} \frac{Q_n}{Q} \tag{2-59}$$

for the monotonic case.

The last equation shows that in the monotonic case the gain loss l^* increases for each stage in proportion to the increase of Q_n over the Q of the reference circuit. But according to Eq. (2-58) in the oscillatory case this loss increases more rapidly and differs from circuit pair to circuit pair.

The loss in gain due to the staggering of resonance frequencies is, of course, totally or partly compensated by the increase in stage gain due to the increase in Q_n as will be apparent from the following gain formulas.

The total gain according to Eq. (2-15) was

$$|G_0| = (1/l) \prod_{n=1}^{n=t} g_n R_n,$$

and with (2-56)

$$|G_0| = \prod_{n=1}^{n=t} g_n R_n / Q_n \sigma_n \tag{2-60}$$

$$= \prod_{n=1}^{n=t} g_n / C_n \omega_{0n} \sigma_n. \tag{2-61}$$

As any circuit pair resonates at frequencies the product of which equals the square of the mid-band frequency, one may replace, in the product, ω_{0n} by ω_0. Furthermore, considering only the case of stages with the same capacities $C_n = C$, and the same transconductance $g_n = g$, the gain becomes:

$$|G_0| = \left[\frac{g}{C\omega_0} \right]^t \prod_{n=1}^{n=t} \frac{1}{\sigma_n}. \tag{2-62}$$

Writing this expression for just one pair of circuits it is easily seen that in the monotonic case the average gain per circuit pair equals the gain of the reference (or middle) circuit.

The average gain per stage is

$$|\bar{G}_0| = \frac{g}{C\omega_0} \left[\prod_{n=0}^{n=t} \frac{1}{\sigma_n} \right]^{1/t}. \tag{2-63}$$

The total band width (with Eqs. (2-22) and (2-23)) is

$$BW = \delta_L f_0 - \frac{f_0}{\delta_L} = f_0 \epsilon_L, \tag{2-64}$$

thus the average gain band with product becomes

$$|\bar{G}_0| BW = \left(\frac{g}{\pi C} \right) \cdot \frac{\epsilon_L}{2} \left[\prod_{n=1}^{n=t} \frac{1}{\sigma_n} \right]^{1/t}. \tag{2-65}$$

For the monotonic case the root equals Q and with (2-52) the expression becomes

$$|\bar{G}_0{}^*| BW = \left(\frac{g}{\pi C} \right) \cdot \tfrac{1}{2} [2d_0]^{1/2t} \tag{2-66}$$

which is exactly the same as the expression derived for the approximate calculation (see Eq. (1-78)).

The factor in parenthesis again is recognized as the theoretical maximum gain band width product and again an efficiency factor may be defined by:

$$\mu = \frac{\epsilon_L}{2} \left[\prod_{n=1}^{n=t} \frac{1}{\sigma_n} \right]^{1/t}, \tag{2-67}$$

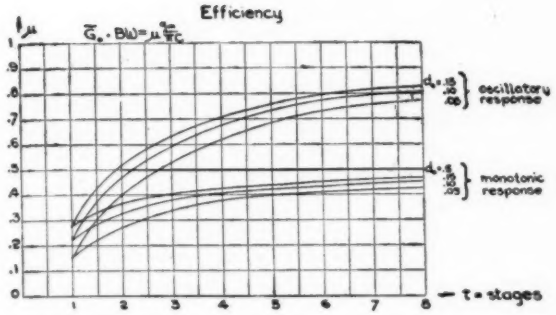

FIG. 2. Efficiency of amplifiers with oscillatory and monotomic response.

or with (2-47):

$$\mu = \tfrac{1}{2} \prod_{n=1}^{n=t} \{\sinh^2 (c/2t) + \cos^2 [(2m+1)\pi/2t]\}^{-1/2t} \quad (2\text{-}68)$$

and in the monotonic case:

$$\mu^* = \tfrac{1}{2}[2d_0]^{1/2t}, \quad (2\text{-}69)$$

the latter approaching rapidly $\frac{1}{2}$ with increasing the number of stages.

The importance of the quantity σ_n in all gain calculations is apparent. With reference to Eq. (2-62) one can say that σ_n defines the relative contribution of each individual stage to the total gain. In order to facilitate the gain calculation, the value of μ and μ^* is plotted in Fig. 2 as a function of t for $d_0 = .05$, $d_0 = .1$, and $d_0 = .15$.

(E) COMPARISON OF MONOTONIC AND OSCILLATORY RESPONSE

The deduced formulas permit the comparison of the performance of amplifiers of monotonic and oscillatory response.

For a given response characteristic, that is for a given maximum gain tolerance d_0 within the pass band and a given minimum attenuation d_m above a given frequency, a monotonic amplifier requires more stages than the oscillatory one. The ratio of their number is, with Eqs. (1-58) and (1-63):

$$\frac{t^*}{t} = \frac{h^*}{h} \cdot \frac{\cosh^{-1} \alpha_m}{\lg \alpha_m}. \quad (2\text{-}70)$$

The first factor almost equals one, so that approximately

$$\frac{t^*}{t} = \frac{\cosh^{-1} \alpha_m}{\lg \alpha_m}, \quad (2\text{-}71)$$

thus if the minimum attenuation is defined anywhere between $\alpha_m = \alpha_m^* = 1.1$ and 2, this ratio varies between 4.5 and 1.9.

For a given gain tolerance within the pass band, and with the same number of stages, the monotonic amplifier has a much flatter cut-off characteristic than the oscillatory one. Thus by setting $t/t^* = 1$ in Eq. (2-71) the frequencies at

TABLE I: Calculation of the Q_n and resonance frequencies.

stage	m	$(2m+1)\pi/t = \theta$	$\cos\theta$	$\cosh c/t + \cos\theta$
1 and 5	0 and 4	36° and 324°	.809	2.006
2 and 4	1 and 3	108° and 252°	−.309	.888
3	2	180°	−1	
Eq.				

stage	$\cosh c/2t \cdot \cos\theta$	σ_n^2	$\sigma_n^2/4$	$(\sigma_n^2/4)^2$	$\tau_n^2/2$
1 and 5	.97	.7	.175	.0305	.343
2 and 4	−.37	.310	.0776	.006	.109
3					
Eq.		(2-47)			(2-48)

stage	σ	$\cosh 2\beta R_n$	$\cos 2\beta T_n$	$2\beta R_n$	$2\beta T_n$	$\Delta\beta_n$
1 and 5	.837	1.345	.995	.797	5.7°	.398
2 and 4	.557	1.136	.980	.516	11.3°	.258
3	.262					0
Eq.	(2-53)	(2-37)	(2-38)			(2-45)

stage	$\sin\beta T_n$	Q_n	δ_n	f_{0n}
1 and 5	.050	10	1.49	17.9 and 8.05 mc
2 and 4	.0984	5.07	1.29	15.5 and 9.3 mc
3		3.82		12 mc
Eq.		(2-46) (2-53)	(2-8)	(2-7)

which a given attenuation is reached are given by

$$\alpha_m^* = \alpha_m + (\alpha_m^2 - 1)^{\frac{1}{2}}. \qquad (2\text{-}72)$$

Within a range of $1.1 < \alpha_m < 2$ the corresponding α_m^* lies between 1.55 and 3.7.

For a given minimum attenuation and a given number of stages the gain variation of the monotonic amplifier is obviously larger.

The average gain band width product, with a given number of stages and a given gain variation, is larger for the oscillatory amplifier by a factor: (Eqs. (2-68) and (2-69))

$$\frac{|\bar{G}_0| \cdot BW}{|\bar{G}_0^*| \cdot BW} = \frac{\mu}{\mu^*}. \qquad (2\text{-}73)$$

The value of μ and μ^* was plotted in Fig. 2.

Whereas the value of μ^* is somewhat smaller than $\frac{1}{2}$ the value of μ is smaller than 1. The limits of μ can be seen to be

$$\mu \to \tfrac{1}{2} \sinh (c/2t) \quad \text{for} \quad \sinh (c/2t) \gg \cos \frac{(2m+1)\pi}{2t}$$

and

$$\mu \to 2^{-1/t} \quad \text{for} \quad \sinh (c/2t) \to 0.$$

The first case corresponds to a very small gain tolerance and a small number of stages. It falls to values below one-half, but is still larger than the corresponding μ^* of the monotonic amplifier.

The other case corresponds to a large gain tolerance and a large number of stages. The average efficiency increases with an increasing number of stages; the total gain band width product tends towards $\frac{1}{2}$, whereas in the monotonic case the average gain band width product tends toward $\frac{1}{2}$.

From the standpoint of amplitude response, which was considered exclusively, the oscillatory amplifier is superior to the monotonic one in every respect.

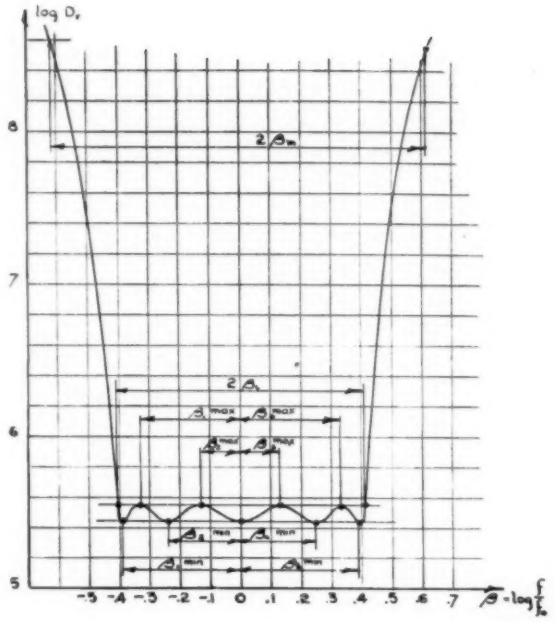

FIG. 3. The resultant response curve shows an oscillatory behavior within the pass band $2\beta_L$, defined by a given gain tolerance d_0. The attenuation exceeds a prescribed minimum value d_m outside a given range $2\beta_m$.

TABLE II.

m	$\frac{(2m+1)\pi}{2t} = \frac{\theta}{2}$	$\cos\frac{\theta}{2}$	$\epsilon_m^{\min}$	$\beta_m^{\min}$	$\delta_m^{\min}$	$f_m^{\min}$
0 and 4	18° and 162°	951	.794	.387	1.473	8.16 and 17.7 mc
1 and 3	54° and 126°	588	.490	.242	1.274	9.42 and 15.3 mc
2	90°	0	0	0	1	12 mc
formula		(2-25)	(2-26)	(2-26)	(2-27)	

TABLE III.

m	$\frac{m\pi}{t}$	$\cos\left(\frac{m\pi}{t}\right)$	$\epsilon_m^{\max}$	$\beta_m^{\max}$	$\delta_m^{\max}$	$f_m^{\max}$
1 and 4	36° and 144°	.809	.675	.331	1.392	8.64 and 16.7 mc
2 and 3	72° and 108°	.309	.258	.129	1.138	10.55 and 13.7 mc

(F) EXAMPLE

A stagger tuned I.F. amplifier is to be designed having a band width from 8 to 18 mc, and having the maximum gain obtainable with 6AK5 tubes, with a gain variation of .1 Nepers within the pass band, with a power attenuation of at least 30 db at 22 mc and the corresponding lower frequency. An oscillatory response is desired. The given quantities are:

$d_0 = .1$ Neper, the admissible gain variation.
$\epsilon^{2d_m} = 1000$, the required power attenuation.
$f_L = 18$ mc and 8 mc, respectively, the upper and lower band limits.
$f_0 = (8.18)^{\frac{1}{2}} = 12$ mc, the geometric mean frequency,

$$f_n = 22 \quad \text{and} \quad \frac{12^2}{22} = 6.55 \text{ mc}$$

the frequencies at which the power drops to the required level. To f_L and f_m correspond detunings:

$$\epsilon_L = .83$$

and

$$\epsilon_m = 1.284$$

which correspond on the logarithmic scale to

$$\beta_L = .407$$

and

$$\beta_m = .607$$

(see Fig. 3). Thus

$$\alpha_m = \epsilon_m/\epsilon_L = 1.542 \quad \text{and} \quad \cosh^{-1}\alpha_m = 1.$$

The minimum number of stages (from (1-58) and (1-59)):

$$2t \geqq h/\cosh^{-1}\alpha_m$$

$$\cosh h = [\epsilon^{2d_m} - (1+d_0)]/d_0$$

$$\leqq 10000$$

$$h = 9.8.$$

$$\geqq 9.8$$

In order to obtain the prescribed response curve, at least 5 stages are required. Calculation of the hyperbolic expressions:

$$c = \cosh^{-1}\frac{1+d_0}{|d_0|} = \cosh^{-1} 11 = 3.09,$$

$$c/2t = \frac{3.09}{10} = .309,$$

$$c/t = .618,$$

$$\cosh (c/2t) = 1.048,$$

$$\sinh (c/2t) = .314,$$

$$\cosh (c/t) = 1.197.$$

The resonance frequencies f_{0n} and the Q_n of the circuits have been calculated in Table I. The result has been plotted on a logarithmic scale in Fig. 1. By addition of the 5 individual response curves the total amplifier response of Fig. 3 is obtained which shows the required oscillatory behavior. The location of minimum attenuation is shown in Table II.

The points of maximum attenuation can be calculated in an analogous way from:

$$\alpha_m{}^{\max} = \cos\left(\frac{m\pi}{t}\right), \quad m = 1, 2, 3 \cdots (t-1), \quad (2\text{-}74)$$

which follows from inspection of Fig. 3 of Part I, (Table III).

The corresponding maximum and minimum values of attenuation within the band turn out to be 5.46 and 5.54. The former checks with the loss in gain if calculated from Eq. (2-58). The difference of .08 checks with the admissible gain variation, as $\log_{10}(1.1)^2 = .08$. (All curves are power response curves.) The minimum attenuation of 30 db = 3 is reached within the prescribed frequency limit $\beta_m = \pm .607$ with an attenuation of 8.57.

Assuming a transconductance of $g = 5000$ mhos and a minimum capacity of $12\mu\mu$f for each stage, the theoretical maximum gain band width product is:

$$9/\pi C = 133 \text{ mc}.$$

The efficiency factor is calculated from Eq. (2-66) with

$$\mu = \frac{.833}{2} \Big/ (.837^2 \times .557^2 \times .262)^{\frac{1}{2}} = .73.$$

The average gain band width product is thus:

$$|\bar{G}_0|\, BW = 133 \times .73 = 98.5 \text{ mc}.$$

With a band width of 10 mc the average gain

becomes

$$|\bar{G}_0| = 98.5/10 = 9.85,$$

and the total gain:

$$|G_0| = 9.85^5 = 92{,}400.$$

This compares very favorably with an amplifier of monotonic response whose best efficiency factor is .5. This gives a maximum gain for 5 stages (with 10 mc band width) of only 13,000.

CONCLUSION

It has been shown that the stagger tuned amplifier problem with oscillatory response can be exactly solved mathematically. The solution is obtained by the same means employed for the solution of the approximate case (with restricted band width), that is—by calculation of the roots of either a parabolic or a Tschebyscheff polynomial.

The Numerical Solution of Laplace's Equation in Composite Rectangular Areas

MAX M. FROCHT*
Illinois Institute of Technology, Chicago, Illinois
(Received January 29, 1946)

An analytical method is developed which yields key values of a harmonic function U in rectangular figures in terms of certain simple combinations of known boundary values, which we call Laplacian perimeters and denote by P. From the key values all the remaining interior values can be directly and rapidly calculated. The basic ideas consist of the introduction of four elementary figures of variable lengths: $3(2+\delta)$, $3(3+\delta)$, $4(2+\delta)$, and $4(3+\delta)$, where $0 \leqslant \delta \leqslant 1$, for which the key values are found algebraically, Eqs. (9.1) to (9.8) inclusive, and of combining analytically these elementary cases to obtain *continuous solutions* for rectangles $(3\times n')$ and $(4\times n')$ for any number n' greater than 2. The general expression for any key value $(u_i)_{m\times n'}$ in a rectangle $(m\times n')$ is

$$(u_i)_{m\times n'} = C_1P_1 + C_2P_2 + \cdots C_iP_i + \cdots C_kp_k,$$

in which C_1, $C_2 \cdots C_k$ are constant coefficients. Analytical relations are established between the coefficients for the last key value u_k in a rectangle $(m\times n)$, where n is an integer, and the coefficients for the next key value u_{k+1} in the rectangle $m(n+\delta)$ or $m(n+\delta+1)$. Specific values of the coefficients are presented in tabular form for rectangles $(3\times n')$ and $(4\times n')$ with the aid of which all key values in such rectangles can be rapidly calculated. The tables also permit the calculation of any one interior key value by itself. A numerical example and further approximate formulas are given, and applications to composite rectangular areas such as angles, channels, etc., are discussed.

1. INTRODUCTION

NUMERICAL or approximate solutions of Laplace's equation

$$\partial^2 U/\partial x^2 + \partial^2 U/\partial y^2 = 0 \qquad (1.1)$$

are generally based on the fact that the value of the function U at an arbitrary point O of the region R to which the function U applies, Fig. 1, must satisfy approximately the general equation†

$$\left(\frac{1}{ac}+\frac{1}{bd}\right)u_o = \frac{u_a}{a(a+c)} + \frac{u_b}{b(b+d)} + \frac{u_c}{c(c+a)} + \frac{u_d}{d(d+b)} \quad \text{(a)} \qquad (1.2)$$

or

$$u_o = k_a u_a + k_b u_b + k_c u_c + k_d u_d, \quad \text{(b)}$$

in which u_a, u_b, u_c, and u_d are the values of the harmonic function U at four neighboring points, A, B, C, and D, respectively, with coordinates as shown in Fig. 1. Equation (1.2) will be referred to as the four-point influence equation, or more briefly the four-point equation.

The procedure in numerical solutions generally consists of drawing a rectangular, equally spaced network distant h apart, and adjusting the values at each point of intersection of the network lines (network points) until they satisfy the four-point equation. When that is attained, an approximate or numerical solution is said to have been found. The distance h between the network

* Professor of Mechanics.

† For a derivation see references 1 and 3 in bibliography at end of paper.

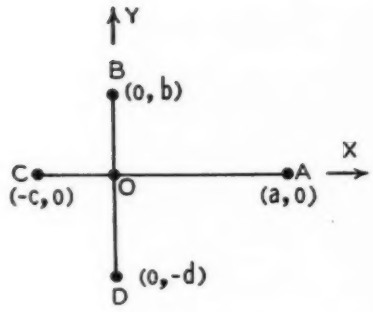

FIG. 1.

lines is called the lattice unit. The points A, B, C, and D may be located on the network lines, or on lines inclined 45° to them. In the first case we speak of normal neighbors, in the second case of diagonal neighbors. In the treatment which follows, both types are used.

Most of the interior network points will have equally spaced neighbors. For such points (1.2) reduces to

$$4u_o = u_a + u_b + u_c + u_d. \tag{1.3}$$

Equation (1.3) is generally called the Liebmann formula.

Another case of special interest is the case in which $a=b$, and $c=d$, Fig. 1. For this case (1.2) reduces to

$$u_o = \frac{c(u_a+u_b)}{2(a+c)} + \frac{a(u_c+u_d)}{2(a+c)}. \tag{1.4}$$

Assuming $a<c$ and $a/c=\delta$, this may be written as

$$u_o = \frac{(u_a+u_b)}{2(\delta+1)} + \frac{\delta(u_c+u_d)}{2(\delta+1)}, \tag{1.5}$$

where δ is a fraction less than unity, or

$$u_o = K_1(u_a+u_b) + K_2(u_c+u_d), \tag{1.6}$$

where K_1 and K_2 are constant coefficients given by

$$\left.\begin{aligned} K_1 &= 1/2(\delta+1), \quad \text{(a)} \\ K_2 &= \delta/2(\delta+1). \quad \text{(b)} \end{aligned}\right\} \tag{1.7}$$

When $b=c=d$, $a<b$, and $a/b=\delta$, we have

$$u_o = \frac{u_a}{(1+\delta)^2} + \frac{\delta u_c}{(1+\delta)^2} + \frac{\delta(u_b+u_d)}{2(1+\delta)}. \tag{1.8}$$

The process of adjustment which makes the values of a harmonic function agree with the four-point influence equation at each network point may be called a process of harmonization. The most commonly used method for harmonization is that of iteration[1] in which, arbitrarily assumed or judiciously selected, initial values are successively improved until practical convergence is obtained. Another procedure which has proved effective is that of relaxation.[2] More recently harmonization in rectangular areas has been effected by a solution of a special system of difference equations.[3]

The object of this paper is to develop an analytical process of harmonization, which yields key values of the harmonic function U in rectangular figures in terms of certain simple combinations of the given boundary values. From the key values all, except two or three, of the remaining interior values can be calculated directly by the simple Liebmann formula (1.3). For two or three points (1.8) may be required. The present treatment is believed to result in simple derivations, a relatively large scope, and a material reduction in the labor required to effect a solution. The method is directly applicable to composite rectangular figures, such as angles, channels, T-figures, Z-figures, etc. The proposed process has been used in numerical cases and found to be rapid and accurate.

The rectangles treated have an arbitrary width m and length n'. The width is always represented by an integer. Specific solutions are obtained for rectangles $(3\times n')$ and $(4\times n')$ for all positive values of n' between 2 and 14. The results are summarized in tables at the end of the paper. The tables are applicable to any value of n greater than 14.

Key Values. Definition

A set of interior values of U, so located in the region R to which the function U applies that, from these values, the values of U at all other network points can be calculated by the Liebmann or four-point formulas, applied either normally or diagonally, is defined as a set of key values. In a square (3×3), Fig. 2(b), any one of the four interior values u_1, u_2, u_3, and u_4 is a key value for the whole region. Thus if u_1 be

known, u_3 can be found from the diagonal neighbors, and u_2, u_4 from the normal neighbors.

Similarly in a rectangle (4×3), Fig. 3(b), either u_1 or u_4 is a key value for the whole region. Thus if u_1 be known, u_3 and u_5 can be found from diagonal neighbors, and u_2, u_4, u_6 from normal neighbors.

A similar condition exists in a (4×4) square, Fig. 5(b), in which u_1, the value at the center of the square, defines the remaining eight interior values. In all three cases one key value is sufficient to obtain a complete numerical solution of Laplace's equation.

In rectangles $(m\times n)$, $m=3$, 4, n an integer, the number of key points k is given by

$$k=(n-2)/2, \quad n\text{-odd},$$
$$k=(n-1)/2, \quad n\text{-even}.$$

In rectangles $(m\times n')$, $n'=n+\delta$, $0\leqslant\delta\leqslant 1$,

$$k=n/2, \quad n\text{-even},$$
$$k=(n-1)/2, \quad n\text{-odd}.$$

The key points are numbered 1, 2, $3\cdots k$ and the corresponding key values are denoted by u_1, u_2, $u_3\cdots u_k$, respectively.

An interior, or unknown, value will always be denoted by u, with a suitable subscript relating it to a given point. Known boundary values will be denoted by a, b, $c\cdots$, etc.

2. KEY VALUES FOR INCOMPLETE AND FULL (3×3) RECTANGLES, FIG. 2

(a) A rectangle $3(2+\delta)$, in which δ is a fraction less than unity, will be spoken of as an incomplete (3×3) square, Fig. 2(a).

In order to find the value u_1 we use (1.6) and (1.3). Thus,

$$\left.\begin{aligned} u_1&=K_1(a_1+a_2)+K_2(a_3+u_3), &(a)\\ 4u_3&=u_1+c_1+c_2+c_3. &(b)\end{aligned}\right\}(2.1)$$

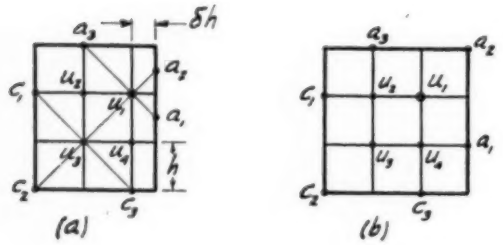

FIG. 2.

Upon solution, eliminating K_1 and K_2 by (1.7), we have

$$(8+7\delta)u_1=4(a_1+a_2)+\delta(4a_3+c_1+c_2+c_3). \quad (2.2)$$

Putting δ equal unity we obtain

$$15u_1=4\sum_{i=1}^{3}a_i+\sum_{i=1}^{3}c_i. \quad (2.3)$$

Equation (2.3) gives the key value for a full (3×3) square.

3. KEY VALUES FOR INCOMPLETE AND FULL (3×4) RECTANGLES, FIG. 3

(a) A rectangle $3(3+\delta)$, Fig. 3(a), will be spoken of as an incomplete (3×4) rectangle. Equations (1.3) and (1.6) give the key value u_1 for this case. Thus

$$\left.\begin{aligned} 4u_1&=u_3+u_5+d_1+d_2, &(a)\\ 4u_3&=u_1+a_1+b_1+c_1, &(b)\\ u_5&=K_1(a_2+b_2)+K_2(u_1+c_1). &(c)\end{aligned}\right\}(3.1)$$

Solving, and eliminating K_1 and K_2, we obtain

$$\left(\frac{15+13\delta}{1+\delta}\right)u_1=(a_1+b_1+c_1+4d_1+4d_2)$$
$$+\left(\frac{2}{1+\delta}\right)(a_2+b_2+\delta c_1). \quad (3.2)$$

Putting δ equal unity, we obtain the key value for a full rectangle (3×4), Fig. 3(b). Thus

$$14u_1=a_1+a_2+2c_1+4(d_1+d_2)+b_1+b_2. \quad (3.3)$$

By putting δ equal zero, changing the notation of the boundary values to agree with that of Fig. 2(b), and observing that when δ becomes zero $a_2=b_2=a_1$ we obtain (2.3), i.e., the key value for a full (3×3) square.

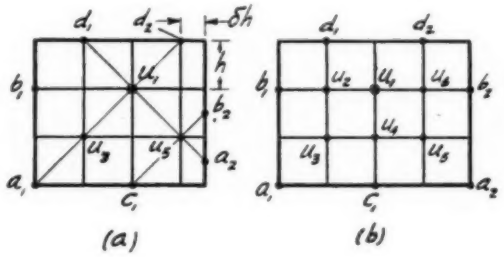

FIG. 3.

4. KEY VALUES FOR INCOMPLETE AND FULL (4×3) RECTANGLES, FIG. 4

(a) A rectangle $4(2+\delta)$, Fig. 4(a), will be spoken of as an incomplete (4×3) rectangle.

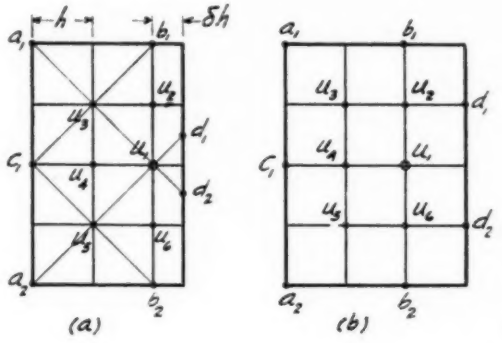

FIG. 4.

To find the key value u_1 we again use (1.6) and (1.3) and obtain the following three equations:

$$\left.\begin{aligned} u_1 &= K_1(d_1+d_2)+K_2(u_3+u_5), && \text{(a)}\\ 4u_3 &= u_1+a_1+b_1+c_1, && \text{(b)}\\ 4u_5 &= u_1+a_2+b_2+c_1. && \text{(c)} \end{aligned}\right\} \quad (4.1)$$

Upon solution we have

$$\left(\frac{4+3\delta}{\delta}\right)u_1=\frac{2}{\delta}(d_1+d_2)+\tfrac{1}{2}(a_1+a_2+b_1+b_2)+c_1. \quad (4.2)$$

(b) Putting δ equal to unity in (4.2) we obtain

$$7u_1=\tfrac{1}{2}(a_1+a_2+b_1+b_2)+2(d_1+d_2)+c_1. \quad (4.3)$$

This is the key value for a full (4×3) rectangle, Fig. 4(b), which agrees with (3.3) giving the key value for a full (3×4) rectangle at the same point.

5. KEY VALUES FOR INCOMPLETE AND FULL (4×4) SQUARE, FIG. 5

(a) A rectangle $4(3+\delta)$ will be spoken of as an incomplete (4×4) square, Fig. 5(a). There are three ways to obtain an expression for the key value u_1. The simplest procedure is to express u_1 in terms of u_2, u_3, u_4, and u_5 and then to express these quantities in terms of u_1. Using (1.3) and (1.6) we obtain the following five expressions:

$$\left.\begin{aligned} 4u_1 &= u_2+u_3+u_4+u_5, && \text{(a)}\\ 4u_3 &= u_1+a_2+c_2+c_3, && \text{(b)}\\ 4u_4 &= u_1+a_3+c_3+c_4, && \text{(c)}\\ u_2 &= K_1(a_1+c_1')+K_2(u_1+c_2), && \text{(d)}\\ u_5 &= K_1(a_4+c_1'')+K_2(u_1+c_4). && \text{(e)} \end{aligned}\right\} \quad (5.1)$$

Upon solution we have

$$\left(\frac{7+5\delta}{1+\delta}\right)u_1=\tfrac{1}{2}(a_2+a_3+c_2+2c_3+c_4)+\frac{1}{(1+\delta)}(a_1+a_4+c_1'+c_1'')+\frac{\delta}{(1+\delta)}(c_2+c_4). \quad (5.2)$$

(b) Putting δ equal unity and observing that then $c_1'=c_1''=c_1$ we obtain

$$6u_1=\tfrac{1}{2}\sum_{i=1}^{4}a_i+\sum_{i=1}^{4}c_i. \quad (5.3)$$

This gives the key value for a full (4×4) square.

(c) Equation (5.3) also yields the key value for a rectangle (4×3). Putting δ equal zero, changing the notation of the boundary values to

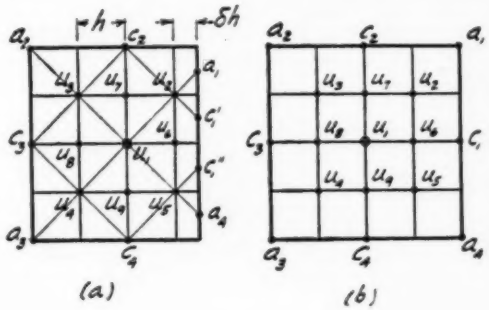

FIG. 5.

agree with that of Fig. 4(b), and observing that when $\delta=0$, $c_1'=a_1=d_1$, and $c_1''=a_4=d_2$, we obtain (4.3) for a full (4×3) rectangle.

6. LAPLACIAN PERIMETERS

In the further development of the method under consideration, extensive use is made of the key values for the basic figures treated in the preceding sections. By combining the results for the elementary rectangles, solutions are built up for longer rectangles. It is therefore convenient to simplify the forms of the expressions of the

key values already derived. Specifically we shall write each key value in the form

$$\left.\begin{aligned} &\alpha u = P + u', && \text{(a)} \\ \text{or,}\quad &\alpha u = P + u' + u'', && \text{(b)} \end{aligned}\right\} \quad (6.1)$$

in which α is a constant, P is a quantity determined by the known boundary values, and u', u, u'' are consecutive key values. The quantity P in (6.1) will, for lack of a better term, be referred to as a Laplacian perimeter or more briefly perimeter. Since we have eight basic rectangles, we shall need eight Laplacian perimeters: four for the incomplete rectangles and four for the full figures. We shall denote these perimeters by the generic symbols p and P, for the incomplete and full rectangles, respectively. As already stated, these perimeters are to contain only known boundary values. It will be seen later that, in each configuration, one or at the most two, boundary values will be characteristically missing in comparison with the full expression for the key value. Thus, incomplete and full (3×3) squares will always be used in such a manner that c_1 will be unknown, and in the full (3×4) rectangle both b_1 and b_2 or at least b_1, will be unknown. In the definitions of the eight Laplacian perimeters that follow, we are guided entirely by such considerations.

7. DEFINITIONS OF LAPLACIAN PERIMETERS

Notation: The notation $P_{m\times n}$ or $(P)_{m\times n}$ denotes a Laplacian perimeter in a rectangle $(m\times n)$.

Full rectangles—P	Incomplete rectangles—p
$P_{3\times3}$—$\bar{P}$,	$p_{3\times3}$—$\bar{p}$,
$P_{3\times4}$—P'',	$p_{3\times4}$—p'',
$P_{4\times3}$—P',	$p_{4\times3}$—p',
$P_{4\times4}$—P,	$p_{4\times4}$—p.

Definitions:

1. Incomplete (3×3) square, Fig. 2(a),

$$\bar{p} = \frac{4}{\delta}(a_1+a_2) + 4a_3 + c_2 + c_3. \quad (7.1)$$

2. Full (3×3) square, Fig. 2(b),

$$\bar{P} = 4\sum_{i=1}^{3} a_i + c_2 + c_3. \quad (7.2)$$

3. Incomplete (3×4) rectangle, Fig. 3(a),

$$p'' = a_1 + c_1 + 4(d_1+d_2) + \left(\frac{2}{1+\delta}\right)(a_2+b_2+\delta c_1). \quad (7.3)$$

4. Full (3×4) rectangle, Fig. 3(b),

$$P'' = (a_1+a_2+2c_1) + 4(d_1+d_2) + \text{known } b\text{'s}. \quad (7.4)$$

5. Incomplete (4×3) rectangle, Fig. 4(a),

$$p' = \tfrac{1}{2}(a_1+a_2+b_1+b_2) + \frac{2}{\delta}(d_1+d_2). \quad (7.5)$$

6. Full (4×3) rectangle, Fig. 4(b),

$$P' = \tfrac{1}{2}(a_1+a_2+b_1+b_2) + 2(d_1+d_2). \quad (7.6)$$

7. Incomplete (4×4) square, Fig. 5(a),

$$p = \tfrac{1}{2}(a_2+a_3+c_2+c_4) + \left(\frac{1}{1+\delta}\right)(a_1+a_4+c_1'+c_1'') + \frac{\delta(c_2+c_4)}{1+\delta}. \quad (7.7)$$

8. Full (4×4) square, Fig. 5(b),

$$P = \tfrac{1}{2}\sum_{i=1}^{4} a_i + \sum \text{known } c\text{'s}. \quad (7.8)$$

8. RELATION BETWEEN $P_{m\times n}$ AND $P_{m\times n'}$

(a) In all figures treated in this paper there are as many Laplacian perimeters as there are key points, or key values.

(b) The numeral subscript in the perimeter refers to the key point of the same number. Thus P_i refers to key point (i) of a key value u_i.

(c) The notation $(P_i)_{m\times n}$ denotes a perimeter at a point (i) in a rectangle $(m\times n)$.

(d) When the length of a rectangular figure is increased by λ, only the last perimeter P_k in the rectangle $(4\times n)$ changes. In rectangles $(3\times n)$ and $(4\times n)$ the relation between the old and

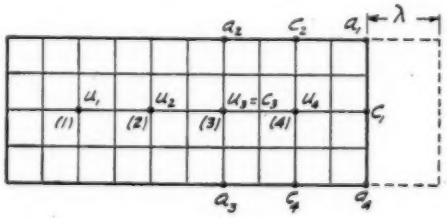

FIG. 6.

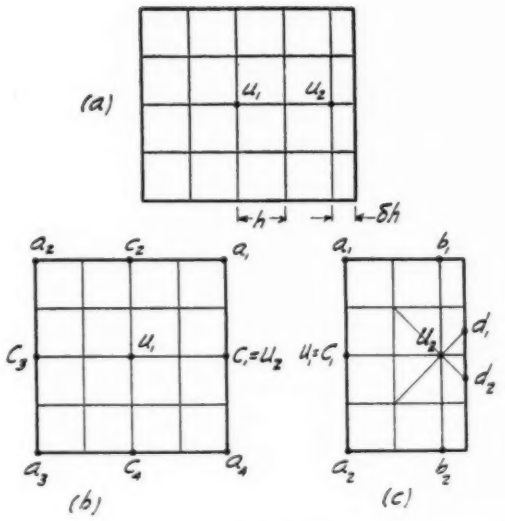

FIG. 7.

new perimeters is

$$(P_k)_{m\times n}=(P_k)_{m\times n'}+u_{k+1}, \qquad (8.1)$$

k referring to the figure $(m\times n)$.

Consider for concreteness the rectangle (4×10), Fig. 6. In the last square having its center at point (4), the Laplacian perimeter $(P_4)_{4\times 10}$ is by definition, (7.8),

$$(P_4)_{4\times 10}=\tfrac{1}{2}\sum_{i=1}^{4} a_i+c_1+c_2+c_4,$$

since $c_3=u_3$ is unknown. If the length $n=10$ is increased by λ

$$(P_4)_{4(10+\lambda)}=\tfrac{1}{2}\sum_{i=1}^{4} a_i+c_2+c_4,$$

since now both $c_1=u_5$, as well as $c_3=u_3$, are unknown, so that

$$(P_4)_{4\times 10}=(P_4)_{4(10+\lambda)}+u_5.$$

We note, however, that P_1, P_2, and P_3 remain unchanged, or in general

$$(P_i)_{m\times n}=(P_i)_{m\times n'}, \quad \text{for} \quad i<k. \qquad (8.2)$$

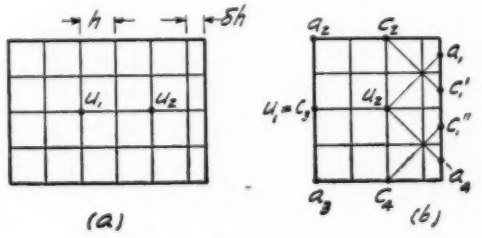

FIG. 8.

9. BASIC KEY VALUES IN TERMS OF P AND p

1. Incomplete (3×3) square, Fig. 2(a). Eq. (2.2) becomes

$$\left.\begin{aligned} \bar{\alpha}u_1&=\bar{p}+c_1, && \text{(a)}\\ \bar{\alpha}&=(8+7\delta)/\delta. && \text{(b)}\end{aligned}\right\} \qquad (9.1)$$

2. Full (3×3) square, Fig. 2(b). Eq. (2.3) becomes

$$15u_1=\bar{P}+c_1. \qquad (9.2)$$

3. Incomplete (3×4) rectangle, Fig. 3(a). Eq. (3.2) becomes

$$\left.\begin{aligned} \alpha''u_1&=p''+b_1, && \text{(a)}\\ \alpha''&=(15+13\delta)/(1+\delta). && \text{(b)}\end{aligned}\right\} \qquad (9.3)$$

4. Full (3×4) rectangle, Fig. 3(b). Eq. (3.3) becomes

$$14u_1=P''+\sum \text{unknown } b\text{'s}. \qquad (9.4)$$

5. Incomplete (4×3) rectangle, Fig. 4(a). Eq. (4.2) becomes

$$\left.\begin{aligned} \alpha'u&=p'+c_1, && \text{(a)}\\ \alpha'&=(4+3\delta)/\delta. && \text{(b)}\end{aligned}\right\} \qquad (9.5)$$

6. Full (4×3) rectangle, Fig. 4(b). Eq. (4.3) becomes

$$7u_1=P'+c_1. \qquad (9.6)$$

7. Incomplete (4×4) square, Fig. 5(a). Eq. (5.2) becomes

$$\left.\begin{aligned} \alpha u_1&=p+c_3, && \text{(a)}\\ \alpha&=(7+5\delta)/(1+\delta). && \text{(b)}\end{aligned}\right\} \qquad (9.7)$$

8. Full (4×4) square, Fig. 5(b). Eq. (5.3) becomes

$$6u_1=P+\sum \text{unknown } c\text{'s}. \qquad (9.8)$$

10. GENERAL METHOD

By combining the solutions for the values of U for the basic cases it is now possible to obtain *continuous* solutions for the key values in rectangles $(m\times n')$, where n' is any positive number greater than 2 and $m=3, 4$.

The general method rests on the following simple proposition: If a solution for the last key value u_k is available for a rectangle $(m\times n)$, n any positive integer, it is possible to extend this solution to u_{k+1} in rectangles $m(n+\delta)$, or $m(n+1+\delta)$. The range of δ is $0\leqslant\delta\leqslant 1$. As a matter of convenience it is best to start with n equal to an even positive integer.

Any rectangle $(m\times n')$ may be viewed as a rectangle $(m\times n)$, n the nearest even integer, overlapped by an incomplete $(m\times 3)$ or $(m\times 4)$. Thus, a rectangle $4(6+\delta)$ may be looked upon as a (4×6) overlapped by an incomplete (4×3), and a rectangle $4(7+\delta)$ may similarly be viewed as a (4×6) overlapped by an incomplete (4×4), Figs. 7 and 8. Now, in the rectangle $(m\times n)$ the last key value u_k may be written as

$$u_k = C_1P_1 + C_2P_2 + \cdots C_kP_k \qquad (10.1)$$

in which the C's are constant coefficients and the P's are perimeters for the rectangle $(m\times n)$. Remembering the relation between $P_{m\times n}$ and $P_{m\times n'}$, (8.1, 8.2) we have

$$u_k = C_1P_1 + C_2P_2 + \cdots C_kP_k + C_ku_{k+1}, \qquad (10.2)$$

in which the C's are the same as (10.1) but the P's now refer to the rectangle $(m\times n')$. Also from the incomplete rectangles $(m\times 3)$ or $(m\times 4)$, Section 9, we have

$$\alpha u_{k+1} = p_{k+1} + u_k. \qquad (10.3)$$

Solving (10.2) and (10.3) we obtain

$$u_{k+1} = (\alpha - C_k)^{-1}(C_1P_1 + C_2P_2 + \cdots C_kP_k) + (\alpha - C_k)^{-1}p_{k+1}. \qquad (10.4)$$

We thus have a general relation between the coefficients for the last key value u_k in the rectangle $(m\times n)$ and the coefficients for the next key value u_{k+1} in the rectangle $m(n+\delta)$, or $m(n+1+\delta)$. Specifically

$$\left.\begin{aligned} C_{k+1} &= (\alpha - C_k)^{-1}, \qquad \text{(a)} \\ \text{and for all other coefficients} & \\ (C_i)_{m\times n'} &= (C_i)_{m\times n}(\alpha - C_k)^{-1}. \qquad \text{(b)} \end{aligned}\right\} (10.5)$$

In using these formulas, it must be remembered that there are four α's, which depend on whether $m=3$ or $m=4$, and on whether n' differs from n by less than unity or by more than unity. Thus, for rectangles $4(n+1+\delta)$ and $4(n+\delta)$ we use α and α', respectively, which are given by (9.7b) and (9.5b). Similarly for rectangles $3(n+1+\delta)$ and $3(n+\delta)$ we use α'' and $\bar{\alpha}$, respectively, given by (9.3b) and (9.1b).

The determination of u_{k+1} reduces the rectangle $(m\times n')$ to that of a rectangle $(m\times n)$ for which a solution for all key values is assumed to be known.

Hence, starting with the expressions for the key value u_1 in a (4×4) square, (9.8), one can successively write down the formulas for the last key values in all subsequent rectangles $(4\times n')$. Similarly, starting with the expression for u_1 in the rectangle (3×4), (9.4), we can write the formulas for all rectangles $(3\times n')$.

11. SUCCESSIVE FACTORS $(\alpha - C_k)^{-1}$

For brevity we simplify our notation and write

$$(\alpha - C_k)_i^{-1} = F_i, \qquad (11.1)$$

and

$$(F, C, \alpha)_{m(n+\delta)} = (F, C, \alpha)_{n+\delta}. \qquad (11.2)$$

We then have

$$F_{4+\delta} = (C_2)_{4+\delta} = [\alpha_{2+\delta} - (C_1)_4]^{-1}, \qquad (11.3)$$

$$F_{5+\delta} = (C_2)_{5+\delta} = [\alpha_{3+\delta} - (C_1)_4]^{-1}, \qquad (11.4)$$

$$F_{6+\delta} = (C_3)_{6+\delta} = [\alpha_{2+\delta} - (C_2)_6]^{-1} = (\alpha_{2+\delta} - F_6)^{-1}, \qquad (11.5)$$

$$F_{7+\delta} = (C_3)_{7+\delta} = [\alpha_{3+\delta} - (C_2)_6]^{-1} = (\alpha_{3+\delta} - F_6)^{-1}, \qquad (11.6)$$

$$F_{8+\delta} = (C_3)_{8+\delta} = [\alpha_{2+\delta} - (C_3)_8]^{-1} = (\alpha_{2+\delta} - F_8)^{-1}. \qquad (11.7)$$

In general, for n an even integer

$$\left.\begin{aligned} F_{n+\delta} &= (\alpha_{2+\delta} - F_n)^{-1}, \qquad \text{(a)} \\ F_{n+1+\delta} &= (\alpha_{3+\delta} - F_n)^{-1}. \qquad \text{(b)} \end{aligned}\right\} (11.8)$$

For example, to find $F_{4(5+\delta)}$ we write

$$F_{4(5+\delta)} = (\alpha_{4(3+\delta)} - F_{4\times 4})^{-1} = [\alpha_{4(3+\delta)} - (C_1)_{4\times 4}]^{-1}. \qquad (11.3)$$

Substituting

$$\alpha_{4(3+\delta)} = (7+5\delta)/(1+\delta), \qquad (9.7b)$$

and

$$(C_1)_{4\times 4} = \tfrac{1}{6}, \qquad (9.8)$$

we have

$$F_{4(5+\delta)} = (41+29\delta)/(1+\delta)6. \qquad (11.9)$$

We can now write down the expression for $(u_2)_{4(5+\delta)}$. Thus by (10.4)

$$(u_2)_{4(5+\delta)} = F_{4(5+\delta)}(C_1)_{4\times 4}P_1 + F_{4(5+\delta)}p_2. \qquad (11.10)$$

Calculating several values of F it is found that these factors converge rapidly, and that

TABLE I.

n'	C_1	C_2	C_3	C_4	C_5	C_6	C_7
$4+\delta$	$(C_1)_4F_{4+\delta}$	$F_{4+\delta}$					
$5+\delta$	$(C_1)_4F_{5+\delta}$	$F_{5+\delta}$					
$6+\delta$	$(C_1)_4F_6F_{6+\delta}$	$F_6F_{6+\delta}$	$F_{6+\delta}$				
$7+\delta$	$(C_1)_4F_6F_{7+\delta}$	$F_6F_{7+\delta}$	$F_{7+\delta}$				
$8+\delta$	$(C_1)_4F_6F_8F_{8+\delta}$	$F_6F_8F_{8+\delta}$	$F_8F_{8+\delta}$	$F_{8+\delta}$			
$9+\delta$	$(C_1)_4F_6F_8F_{9+\delta}$	$F_6F_8F_{9+\delta}$	$F_8F_{9+\delta}$	$F_{9+\delta}$			
$10+\delta$	$(C_1)_4F_6F_8F_{10}F_{10+\delta}$	$F_6F_8F_{10}F_{10+\delta}$	$F_8F_{10}F_{10+\delta}$	$F_{10}F_{10+\delta}$	$F_{10+\delta}$		
$11+\delta$	$(C_1)_4F_6F_8F_{10}F_{11+\delta}$	$F_6F_8F_{10}F_{11+\delta}$	$F_8F_{10}F_{11+\delta}$	$F_{10}F_{11+\delta}$	$F_{11+\delta}$		
$12+\delta$	$(C_1)_4F_6F_8F_{10}F_{12}F_{12+\delta}$	$F_6F_8F_{10}F_{12}F_{12+\delta}$	$F_8F_{10}F_{12}F_{12+\delta}$	$F_{10}F_{12}F_{12+\delta}$	$F_{12}F_{12+\delta}$	$F_{12+\delta}$	
$13+\delta$	$(C_1)_4F_6F_8F_{10}F_{12}F_{13+\delta}$	$F_6F_8F_{10}F_{12}F_{13+\delta}$	$F_8F_{10}F_{12}F_{13+\delta}$	$F_{10}F_{12}F_{13+\delta}$	$F_{12}F_{13+\delta}$	$F_{13+\delta}$	
$14+\delta$	$(C_1)_4F_6F_8F_{10}F_{12}F_{14}F_{14+\delta}$	$F_6F_8F_{10}F_{12}F_{14}F_{14+\delta}$	$F_8F_{10}F_{12}F_{14}F_{14+\delta}$	$F_{10}F_{12}F_{14}F_{14+\delta}$	$F_{12}F_{14}F_{14+\delta}$	$F_{14}F_{14+\delta}$	$F_{14+\delta}$
$15+\delta$	$(C_1)_4F_6F_8F_{10}F_{12}F_{14}F_{15+\delta}$	$F_6F_8F_{10}F_{12}F_{14}F_{15+\delta}$	$F_8F_{10}F_{12}F_{14}F_{15+\delta}$	$F_{10}F_{12}F_{14}F_{15+\delta}$	$F_{12}F_{14}F_{15+\delta}$	$F_{14}F_{15+\delta}$	$F_{15+\delta}$

they become essentially constant at $n=6$ when $m=4$, and at $n=4$ when $m=3$. Thus, to five decimal places,

$$\left.\begin{aligned} F_{4(n+\delta)} &= F_{4(7+\delta)}, \quad n \text{ odd}; \quad \text{(a)} \\ F_{4(n+\delta)} &= F_{4(8+\delta)}, \quad n \text{ even}; \quad \text{(b)} \\ F_{3(n+\delta)} &= F_{3(5+\delta)}, \quad n \text{ odd}; \quad \text{(c)} \\ F_{3(n+\delta)} &= F_{3(6+\delta)}, \quad n \text{ even}. \quad \text{(d)} \end{aligned}\right\} \tag{11.11}$$

It is easy to verify (11.11) for integral values of n, i.e., $\delta=0$. For example

$$F_{4\times 15}-F_{4\times 7}=.0000031,$$
$$F_{4\times 16}-F_{4\times 8}=.0000042,$$
$$F_{3\times 15}-F_{3\times 5}=.00000165,$$
$$F_{3\times 16}-F_{3\times 6}=.00000189.$$

But by (11.8) for n an even or odd integer

$$F_{n+2+\delta}-F_{n+\delta}=(\alpha-F_{n+2})^{-1}-(\alpha-F_n)^{-1}.$$

Since the α's are the same, and for integral values of n, $F_{n+2}=F_n$, for $n>6$, $m=4$, and $n>4$, $m=3$ it follows that the relations given in (11.11) are correct to five decimal places.

12. TABLE OF MASTER COEFFICIENTS FOR THE LAST KEY VALUE u_{k+1}

From (10.5) it is possible to write down all coefficients from C_1 to C_{k+1} for the last key value in all rectangles $(m\times n')$. Thus using the abridged notation from the preceding section and the general relation

$$(C_i)_{n'}=(C_i)_nF_{n'}, \tag{10.5b}$$

we have

$$\left.\begin{aligned} (C_1)_{4+\delta} &= (C_1)_4F_{4+\delta}, \quad \text{(a)} \\ (C_1)_{5+\delta} &= (C_1)_4F_{5+\delta}, \quad \text{(b)} \\ (C_1)_{6+\delta} &= (C_1)_6F_{6+\delta}=(C_1)_4F_6F_{6+\delta}, \quad \text{(c)} \\ (C_1)_{7+\delta} &= (C_1)_6F_{7+\delta}=(C_1)_4F_6F_{7+\delta}, \text{ etc.} \quad \text{(d)} \end{aligned}\right\} \tag{12.1}$$

Similarly,

$$\left.\begin{aligned} (C_2)_{4+\delta} &= F_{4+\delta}, \quad \text{(a)} \\ (C_2)_{5+\delta} &= F_{5+\delta}, \quad \text{(b)} \\ (C_2)_{6+\delta} &= (C_2)_6F_{6+\delta}=F_6F_{6+\delta}, \quad \text{(c)} \\ (C_2)_{7+\delta} &= (C_2)_6F_{7+\delta}=F_6F_{7+\delta}, \quad \text{etc.} \quad \text{(d)} \end{aligned}\right\} \tag{12.2}$$

A summary of all coefficients for the last key value in rectangle $(m\times n')$, $m=3,\ 4,\ 4\leqslant n\leqslant 16$ is given in Table I. Hereafter the last key value will be denoted by u_k in all rectangles.

13. GENERAL RELATIONS BETWEEN THE COEFFICIENTS IN TABLE I

Inspection of Table I shows three important relations between the coefficients for the last key value.

(a) For any fixed value n'

$$\begin{aligned} &(C_1)_{n'}=(C_1)_4F_6F_8F_{10}\cdots F_{n'}; \quad C_2=C_1/(C_1)_4; \\ &C_3=C_2/F_6; \quad C_4=C_3/F_8; \\ &C_i=C_{i-1}/F_{2i}; \quad C_k=F_{n'}. \end{aligned} \tag{13.1}$$

(b) The last four coefficients C_k, C_{k-1}, C_{k-2}, C_{k-3} become constant for all even values of n, and for all odd values of n, at $n\geqslant 12$. Thus in rectangles $m(n+\delta)$ for n even,

$$C_k = F_{n+\delta}; \quad C_{k-1} = F_n F_{n+\delta};$$
$$C_{k-2} = F_{n-2} F_n F_{n+\delta}, \quad C_{k-3} = F_{n-4} F_{n-2} F_n F_{n+\delta}. \tag{13.2}$$

For n odd,

$$C_k = F_{n+\delta}; \quad C_{k-1} = F_{n-1} F_{n+\delta};$$
$$C_{k-2} = F_{n-3} F_{n-1} F_{n+\delta}; \tag{13.3}$$
$$C_{k-3} = F_{n-5} F_{n-3} F_{n-1} F_{n+\delta}.$$

Introducing the approximations of (11.1) we have for n even,

$$C_k = F_{8+\delta}; \quad C_{k-1} = F_8 F_{8+\delta};$$
$$C_{k-2} = F_8^2 F_{8+\delta}; \quad C_{k-3} = F_8^3 F_{8+\delta}. \tag{13.4}$$

For n odd,

$$C_k = F_{7+\delta}; \quad C_{k-1} = F_8 F_{7+\delta};$$
$$C_{k-2} = F_8^2 F_{7+\delta}; \quad C_{k-3} = F_8^3 F_{7+\delta}. \tag{13.5}$$

(c) For n greater than six, assuming $F_8 = F_{10} = F_{12}$, etc.

$$(C_i)_{n'+2} = (C_i)_{n'} F_8. \tag{13.6}$$

14. MAIN TABLES AND THEIR USE

From the expressions given in Table I, and the simplifications for F made in Section 11, it is possible to calculate the coefficients $C_1, C_2 \cdots C_k$ for the 1st key value in a rectangle of arbitrary length n'. Such calculations were made for $m(n+\delta)$, $m = 3, 4$; $n = 2, 3, 4, 5, 6 \cdots 13$, and $\delta = .1, .2, .3 \cdots .8, .9, 1.0$. The results are given in Tables II and III.

These tables are sufficient to determine all key values in rectangles $(m \times n')$, for values of n' between 2 and infinity. The procedure is as follows.

First we calculate the last key value u_k using the appropriate coefficients in the tables. We can then treat the rectangle as if it were shorter and its length n was an even integer. Next we find u_{k-1} and then view the rectangle as if it were further shortened by 2 units. We thus can find u_{k-2}, u_{k-3}, etc. and continue the process until all key values are found.

It should be observed that in calculating u_{k-1} the last perimeter P_{k-1} must be modified by the addition of u_k. In general, in calculating u_i we add u_{i+1} to P_i. Thus

$$u_i = C_1 P_1 + C_2 P_2 + \cdots C_i (P_i + u_{i+1}). \tag{14.1}$$

TABLE II. $3(n+\delta)$.

u_k	n ↓	$\delta \rightarrow$	.1	.2	.3	.4	.5	.6	.7	.8	.9	1.0
u_1	2	C_1	.01149	.02128	.02970	.03704	.04348	.04918	.05426	.05882	.06294	.06667
u_1	3	C_1	.06748	.06818	.06878	.06931	.06977	.07018	.07054	.07087	.07116	.07143
u_2	4	C_1	.00082	.00152	.00213	.00265	.00312	.00353	.00389	.00422	.00452	.00478
		C_2	.01150	.02131	.02977	.03714	.04361	.04935	.05447	.05907	.06322	.06699
u_2	5	C_1	.00484	.00490	.00494	.00498	.00501	.00504	.00506	.00509	.00511	.00513
		C_2	.06781	.06852	.06912	.06965	.07012	.07053	.07090	.07123	.07152	.07179
u_3	6	C_1	.00006	.00011	.00015	.00019	.00022	.00025	.00028	.00030	.00032	.00034
		C_2	.00083	.00153	.00214	.00267	.00313	.00354	.00391	.00424	.00454	.00481
		C_3	.01150	.02131	.02977	.03714	.04361	.04935	.05448	.05907	.06322	.06699
u_3	7	C_1	.00035	.00035	.00035	.00036	.00036	.00036	.00036	.00037	.00037	.00037
		C_2	.00487	.00492	.00496	.00500	.00503	.00506	.00509	.00511	.00514	.00515
		C_3	.06781	.06852	.06912	.06965	.07012	.07053	.07090	.07123	.07153	.07180
u_4	8	C_1	.00000	.00001	.00001	.00001	.00002	.00002	.00002	.00002	.00002	.00002
		C_2	.00006	.00011	.00015	.00019	.00022	.00025	.00028	.00030	.00033	.00035
		C_3	.00083	.00153	.00214	.00267	.00313	.00354	.00391	.00424	.00454	.00481
		C_4	.01150	.02131	.02977	.03714	.04361	.04935	.05448	.05907	.06322	.06699
u_4	9	C_1	.00002	.00003	.00003	.00003	.00003	.00003	.00003	.00003	.00003	.00003
		C_2	.00035	.00035	.00035	.00036	.00036	.00036	.00036	.00037	.00037	.00037
		C_3	.00487	.00492	.00496	.00500	.00503	.00506	.00509	.00511	.00514	.00515
		C_4	.06781	.06852	.06912	.06965	.07012	.07053	.07090	.07123	.07153	.07180

TABLE III. $4(n+\delta)$.

u	n ↓	$\delta\rightarrow$	.1	.2	.3	.4	.5	.6	.7	.8	.9	1.0
u_1	2	C_1	.02326	.04348	.06122	.07692	.09091	.10345	.11475	.12500	.13433	.14286
u_1	3	C_1	.14667	.15000	.15294	.15556	.15789	.16000	.16190	.16364	.16522	.16667
u_2	4	C_1	.00389	.00730	.01031	.01299	.01538	.01754	.01950	.02128	.02290	.02439
		C_2	.02335	.04380	.06186	.07792	.09231	.10526	.11699	.12766	.13740	.14634
u_2	5	C_1	.02506	.02564	.02616	.02662	.02703	.02740	.02773	.02804	.02832	.02857
		C_2	.15034	.15385	.15694	.15970	.16216	.16438	.16639	.16822	.16990	.17143
u_3	6	C_1	.00067	.00125	.00177	.00223	.00264	.00301	.00334	.00365	.00393	.00418
		C_2	.00400	.00751	.01061	.01336	.01583	.01805	.02007	.02190	.02357	.02510
		C_3	.02335	.04380	.06187	.07795	.09235	.10532	.11706	.12774	.13749	.14644
u_3	7	C_1	.00430	.00440	.00449	.00457	.00464	.00470	.00476	.00481	.00486	.00490
		C_2	.02579	.02639	.02692	.02740	.02782	.02820	.02855	.02886	.02915	.02941
		C_3	.15045	.15396	.15706	.15982	.16229	.16451	.16653	.16836	.17003	.17157
u_4	8	C_1	.00011	.00021	.00030	.00038	.00045	.00052	.00057	.00063	.00067	.00072
		C_2	.00069	.00129	.00182	.00229	.00272	.00310	.00344	.00376	.00404	.00431
		C_3	.00401	.00752	.01062	.01337	.01584	.01807	.02008	.02192	.02359	.02513
		C_4	.02335	.04381	.06187	.07795	.09235	.10532	.11706	.12774	.13750	.14645
u_4	9	C_1	.00074	.00075	.00077	.00078	.00080	.00081	.00082	.00083	.00083	.00084
		C_2	.00443	.00453	.00462	.00470	.00477	.00484	.00490	.00495	.00500	.00505
		C_3	.02581	.02642	.02695	.02742	.02784	.02823	.02857	.02889	.02917	.02944
		C_4	.15045	.15396	.15706	.15982	.16229	.16452	.16653	.16836	.17004	.17157
u_5	10	C_1	.00002	.00004	.00005	.00007	.00008	.00009	.00010	.00011	.00012	.00012
		C_2	.00012	.00022	.00031	.00039	.00047	.00053	.00059	.00064	.00069	.00074
		C_3	.00069	.00129	.00182	.00229	.00272	.00310	.00345	.00376	.00405	.00431
		C_4	.00401	.00752	.01062	.01337	.01584	.01807	.02008	.02192	.02359	.02513
		C_5	.02335	.04381	.06187	.07795	.09235	.10532	.11706	.12774	.13750	.14645
u_5	11	C_1	.00013	.00013	.00013	.00013	.00014	.00014	.00014	.00014	.00014	.00014
		C_2	.00076	.00078	.00079	.00081	.00082	.00083	.00084	.00085	.00086	.00087
		C_3	.00443	.00453	.00462	.00470	.00478	.00484	.00490	.00496	.00501	.00505
		C_4	.02581	.02642	.02695	.02742	.02784	.02823	.02857	.02889	.02917	.02944
		C_5	.15045	.15396	.15706	.15982	.16229	.16452	.16653	.16836	.17004	.17157
u_6	12	C_1	.00000	.00001	.00001	.00001	.00001	.00002	.00002	.00002	.00002	.00002
		C_2	.00002	.00004	.00005	.00007	.00008	.00009	.00010	.00011	.00012	.00013
		C_3	.00012	.00022	.00031	.00039	.00047	.00053	.00059	.00065	.00069	.00074
		C_4	.00069	.00129	.00182	.00229	.00272	.00310	.00345	.00376	.00405	.00431
		C_5	.00401	.00752	.01062	.01337	.01584	.01807	.02008	.02192	.02359	.02513
		C_6	.02335	.04381	.06187	.07795	.09235	.10532	.11706	.12774	.13750	.14645
u_6	13	C_1	.00002	.00002	.00002	.00002	.00002	.00002	.00002	.00002	.00002	.00002
		C_2	.00013	.00013	.00013	.00014	.00014	.00014	.00014	.00015	.00015	.00015
		C_3	.00076	.00078	.00079	.00081	.00082	.00083	.00084	.00085	.00086	.00087
		C_4	.00443	.00453	.00462	.00470	.00478	.00484	.00490	.00496	.00501	.00505
		C_5	.02581	.02642	.02695	.02742	.02784	.02823	.02857	.02889	.02917	.02944
		C_6	.15045	.15396	.15706	.15982	.16229	.16452	.16653	.16836	.17004	.17157

Inspection of Tables II and III shows that the coefficients for u_k rapidly approach convergence. In rectangles $(3\times n')$, Table II, convergence is reached at $n=9$. For values of n greater than 9, C_k, C_{k-1}, C_{k-2}, C_{k-3} are the same as C_4, C_3, C_2, and C_1, respectively, at $n=9$ or $n=8$ depending on whether n is odd or even.

In rectangles $(4\times n')$ convergence is reached at $n=13$. The coefficients for values of δ other than those given in Tables II and III can be found by interpolation.

15. AUXILIARY TABLES

It is sometimes desirable to be able to find directly a value of $u_i \mp u_k$ without having to find first u_k, $u_{k-1}\cdots u_{i+1}$. This is especially useful in very long rectangles. This can be done by means of Tables IV and V, which give the coefficients

for any $u_i \neq u_k$ independent of all other key values. Tables IV and V are for regular rectangles, with integral lengths. If the length is not an integer it is necessary first to find u_k.

Another advantage of Tables IV and V lies in the fact that all key values are given in terms of the one set of P's calculated for the rectangle $(m \times n)$, and no modification of these are needed.

Inspection of Tables IV and V shows that when n equals 14 the coefficients have become stabilized and that these coefficients may be used for all subsequent values of n. Specifically, for any integral value of n greater than 14.

(a) The coefficients of u_1, u_2, and u_3 are the same as of u_1, u_2, and u_3 for $n=14$.

(b) For n even, the coefficients C_{k-1}, C_{k-2}, etc. of u_{k-1} and u_{k-2} are the same as of u_5 and u_4, respectively, at $n=14$. For n odd, the corresponding coefficients are the same as of u_5 and u_4, respectively, at $n=13$.

(c) The coefficients of u_i, $(3<i<k-2)$, are constant, and essentially the same as for u_3 in $n=14$. Thus, to four decimal places, n odd or even,

$$\left.\begin{aligned}(u_i)_{3\times n} &= .0722P_i + .0052(P_{i-1}+P_{i+1}) \\ &\quad + .0004(P_{i-2}+P_{i+2}), \quad \text{(a)} \\ (u_i)_{4\times n} &= .1768P_i + .0303(P_{i-1}+P_{i+1}) \\ &\quad + .0052(P_{i-2}+P_{i+2}) \\ &\quad + .0009(P_{i-3}+P_{i+3}), \quad \text{(b)}\end{aligned}\right\} \quad (15.1)$$

since the last perimeter in (15.1) is $P_{i\pm3}$ it follows that u_i is affected by a relatively small length of immediately adjacent boundaries. If we limit the accuracy of the coefficient to four

TABLE IV. $(3\times n)$.

n	u	C_1	C_2	C_3	C_4	C_5	C_6
5	u_1	.07177	.00478				
6	u_1	.07179	.00513				
7	u_1	.07180	.00515	.00034			
	u_2	.00515	.07214	.00481			
8	u_1	.07180	.00515	.00037			
	u_2	.00515	.07216	.00515			
9	u_1	.07180	.00515	.00037	.00002		
	u_2	.00515	.07217	.00518	.00035		
	u_3	.00037	.00518	.07214	.00481		
10	u_1	.07180	.00515	.00037	.00003		
	u_2	.00515	.07217	.00518	.00037		
	u_3	.00037	.00518	.07217	.00515		
11	u_1	.07180	.00515	.00037	.00003	.00000	
	u_2	.00515	.07217	.00518	.00037	.00002	
	u_3	.00037	.00518	.07217	.00518	.00035	
	u_4	.00003	.00037	.00518	.07214	.00481	
12	u_1	.07180	.00515	.00037	.00003	.00000	
	u_2	.00515	.07217	.00518	.00037	.00003	
	u_3	.00037	.00518	.07217	.00518	.00037	
	u_4	.00003	.00037	.00518	.07217	.00515	
13	u_1	.07180	.00515	.00037	.00003	.00000	.00000
	u_2	.00515	.07217	.00518	.00037	.00003	.00000
	u_3	.00037	.00518	.07217	.00518	.00037	.00002
	u_4	.00003	.00037	.00518	.07217	.00518	.00035
	u_5	.00000	.00003	.00037	.00518	.07214	.00481
14	u_1	.07180	.00515	.00037	.00003	.00000	.00000
	u_2	.00515	.07217	.00518	.00037	.00003	.00000
	u_3	.00037	.00518	.07217	.00518	.00037	.00003
	u_4	.00003	.00037	.00518	.07217	.00518	.00037
	u_5	.00000	.00003	.00037	.00518	.07217	.00515

TABLE V. $(4\times n)$.

n	u	C_1	C_2	C_3	C_4	C_5	C_6
5	u_1	.17073	.02439				
6	u_1	.17143	.02857				
7	u_1	.17155	.02929	.00418			
	u_2	.02029	.17573	.02510			
8	u_1	.17157	.02941	.00490			
	u_2	.02941	.17647	.02941			
9	u_1	.17157	.02943	.00503	.00072		
	u_2	.02943	.17660	.03015	.00431		
	u_3	.00503	.03015	.17588	.02513		
10	u_1	.17157	.02944	.00505	.00084		
	u_2	.02944	.17662	.03028	.00505		
	u_3	.00505	.03028	.17662	.02944		
11	u_1	.17157	.02944	.00505	.00086	.00012	
	u_2	.02944	.17662	.03030	.00517	.00074	
	u_3	.00505	.03030	.17675	.03018	.00431	
	u_4	.00086	.00517	.03018	.17588	.02513	
12	u_1	.17157	.02944	.00505	.00087	.00014	
	u_2	.02944	.17662	.03030	.00519	.00087	
	u_3	.00505	.03030	.17677	.03030	.00505	
	u_4	.00087	.00519	.03030	.17662	.02944	
13	u_1	.17157	.02944	.00505	.00087	.00015	.00002
	u_2	.02944	.17662	.03030	.00519	.00089	.00013
	u_3	.00505	.03030	.17677	.03032	.00518	.00074
	u_4	.00087	.00520	.03032	.17675	.03018	.00431
	u_5	.00015	.00089	.00518	.03018	.17589	.02513
14	u_1	.17157	.02944	.00505	.00087	.00015	.00002
	u_2	.02944	.17662	.03030	.00520	.00089	.00015
	u_3	.00505	.03030	.17677	.03033	.00520	.00087
	u_4	.00087	.00520	.03033	.17677	.03030	.00505
	u_5	.00015	.00089	.00520	.03030	.17662	.02944

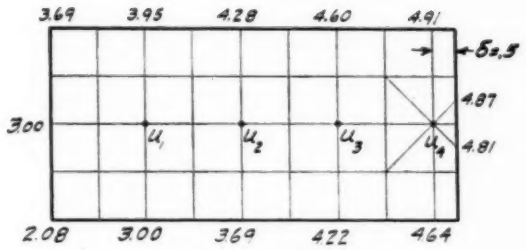

FIG. 9.

decimal places it is seen that in rectangles $(4\times n)$ the length of the influencing boundary does not extend beyond six lattice units measured from point (i) in either direction. In rectangles $(3\times n)$ the corresponding length is only four lattice units. These facts are useful in approximate solutions.

16. NUMERICAL EXAMPLE

Given a rectangle 4×8.5 with boundary values as shown in Fig. 9. Required to find all key values. Solution:

(a) We begin by calculating P_1, P_2, P_3, and p_4. The necessary Eqs. are (7.8) and (7.6). Thus

$$P_1=.5(4.28+3.69+2.08+3.69)+3.95+3.00+3.00=16.82,$$
$$P_2=.5(4.60+3.95+3.00+4.22)+4.28+3.69=15.86,$$
$$P_3=.5(4.91+4.28+3.69+4.64)+4.60+4.22=17.58,$$
$$p_4=.5(4.60+4.22+4.91+4.64)+4(4.87+4.81)=47.91.$$

We next find $u_k=u_4$. From Table III we have

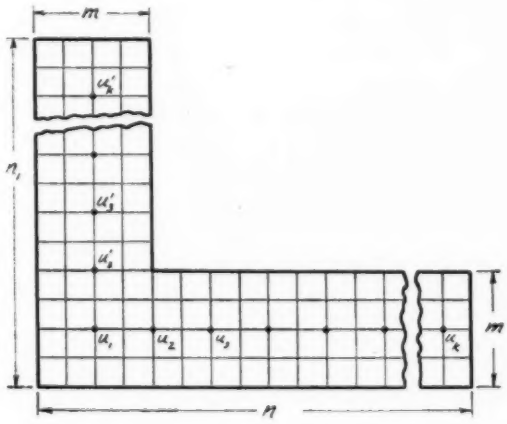

FIG. 10.

$$u_4=.00045P_1+.00272P_2+.01584P_3+.09235p_4=4.754.$$

We now view the rectangle as a (4×8) and find u_3. Thus

$$u_3=.00490P_1+.02941P_2+.17157(P_3+u_4)=4.381.$$

Considering the remaining figure as a (4×6) we have

$$u_2=.02857P_1+.17143(P_2+u_3)=3.950.$$

Lastly

$$u_1=.16667(P_1+u_2)=3.462.$$

(b) Alternate procedure for u_1 and u_2. After finding u_4 and u_3, we take coefficients from Table IV and write

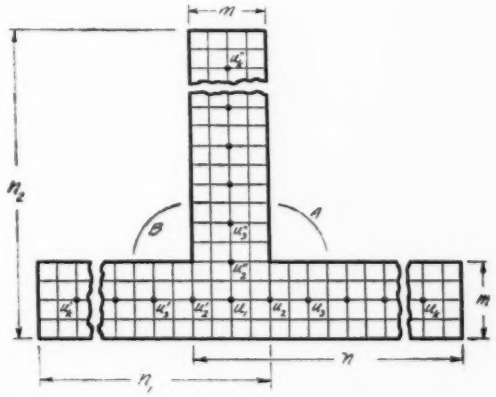

FIG. 11.

$$u_2=.02941P_1+.17647P_2+.02941(P_3+u_3)=3.939,$$
$$u_1=.17155P_1+.02941P_2+.00490(P_3+u_3)=3.460.$$

The exact values of u_4, u_3, u_2, and u_1 are 4.7536, 4.3820, 3.9512, 3.4657, which differ but slightly from those given by our method. From the key values all remaining values can be calculated by the Liebmann formula.

17. COMPOSITE RECTANGULAR AREAS

(a) Angles. The proposed method and tables are applicable to composite rectangular areas. Consider the angle of Fig. 10. This configuration may be viewed as the composite of two rectangles $(m\times n)$ and $(m\times n_1)$. The key values

$u_1, u_2 \cdots u_k$ in rectangle $(m \times n)$ could be found by means of the coefficients in the tables if u_2' were known. Similarly $u_1, u_2' \cdots u_k'$ in the rectangle $(m \times n_1)$ could be calculated if u_2 were known. The necessary key values u_2 and u_2' can be found from the following two equations:

$$\left.\begin{aligned} u_2 &= C_1(P_1+u_2')+C_2(P_2+.5u_2') \\ &\quad +C_3P_3+\cdots C_kP_k, \quad \text{(a)} \\ u_2' &= C_1'(P_1'+u_2)+C_2'(P_2'+.5u_2) \\ &\quad +C_3'P_3'+\cdots C_{k'}'P_{k'}', \quad \text{(b)} \end{aligned}\right\} (17.1)$$

in which the coefficients C and C' are taken directly from the tables, and most perimeters are calculated from the basic expression

$$P = .5 \sum \text{known } a\text{'s} + \sum \text{known } c\text{'s}, \quad (17.2)$$

using only the boundary values on the angle.

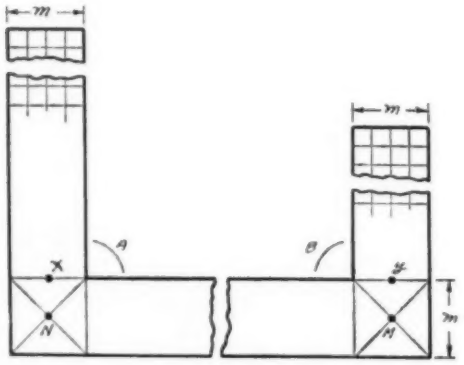

FIG. 12.

We denote the results from (17.1) by

$$\left.\begin{aligned} u_2 &= f(C, C', P, P'), \quad \text{(a)} \\ u_2' &= f_1(C, C', P, P'). \quad \text{(b)} \end{aligned}\right\} (17.3)$$

(b) T-figures. A configuration such as shown in Fig. 11 may be viewed as the composite of two overlapping angles. Observing that P_1 in angle A equals P_1 in the T-figure plus u_2', and that P_1' in angle B equals P_1' in the T-figure plus u_2 we have by (17.3)

$$\begin{aligned} u_2 &= f(C, P, C'', P'', u_2'), \\ u_2' &= f_1(C', P', C'', P'', u_2). \end{aligned} \quad (17.4)$$

Upon solution the problem is reduced to angles.

An alternate procedure is to view Fig. 11 as consisting of three overlapping rectangles of length n, n_1, and n_2. The resulting equations are:

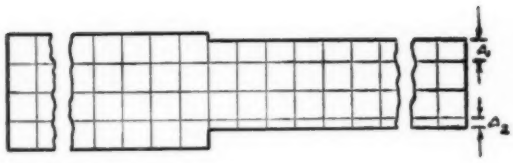

FIG. 13.

$$\left.\begin{aligned} u_2 &= C_1(P_1+u_2'+u_2'') \\ &\quad +C_2(P_2+.5u_2'')+C_3P_3+\cdots C_kP_k, \quad \text{(a)} \\ u_2' &= C_1'(P_1'+u_2+u_2'') \\ &\quad +C_2'(P_2'+.5u_2'') \\ &\quad +C_3'P_3'+\cdots C_k'P_k', \quad \text{(b)} \\ u_2'' &= C_1''(P_1''+u_2+u_2') \\ &\quad +C_2''(P_2''+.5u_2+.5u_2') \\ &\quad +C_3''P_3''+\cdots C_{k''}''P_{k''}''. \quad \text{(c)} \end{aligned}\right\} (17.5)$$

Upon solution the figure is reduced to rectangles.

(c) Channels. A channel, Fig. 12, may be viewed as the composite of two overlapping angles A and B. We observe that

$$\left.\begin{aligned} (P_M)_{\angle A} &= (P_M)_{\text{channel}}+y, \quad \text{(a)} \\ (P_N)_{\angle B} &= (P_N)_{\text{channel}}+x. \quad \text{(b)} \end{aligned}\right\} (17.6)$$

Hence by (17.3)

$$\left.\begin{aligned} x &= f(C, C', P, P', y), \quad \text{(a)} \\ y &= f_1(C, C', P, P', x). \quad \text{(b)} \end{aligned}\right\} (17.7)$$

Upon solution we obtain x and y and the problem is reduced to angles. When the length $n > 3m$ the value y may be neglected in the calculation of x, and x may be neglected in the calculation of y. Equations (17.7) then reduce to (17.3). A figure having a Z-shape can be treated in the same manner.

(d) H or I shapes may be viewed as overlapping channels. The method is also applicable to rectangles of variable widths, Fig. 13. It should, however, be added that in complicated areas the method of block iteration may be shorter.[4]

SHORT BIBLIOGRAPHY

1. G. H. Shortly and R. Weller, "The numerical solution of Laplace's equation," J. App. Phys. **9**, 334–348 (1938).

2. D. G. Christopherson and R. V. Southwell, "Relaxation methods applied to engineering problems," Proc. Roy. Soc. **A168**, 317–350 (1938). See also—H. W. Emmons, "The numerical solutions of heat conduction problems," Trans. A.S.M.E. **65**, 607–615 (1943).

3. David Moskovitz, "The numerical solution of Laplace's and Poisson's equations," Quart. Appl. Math. **2**, No. 2, 148–163 (July 1944).

4. Max M. Frocht, *Photoelasticity* (John Wiley and Sons, Inc., New York), Vol. II, Chap. 8, now in press.

Erratum

Correction of Diffraction Amplitudes for Lorentz and Polarization Factors

[J. App. Phys. 17, 285 (April 1946)]

M. J. Buerger and Gilbert E. Klein

THE values of the functions in Tables III and VIII are each misplaced in the region 90–179.9° so that they are found at a value of the given argument 0.1° lower than the correct argument. The tables may be utilized in this region by subtracting 0.1° from the desired value of Υ and looking up the function for this altered (false) argument. For example, if one desires the function for 147.3°, it should be looked up under the altered (false) argument 147.2°.

The Thermoluminescence and Conductivity of Phosphors

Robert C. Herman and Charles F. Meyer
Applied Physics Laboratory, Johns Hopkins University, Silver Spring, Maryland

(Received May 3, 1946)

A simple theoretical treatment is given for the emission of light and associated variations of dark current that occur on warming zinc sulphide and zinc silicate type phosphors previously irradiated with ultraviolet light at low temperatures. Reasonably good agreement is found between the calculated and observed glow curve for Willemite. The same type of treatment is applied to the case of infra-red illumination of phosphors at low temperatures.

1. INTRODUCTION

THE phenomena of thermoluminescence and the associated increase in conductivity in certain phosphors such as zinc sulphide and zinc silicate are sufficiently interesting to warrant further study. Recently there has arisen a great deal of interest in the storage and release of energy in solids, particularly with respect to infra-red-sensitive phosphors. Simple models based on the energy-band theory of solids have been shown to be in agreement with experimental data by various investigators.[1–3] It is now generally accepted that a phosphor is an insulating crystal which can be made luminescent by the addition of a small concentration of impurity or activator atoms. Figure 1 shows the spectrum of energy states of electrons in the crystal. Between the uppermost filled band, A, and the next highest band, B, the conduction band which is normally empty, there are localized electron states, such as C, D, and E. The narrow energy states C and D which lie in the forbidden region are the impurity states associated with the activator atoms whereas the states E represent the so-called trapping states which are associated with lattice imperfections such as strains, cracks, surfaces, etc. The trapping states, E, are populated with electrons to an extent which depends on the previous history of the phosphor. Photoconductivity arises when an electron is raised into the conduction band from states A, C, or E

[1] F. Seitz and R. P. Johnson, J. App. Phys. **8**, 84, 186, 246 (1937).
[2] N. F. Mott, Trans. Faraday Soc. **34**, 822 (1938).
[3] R. P. Johnson, J. Opt. Soc. Am. **29**, 387 (1939).

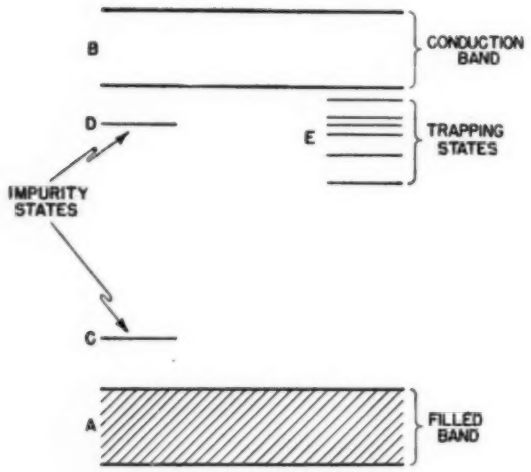

FIG. 1. Energy states of electron in phosphor.

by the absorption of a quantum of light. However, no photo-conductivity is observed when an electron is raised to an excited state at D.

In an excited phosphor, electrons return to the ground state by dropping from the conduction band to a state at D and then may make a radiative transition from D to C. Electrons in the conduction band may also be captured in the trapping states E. They can be released either thermally or by the absorption of radiation and thus return to the conduction band. The phenomena of phosphorescence and thermoluminescence are caused by the storage of electrons in excited states of the activator atoms and in the trapping states. Recently, Randall and Wilkins[4] have discussed the phenomenon of thermoluminescence or glow and presented a series of significant experiments. The storage of light at low temperatures which can be recovered by warming is well known and has been discussed frequently. The glow curve for zinc silicate obtained by warming a phosphor or crystal previously illuminated at liquid air temperatures with ultraviolet light is accompanied by a large dark current peak at about the same temperature as the glow peak.[5] This observation demonstrates that electrons thermally released from trapping states pass through the conduction band during the glow process. This conclusion is supported by the fact that a glow is produced in phosphorescent zinc silicate by the application of an electric field.[6] As previously suggested, it would prove interesting to observe the variations of dark current in zinc-silicate type phosphors during the glow experiment.[5] Also, dark current measurements would permit a study of trapping state distributions in non-fluorescent solids.[4]

It is the purpose of the present paper to discuss theoretically both the emission of light and variations in conductivity that occur in phosphors of the zinc silicate and zinc sulphide varieties. This has been done with a simplified model in which the only energy states considered are those in the uppermost filled band, the next highest normally empty conduction band and in the trapping state distribution. For the sake of simplicity, the analysis which follows deals with discrete sets of trapping states. This may be extended to various distributions as will be mentioned later.

2. LUMINESCENCE AND CONDUCTIVITY DURING WARMING

Let N_i be the number of trapping states per cm^3 at an energy ϵ_i below the conduction band, n_0 the number of positive holes per cm^3 in the uppermost filled band, n the number of electrons per cm^3 in the conduction band, and n_i the number of electrons per cm^3 in the trapping states in $d\epsilon_i$ at ϵ_i. If a phosphor of the type under discussion is irradiated with light of the proper wave-length at a sufficiently low temperature, the trapping states will become populated and remain so for considerable lengths of time so long as $\exp(-\epsilon_i/kT)$ is very small. With regard to the warming experiment, the initial condition of the crystal or phosphor chosen is that the number of electrons trapped in the states in $d\epsilon_i$ at an energy ϵ_i below the conduction band is $(n_i)_0$, $n=0$ and $(n_0)_0$ the number of holes, originally equal to the number of trapped electrons. In general, $n_0=n+n_i$. If the crystal is allowed to warm up the light emission and variations in dark current may be found from the following set of equations:

[4] J. T. Randall and M. H. F. Wilkins, Proc. Roy. Soc. **A184**, 366 (1945).
[5] R. C. Herman and R. Hofstadter, Phys. Rev. **57**, 936 (1940).
[6] J. Frenkel, Tech. Phys. U.S.S.R. **5**, 685 (1938).

$$dn_0/dt = -An_0n, \tag{1a}$$

$$\frac{dn}{dt} = -An_0n + \sum s_i \exp(-\epsilon_i/kT)n_i - \sum K_i[(n_i)_0 - n_i]n, \tag{1b}$$

$$\frac{dn_i}{dt} = -s_i \exp(-\epsilon_i/kT)n_i + K_i[(n_i)_0 - n_i]n, \tag{1c}$$

where A is the recombination coefficient and is equal to σV; σ the cross section for capture by an impurity center of an electron in the conduction band and subsequent radiation; V the velocity of the conduction electron; s_i the frequency factor in sec.$^{-1}$ or the number of times per second an electron strikes the potential barrier in a trap; and K_i is similar to A but refers to the various sets of trapping states. De Groot[7] has solved graphically a similar set of equations in his studies of the fluorescence and phosphorescence of zinc sulphide phosphors. Following Randall and Wilkins[8] who point out that the effect of retrapping is not very large, we have solved the equations for the case $K_i=0$ or:

$$dn_0/dt = -An_0n, \tag{2a}$$

$$\frac{dn}{dt} = -An_0n_1 + \sum s_i \exp(-\epsilon_i/kT)n_i, \tag{2b}$$

$$\frac{dn_i}{dt} = -s_i \exp(-\epsilon_i/kT)n_i. \tag{2c}$$

Equation (2c), which expresses the rate at which trapped electrons leave the states in $d\epsilon_i$ at ϵ_i, can be integrated yielding:

$$n_i = (n_i)_0 \exp\left\{-s_i \int_0^t \exp(-\epsilon_i/kT)dt\right\} \tag{3}$$

where $(n_i)_0$ is the number of electrons originally trapped in $d\epsilon_i$ at ϵ_i. If a constant rate of warming is used so that $T=\alpha t+T_0$, then $dT=\alpha dt$ and

$$n_i = (n_i)_0 \times \exp\left\{-(s_i/\alpha)\int_{T_0}^{T} \exp(-\epsilon_i/kT)dT\right\}. \tag{4}$$

The general case involving electrons trapped in complicated trapping distributions can be handled by a numerical integration of Eq. (4) over all trapping states.

In the case where there are sets of states at discrete energies the problem is much simpler and Eq. (4) becomes for a single trap energy:

$$n_1 = N_1 \exp\left\{(s\epsilon/\alpha k)\int_{x_0}^{x} x^{-2}e^{-x}dx\right\}, \tag{5}$$

where

$$x=\epsilon/kT, \quad x_0=\epsilon/kT_0,$$

and it is assumed that N_1 traps at the energy ϵ are filled with electrons when $T=T_0$. Equation (5) can be rewritten in the form

$$n_1 = N_1 \exp\{-(s\epsilon/\alpha k) \times [x^{-1}e^{-x} + Ei(-x) - f_0]\}, \tag{6}$$

where

$$-Ei(-x) = \int_x^{\infty} u^{-1}e^{-u}du$$

and

$$f_0 = x_0^{-1}\exp(-x_0) + Ei(-x_0).$$

Substitution of n_1 from Eq. (6) into (2a) yields an equation that can be expressed in terms of known functions, but which requires numerical solution. It was found convenient to solve the differential equation numerically in the form:

$$\frac{d\eta}{dx} = \frac{AN_1\epsilon}{\alpha k}\frac{\eta}{x^2}(\eta-\zeta), \tag{7}$$

where

$$\eta = n_0/N_1, \quad \zeta = n_1/N_1 \quad \text{and} \quad \xi = n/N_1 = \eta - \zeta.$$

The solution of these equations yields both the luminescent intensity, I, and the conduction current, i, in an applied electric field since $I \propto \eta\xi$ and $i \propto \xi$.

Randall and Wilkins[8] have shown that for many of the phosphors the glow curves can be interpreted on the basis of a reasonably broad distribution of trapping states. For example, the broad glow curves for zinc sulphide phosphors originate in this manner. However, the three glow-curve peaks for Willemite+1 percent Mn seemed sufficiently sharp to be accounted for by a set of three discrete trap energies.

The light intensity and current have been computed for this case by solving Eq. (7) numerically using the value of the constants shown in Table I. The solutions to these equations are shown in Fig. 2 where η, ξ, and ζ are

[7] W. de Groot, Physica **6**, 275 (1939).
[8] J. T. Randall and M. H. F. Wilkins, Proc. Roy. Soc. **A184**, 390 (1945).

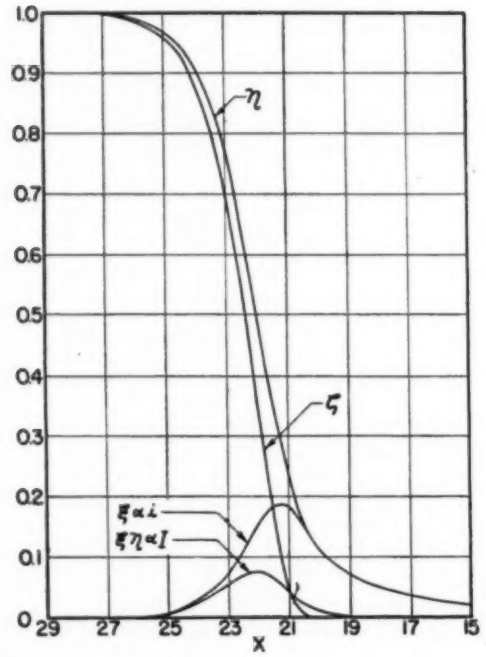

FIG. 2. Curves showing temperature dependence of luminescence and current during linear warming of a Willemite phosphor in an electric field, for the case of peak C (see Fig. 3).

plotted against x for the largest peak labeled C in Fig. 3. It is to be noted that the experimental fit seems to be good, particularly in that the long tail is predicted. For long times when the number of trapped electrons is small (or $\zeta \to 0$) Eq. (7) reduces to a form having a solution of the type

$$\eta = \xi = [x/(1+cx)]. \tag{8}$$

Thus, for long times bimolecular decay applies. In the event that positive holes are originally present the decay would be more rapid and in fact exponential if there are a large number of holes present originally.

The conduction current is proportional to ξ and has not been plotted on a temperature scale since complete experimental data is not available for comparison. However, Herman and Hofstadter[5] found a sudden increase in dark current at about $-60°$C which agrees with the predicted curve shown in Fig. 2.

Since the areas under the light emission curves are proportional to the number of trapped electrons, the relative number of trapping states at the three energies could be obtained. Since the peaks A and B overlap, it would be necessary

TABLE I.

Constants	Peak A	Peak B	Peak C
A(cm³/sec.)	10^{-13}	10^{-13}	10^{-13}
s(sec.$^{-1}$)	10^{9}	10^{9}	10^{9}
ϵ(ev)	0.223	0.291	0.500
N_1(cm^{-3})	1.4×10^{12}	$\sim5\times10^{11}$	1×10^{13}
α(deg./sec.)*	5	5	3

* The experimental data of Randall and Wilkins (reference 4) shows a non-uniform rate of warming for this case.

to solve Eq. (7) in the form

$$\frac{d\eta}{dT} = -\frac{AN}{\alpha}\eta[\eta - \zeta(T)],$$

where $N\zeta(T)$ is the number of electrons trapped in both sets of levels. However, for the sake of simplicity each set of trapping states was handled separately and the result is shown in Fig. 3. Since overlapping light emission and current peaks are more difficult to analyze, it would be desirable to have a slow linear increase in temperature since this will lead to better resolution. This has been done by Williams and Eyring.[9]

3. LUMINESCENCE AND CONDUCTIVITY DURING INFRA-RED ILLUMINATION

Some time ago Gisolf[10] performed a series of qualitative experiments with ZnS phosphors which showed that electrons in trapping states absorb infra-red radiation. The electrons can be freed by infra-red illumination and since changes in conductivity occur it is evident that the electrons pass through the conduction band. On first illuminating the phosphor the photo-current increases and then decreases as a consequence of recombination of electrons with positive holes. A more quantitative study by Reimann[11] shows that the resistance of a ZnS phosphor containing trapped electrons increases linearly with time when the phosphor is irradiated with infra-red light. The simple theory for sufficiently long time after beginning the illumination has been given by Reimann and others.[12,13]

[9] F. E. Williams and H. Eyring, "Mechanism of luminescence of solids," Bull. Am. Phys. Soc. **21**, 17 (A) (Jan. 24, 1946). We wish to thank Professor H. Eyring and Mr. F. E. Williams for interesting discussions.

[10] J. H. Gisolf, Ned. T. Natuurk **5**, 289 (1938).

[11] A. L. Reimann, Nature **140**, 501 (1937).

[12] N. F. Mott and R. W. Gurney, *Electronic Processes in Ionic Crystals* (Oxford University Press, New York, 1940).

[13] F. Seitz, *The Modern Theory of Solids* (McGraw-Hill Book Company, Inc., New York, 1940).

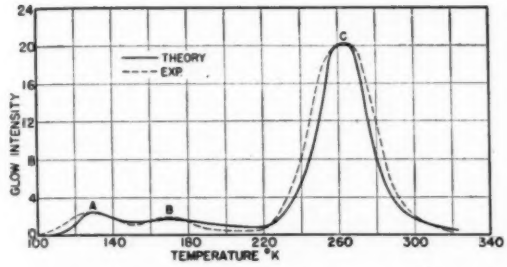

FIG. 3. Comparison of theoretical glow curve with experimental results of Randall and Wilkins (reference 4) for Willemite +1 percent Mn.

It is evident that the resistance of such a phosphor must decrease and then increase in a manner which depends upon the infra-red light intensity, the cross section of a trapped electron for an infra-red photon, the total number of trapped electrons, and the probability that a conduction electron will recombine with a positive hole. Since a general theory involving complicated trap distributions leads to tedious solutions, attention has been confined to the case of a single set of trapping states all at the same energy below the conduction band.

The equations are similar to those employed in the previous case except that the temperature is kept constant and the rate of release of electrons from trapping states is given by

$$\frac{dn_1}{dt}=-\frac{I_0}{h\nu}\sigma n_1, \tag{9}$$

where I_0 is the intensity of the infra-red light, σ the cross section of a trapped electron for an infra-red photon, and n_1 the number of trapped electrons. For constant intensity of illumination, I_0, Eq. (9) yields

$$n_1=N_1\exp(-C_0t), \tag{10}$$

where

$$C_0=I_0\sigma/h\nu,$$

and N_1 is the number of electrons originally trapped. Substitution of Eq. (10) into (2a) yields

$$\frac{dn_0}{dt}=-An_0[n_0-N_1\exp(-C_0t)]. \tag{11}$$

The solution of Eq. (11) is

$$\frac{1}{\eta}=1-\frac{AN_1}{C_0}[Ei(-y)-Ei(-y_0)]e^y, \tag{12}$$

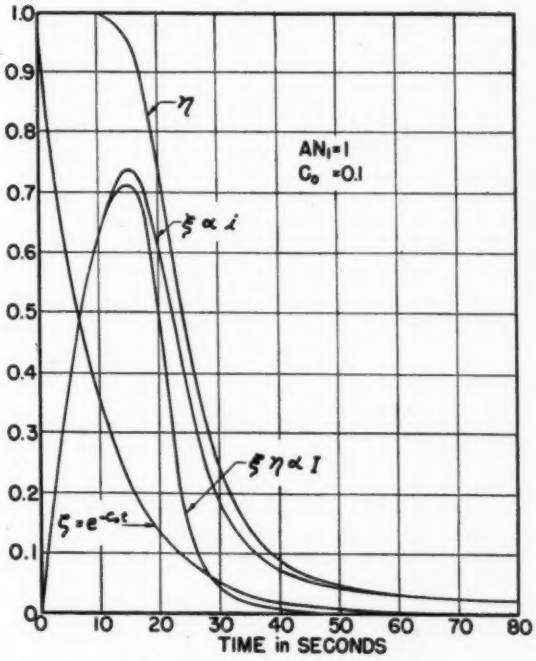

FIG. 4. Time dependence of luminescence and current for a phosphor in an electric field, that is illuminated with infra-red light at constant temperature.

where

$$y=(AN_1/C_0)\exp(-C_0t),\quad y_0=AN_1/C_0$$

and

$$\eta=n_0/N_1.$$

When t is sufficiently large $\xi=(n/N_1)$ is equal to η and the resistance which is proportional to $(1/\xi)$ increases linearly with the time.

The solutions for the glow intensity and the current are shown in Fig. 4 for the case of $AN_1=1$ sec.$^{-1}$ and $C_0=0.1$ sec.$^{-1}$. The equations have also been solved for various values of AN_1 and C_0 and the resistance computed as a function of time. These results are shown in Fig. 5. It is apparent that if the infra-red intensity or the cross section is smaller, the resistance minimum is broader. On the other hand, if the total number of electrons originally trapped or the recombination coefficient is smaller, then the resistance begins to rise linearly at an earlier time. Since the resistance in the dark is finite, it is necessary to add a constant term to the conductivity calculated. However, if the peak current is large compared to the dark current, deviations from linearity will occur only at very long times.

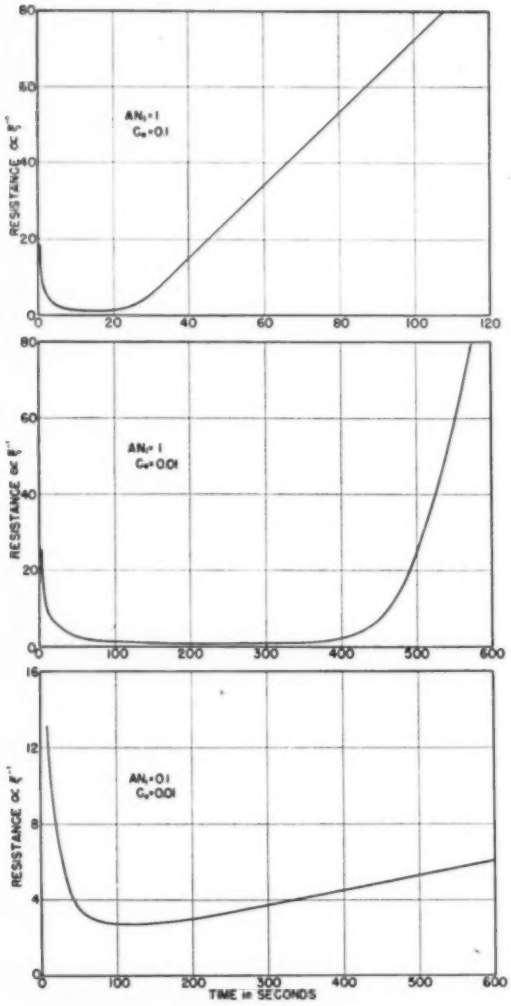

FIG. 5. Variation of resistance $\propto 1/\xi$ with time, for a phosphor in an electric field during infra-red illumination and the dependence on phosphor characteristics as well as light intensity.

4. APPENDIX

The exponential integral

$$-Ei(-x)=\int_x^\infty \frac{e^{-u}}{u}du$$

employed in the calculation of the glow intensity curves, etc., has been tabulated in various references[14–16] for $0\leqq x\leqq 15$ and $20\leqq x\leqq 50$. We have been unable to find tabulated values of $-Ei(-x)$ in the range $15<x<20$. These have been calculated using the asymptotic expansion

$$-Ei(-x)=e^{-x}\left[\frac{1}{x}-\frac{1}{x^2}+\frac{2!}{x^3}-\frac{3!}{x^4}+\frac{4!}{x^5}-\cdots\right]$$

and are given in Table II together with second differences, Δ_2, in the hope that they may be found useful by others.

TABLE II. Exponential integral $-Ei(-x)=\int_x^\infty(e^{-u}/u)du$.

x	$-Ei(-x)$	Δ_2
15.0	1.91863×10^{-8}	0.02178×10^{-8}
15.1	1.72520×10^{-8}	0.01956×10^{-8}
15.2	1.55133×10^{-8}	0.01756×10^{-8}
15.3	1.39502×10^{-8}	0.01581×10^{-8}
15.4	1.25452×10^{-8}	0.01419×10^{-8}
15.5	1.12821×10^{-8}	0.01276×10^{-8}
15.6	1.01466×10^{-8}	0.01146×10^{-8}
15.7	9.12573×10^{-9}	0.01030×10^{-8}
15.8	8.20784×10^{-9}	0.09013×10^{-9}
15.9	7.38008×10^{-9}	0.08818×10^{-9}
16.0	6.64050×10^{-9}	0.07229×10^{-9}
16.1	5.97321×10^{-9}	0.06727×10^{-9}
16.2	5.37319×10^{-9}	0.06042×10^{-9}
16.3	4.83359×10^{-9}	0.05434×10^{-9}
16.4	4.34833×10^{-9}	0.04886×10^{-9}
16.5	3.91193×10^{-9}	0.04390×10^{-9}
16.6	3.51943×10^{-9}	0.03949×10^{-9}
16.7	3.16642×10^{-9}	0.03550×10^{-9}
16.8	2.84891×10^{-9}	0.03191×10^{-9}
16.9	2.56331×10^{-9}	0.02872×10^{-9}
17.0	2.30643×10^{-9}	0.02580×10^{-9}
17.1	2.07535×10^{-9}	0.02321×10^{-9}
17.2	1.86748×10^{-9}	0.02088×10^{-9}
17.3	1.68049×10^{-9}	0.01876×10^{-9}
17.4	1.51226×10^{-9}	0.01688×10^{-9}
17.5	1.36091×10^{-9}	0.01519×10^{-9}
17.6	1.22475×10^{-9}	0.01366×10^{-9}
17.7	1.10225×10^{-9}	0.01227×10^{-9}
17.8	9.92022×10^{-10}	0.01106×10^{-9}
17.9	8.92850×10^{-10}	0.10031×10^{-10}
18.0	8.03609×10^{-10}	0.08843×10^{-10}
18.1	7.23311×10^{-10}	0.08041×10^{-10}
18.2	6.51054×10^{-10}	0.07233×10^{-10}
18.3	5.86030×10^{-10}	0.06509×10^{-10}
18.4	5.27515×10^{-10}	0.05859×10^{-10}
18.5	4.74859×10^{-10}	0.05263×10^{-10}
18.6	4.27466×10^{-10}	0.04741×10^{-10}
18.7	3.84814×10^{-10}	0.04267×10^{-10}
18.8	3.46429×10^{-10}	0.03835×10^{-10}
18.9	3.11879×10^{-10}	0.03454×10^{-10}
19.0	2.80783×10^{-10}	0.03042×10^{-10}
19.1	2.52729×10^{-10}	0.02924×10^{-10}
19.2	2.27599×10^{-10}	0.02453×10^{-10}
19.3	2.04922×10^{-10}	0.02263×10^{-10}
19.4	1.84508×10^{-10}	0.02037×10^{-10}
19.5	1.66131×10^{-10}	0.01835×10^{-10}
19.6	1.49589×10^{-10}	0.01651×10^{-10}
19.7	1.34698×10^{-10}	0.01484×10^{-10}
19.8	1.21291×10^{-10}	0.01337×10^{-10}
19.9	1.09221×10^{-10}	0.01204×10^{-10}
20.0	9.83555×10^{-11}	0.01083×10^{-10}

[14] *Tables of Sine, Cosine, and Exponential Integrals* (Federal Works Agency, WPA, 1940), Vol. 1 and 2.

[15] *British Assoc. Adv. Sci. Math. Tables* (Cambridge University Press, New York, 1931), Vol. 1.

[16] T. Akahira, Sci. Pap. Inst. Phys. Chem. Res. Tokio, 181 (June, 1929), Table No. 3.

Oscillation Conditions in Single Tuned Amplifiers

WILLIAM R. FAUST AND HUGO M. BECK
Naval Research Laboratory, Washington, D. C.
(Received May 31, 1946)

An application of the calculus of finite differences has been made in obtaining the complete expression for the voltage gain of an n-stage amplifier having identical grid-to-plate impedances and plate loads when driven by a generator of any given internal impedance. An application of these results was made in determining the conditions of oscillation in a multi-stage amplifier using single-tuned circuits. It was found that there is a certain minimum grid-to-plate capacitance required to cause oscillation. If the actual grid-to-plate capacitances are below this value, the system will not oscillate. There also exists a region of stable gain, zero to $2^{1/n}$, wherein it is impossible to make the amplifier oscillate even with grid-to-plate capacitance arbitrarily large.

1. INTRODUCTION

THE calculus of finite differences has been applied to cascaded systems of vacuum tube amplifiers,[1] but apparently the full power and usefulness of the method has not been realized. It is obvious that a system of cascaded amplifiers lends itself quite readily to the methods of finite differences. The equivalent circuit of multitube amplifiers resembles, to a very great extent, an artificial transmission line made up of Pi or T sections with the exception that the amplifier contains internal current generators. Nevertheless, the difference equations for the two systems are quite similar in form and become identical when the g_m (mutual conductance) of the tubes vanishes.

The purpose of this paper is twofold: First, that of obtaining a complete expression for the voltage gain of a multi-stage amplifier. Such an expression describes the effect of the feedback between the grid and plates of the various stages. Second, that of applying the general expression for voltage gain to specific cases and using it to compute the conditions necessary for sustained oscillations to exist in a multi-stage, single-tuned amplifier.

2. DEVELOPMENT OF FUNDAMENTAL RELATIONS

The circuit of Fig. 1 is a cascaded multi-stage amplifier driven by a generator of e.m.f. e_{in} and internal impedance Z_g with identical plate load impedances Z_2'. The circuit of Fig. 2 is an equivalent circuit of Fig. 1, wherein Z_1 represents the grid to plate impedance which is assumed to be perfectly general at the present time. For simplicity the circuit of Fig. 2 will be shown as in Fig. 2*a*, where Z_2 is the parallel combination of R_p and Z_2', i.e.,

$$Z_2 = R_p Z_2'/(Z_2'+R_p).$$

The voltage relationship between the k and $k+1$ stages is

$$e_{k+1} - Z_1 i_k - e_k = 0, \tag{1}$$

and the currents at the plate of the kth stage are related by

$$i_k - i_{k-1} - e_k/Z_2 - g_m e_{k-1} = 0. \tag{2}$$

Equations (1) and (2) are the difference equations of the amplifier for which a solution satisfying the boundary conditions must be found. To find a solution, it is assumed that

$$e_k = U(\exp \gamma_1 k) + V(\exp -\gamma_2 k), \tag{3}$$

$$i_k = W(\exp \gamma_1 k) + X(\exp -\gamma_2 k), \tag{4}$$

where U, V, W, and X are complex constants and γ_1 and γ_2 are the complex propagation constants of the system. There are not four independent

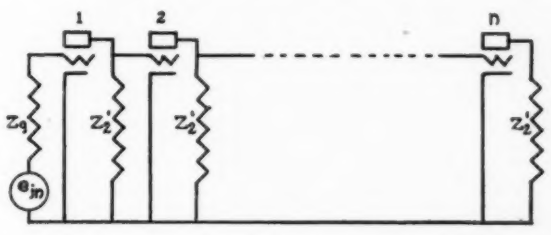

FIG. 1. Radiofrequency circuit of n-stage amplifier.

[1] A. C. Bartlett, *The Theory of Electrical Artificial Line and Filters* (John Wiley and Sons, Inc., New York, 1931), pp. 143–150.

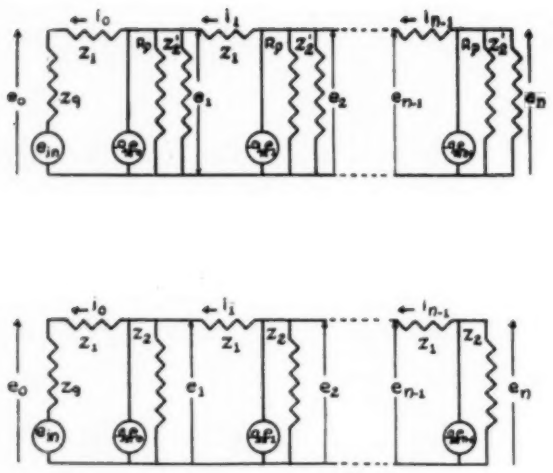

FIG. 2. Equivalent circuits. (a) Equivalent circuit of Fig. 1. (b) Simplified equivalent where $Z_2=R_pZ_2'/(Z_2'+R_p)$.

constants U, V, W, X but only two, as a relationship between U and W, and V and X can be found. By substituting the assumed solutions (3) and (4) into Eq. (1), it follows that

$$(\exp \gamma_1 k)[U(-1+\exp \gamma_1)-Z_1W] +(\exp -\gamma_2 k)[V(-1+\exp -\gamma_2)-Z_1X]=0. \quad (5)$$

Since this expression must hold for all values of k, it is necessary that the coefficients of $\exp \gamma_1 k$ and $\exp \gamma_2 k$ vanish independently, i.e.,

$$W=U[(\exp \gamma_1)-1]/Z_1, \quad (6)$$

$$X=V[(\exp -\gamma_2)-1]/Z_1. \quad (7)$$

Equation (4) then becomes

$$i_k=U(-1+\exp \gamma_1) \times(\exp \gamma_1 k)/Z_1+V(-1+\exp -\gamma_2) \times(\exp -\gamma_2 k)/Z_1. \quad (8)$$

To determine the "propagation constants" γ_1 and γ_2 so that the assumed solutions will satisfy the difference equations, substitute the solutions (3) and (8) into Eq. (2), which then becomes

$$\begin{aligned} U\{&[-1+\exp \gamma_1][\exp \gamma_1 k]/Z_1 \\ &-[-1+\exp \gamma_1][\exp \gamma_1(k-1)]/Z_1 \\ &+-[\exp \gamma_1 k]/Z_2-g_m[\exp \gamma_1(k-1)]\} \\ &+V\{[-1+\exp -\gamma_2][\exp -\gamma_2 k]/Z_1 \\ &+-[-1+\exp -\gamma_2][\exp -\gamma_2(k-1)]/Z_1 \\ &-[\exp -\gamma_2 k]/Z_2 \\ &-g_m[\exp -\gamma_2(k-1)]\}=0. \end{aligned} \quad (9)$$

Because this must be satisfied for every value of k, it is necessary that the coefficients of U and V vanish; and since U and V are assumed not to equal zero, it follows that

$$\exp \gamma_1=1+Z_1/2Z_2 \pm[Z_1/Z_2+(Z_1/2Z_2)^2+g_mZ_1]^{\frac{1}{2}}, \quad (10)$$

and

$$\exp \gamma_2=1+Z_1/2Z_2 \pm[Z_1/Z_2+(Z_1/2Z_2)^2+g_mZ_1]^{\frac{1}{2}}/(1-g_mZ_1). \quad (11)$$

The exact choice of the signs in (10) and (11) will be determined later. It should be pointed out, however, that $(\exp \gamma_1)\neq(\exp -\gamma_2)$ as such a choice of signs would lead to a solution not consistent with the physical facts. It has been shown that Eqs. (3) and (8) are solutions of the difference equations where γ_1 and γ_2 are as defined above and U and V determined by the boundary conditions.

3. BOUNDARY CONDITIONS

The boundary conditions are very similar to those for a transmission line and should require but little discussion. It will be assumed that the amplifier has n stages, so the corresponding boundary condition is simply

$$i_n=0, \quad (12)$$

from which it follows that

$$V=-U[\exp n(\gamma_1+\gamma_2)] \times[-1+\exp \gamma_1]/(-1+\exp -\gamma_2). \quad (13)$$

Since the amplifier is driven by a generator of e.m.f. e_{in} and internal impedance Z_g, the corresponding boundary condition is

$$e_0=e_{in}+Z_gi_0. \quad (14)$$

By the use of Eqs. (1), (8), and (13) Eq. (14) becomes

$$\begin{aligned} e_{in}=U\{&1-[\exp n(\gamma_1+\gamma_2)] \\ &\times[-1+\exp \gamma_1]/(-1+\exp -\gamma_2) \\ &+-Z_g(-1+\exp \gamma_1) \\ &\times[1-\exp n(\gamma_1+\gamma_2)]/Z_1\}. \end{aligned} \quad (15)$$

Consequently, the expression for the voltage gain between the generator and the kth stage becomes

$$\frac{e_k}{e_{in}}=\frac{[\exp\gamma_1 k]-[\exp n(\gamma_1+\gamma_2)][-1+\exp\gamma_1][\exp-\gamma_2 k]/[-1+\exp-\gamma_2]}{1-\{[\exp n(\gamma_1+\gamma_2)][-1+\exp\gamma_1]/[-1+\exp-\gamma_2]\}} \tag{16}$$
$$-\left\{\frac{Z_g}{Z_1}[-1+\exp\gamma_1][1-\exp n(\gamma_1+\gamma_2)]\right\}$$

Usually the over-all gain of the system is of interest rather than the gain up to a certain stage, so the expression for e_n/e_{in} will be considered. This is obtained from (16) simply by setting $k=n$,

$$\frac{e_n}{e_{in}}=\frac{(\exp-\gamma_2)-(\exp+\gamma_1)}{[\exp-n\gamma_1][-1+\exp-\gamma_2]-[\exp n\gamma_2][-1+\exp\gamma_1]} \tag{17}$$
$$-\frac{Z_g}{Z_1}[-1+\exp\gamma_1][-1+\exp-\gamma_2][(\exp-n\gamma_1)-(\exp n\gamma_2)]$$

4. SPECIAL CASES

Equation (17), as it stands, is of little practical value; and the exponentials must be replaced by their values in terms of the parameters of the system. For simplicity in the manipulation of the expression, it will be convenient to set

$$A=1+Z_1/2Z_2,$$

and

$$B=[Z_1/Z_2+(Z_1/2Z_2)^2+g_mZ_1]^{\frac{1}{2}},$$

so that

$$\exp\gamma_1=A-B \quad \text{or} \quad \exp-\gamma_1=(A+B)/(1-Z_1g_m),$$

and

$$\exp\gamma_2=(A-B)/(1-g_mZ_1).$$

The relationships may be simplified by setting $Z_g=Z_2$. This is the usual case and should not detract from the utility of the results. Substitution of these values in (17) produces

TABLE I.

No. of stages, n	Gain
0	1
1	$\dfrac{Z_2-g_mZ_2Z_1}{2Z_2+Z_1+g_mZ_2^2}$
2	$\dfrac{(1-g_mZ_1)^2Z_2^2}{(Z_1+3Z_2+2g_mZ_2^2)(Z_1+Z_2)}$
3	$\dfrac{(1-g_mZ_1)^3Z_2^3}{Z_1^3+3Z_1^2Z_2(2+g_mZ_2)+Z_1Z_2^2(10+8g_mZ_2+g_m^2Z_2^2)+Z_2^3(4+3g_mZ_2)}$
4	$\dfrac{(1-g_mZ_1)^4Z_2^4}{(Z_1^2+3Z_1Z_2+g_mZ_1Z_2^2)(Z_1^2+5Z_1Z_2+3g_mZ_1Z_2^2+5Z_2^2+4g_mZ_2^3)}$
5	$\dfrac{(1-g_mZ_1)^5Z_2^5}{Z_1^5+5Z_1^4Z_2(2+g_mZ_2)+2Z_1^3Z_2^2(18+16g_mZ_2+3g_m^2Z_2^2)+Z_1^2Z_2^3(g_m^2Z_2^3+56+18g_m^2Z_2^2+63g_mZ_2)+5Z_1Z_2^4(7+8g_mZ_2+2g_m^2Z_2^2)+Z_2^5(6+5g_mZ_2)}$
6	$\dfrac{(1-g_mZ_1)^6Z_2^6}{(Z_1^3+7Z_1^2Z_2+4g_mZ_2^2Z_1^2+14Z_1Z_2^2+13g_mZ_1Z_2^3+2g_m^2Z_1Z_2^4+Z_2^3+6g_mZ_2^4)\times(Z_1^3+5Z_1^2Z_2+2g_mZ_1^2Z_2^2+6Z_1Z_2^3+3g_mZ_1Z_2^3+Z_2^3)}$

$$\frac{e_n}{e_{in}}=\frac{2B(1-g_mZ_1)^n}{(A+B)^n(A+B-1)-(A-B)^n(A-B-1)-(A-B-1)(A+B-1)[(A+B)^n-(A-B)^n]\dfrac{Z_2}{Z_1}}, \quad (18)$$

which may be written in the form

$$e_n/e_{in}=\frac{2B(1-g_mZ_1)^n}{(A+B)^n[(A+B)+g_mZ_2]-(A-B)^n[(A-B)+g_mZ_2]}. \quad (19)$$

By expanding Eq. (19), it is easy to obtain

$$e_n/e_{in}=\frac{(1-g_mZ_1)^n}{(n+1)\left[A^n+\dfrac{n(n-1)A^{n-2}B^2}{3!}+\dfrac{n(n-1)(n-3)A^{n-4}B^4}{5!}+\cdots\right]+g_mZ_2\left[nA^{n-1}+\dfrac{n(n-1)(n-2)A^{n-3}B^2}{3!}+\dfrac{n(n-1)(n-2)(n-3)(n-4)A^{n-5}B^4}{5!}+\cdots\right]}. \quad (20)$$

Equation (20) is the general expression for the gain of a cascaded n-stage amplifier and, as such, is much too general to deduce any results. In Table I, Eq. (20) has been evaluated for various values of n; the appropriate values of A and B as given previously have also been included.

That these equations are correct in the limit may be shown by letting Z_1 become very large; the general form of the expressions in Table I then becomes $(-g_mZ_2)^n$, which is the proper form for the gain of an n-stage amplifier.

5. CONDITIONS FOR OSCILLATION

It is now desired to determine what conditions must exist in order to produce sustained oscillation. Obviously the system under consideration is oscillating when a finite output $e_n \neq 0$ exists for $e_{in}=0$. In order that the above conditions obtain, it is necessary that the denominators of the various expressions in Table I vanish. To apply the above results to a practical case, Z_1 will be taken as the plate to grid impedance of a vacuum tube which is mainly capacitive, i.e.,

$$Z_1=1/j\omega C. \quad (21)$$

The effective plate impedance Z_2 will be taken as that of a single tuned circuit consisting of an inductance L_0, capacitance C_0, and resistance, all in parallel; hence[2]

$$Z_2=R/(1+JQF), \quad (22)$$

where

$Q=R(C_0/L_0)^{\frac{1}{2}}$,

$F=(\omega/\omega_0-\omega_0/\omega)$,

$\frac{\omega_0}{2\pi}$ = Resonant frequency of single-tuned circuit $=1/2\pi(L_0C_0)^{\frac{1}{2}}$,

$\frac{\omega}{2\pi}$ = The frequency under consideration, and

R = Dynamic resistance $=R'R_p/(R_p+R')\approx R'$ (for pentodes).

One Stage

From Table I, it is seen that the conditions of oscillation are to be determined from

$$2Z_2+Z_1+g_mZ_2^2=0. \quad (23)$$

By substituting the values of Z_1 and Z_2 from Eqs. (21) and (22) and separating the real and imaginary parts, there is obtained

$$(QF)^2+2(R\omega C)(QF)-1=0 \text{ (Real part)}, \quad (24)$$

and

$$2(QF)+2(R\omega C)-g_mR(R\omega C)=0. \text{ (Imaginary part)}. \quad (25)$$

[2] S. A. Schelkunoff, *Electromagnetic Waves* (D. Van Nostrand Company, Inc., New York, 1943), pp. 119–120.

A simultaneous solution of these two expressions results in

$$QF=\pm[(2+g_mR)/(g_mR-2)]^{\frac{1}{2}}, \quad (26)$$

and

$$C=\mp 2/\omega R[(g_mR)^2-4]^{\frac{1}{2}}. \quad (27)$$

The negative sign must be chosen in Eq. (26) so that C will be positive in Eq. (27). The frequency of oscillation ω is determined from

$$QF=(\omega/\omega_0-\omega_0/\omega)Q=(\omega^2-\omega_0^2)Q/\omega\omega_0 = -[(2+g_mR)/(g_mR-2)]^{\frac{1}{2}}, \quad (28)$$

which gives

$$\omega=\frac{\omega_0}{2Q}\left\{-\left[\frac{(g_mR+2)}{(g_mR-2)}\right]^{\frac{1}{2}} \pm\left[\frac{(g_mR+2)}{(g_mR-2)}+4Q^2\right]^{\frac{1}{2}}\right\}. \quad (29)$$

The positive sign of the second term in (29) must be chosen so as to produce a frequency of oscillation that has physical meaning. After ω is eliminated from Eqs. (27) and (29) there results,

$$C=\frac{4Q}{R\omega_0\{[(g_mR+2)^2+4Q^2(g_m^2R^2-4)]^{\frac{1}{2}}-(g_mR+2)\}}. \quad (30)$$

It is interesting to note that if $g_mR\leqslant 2$, the system will never oscillate, as C becomes indefinitely large when $g_mR=2$, and is imaginary if $g_mR<2$. For a high stage gain, these results differ but little from previous results.[3,4] For an amplifier of low gain (g_mR of the order of 2) and low Q, there is a wide difference; and these results indicate that the system will be intrinsically stable. This situation is illustrated in the curves of Fig. 3 in which Eqs. (24) and (25) are plotted with (QF) as the independent variable and (g_mR) a parameter. Equation (24) is a hyperbola and (25) is a straight line whose slope is dependent upon the parameter g_mR. The intersection of these two curves represents the simultaneous solution of the real and imaginary parts of the defining equation. In order to obtain positive values of $(R\omega C)$, the intersection of the two curves must occur in the second quadrant. Since the asymptote to the hyperbola corresponds to the straight line with $g_mR=2$, it follows that there can be no real simultaneous solution of the two equations between $g_mR=0$ and $g_mR=2$. Consequently, the system will be inherently stable within these limits.

Two Stages

The defining equation in this case is

$$(Z_1+Z_2)(Z_1+3Z_2+2g_mZ_2^2)=0. \quad (31)$$

The second factor may be separated into its real and imaginary parts giving

$$(QF)^2+3(R\omega C)(QF)-1=0 \text{ (Real part)}, \quad (32)$$

and

$$2(QF)+3(R\omega C)+2g_mR(R\omega C)=0. \text{ (Imaginary part)}, \quad (33)$$

which when solved simultaneously produces

$$QF=\pm[(2g_mR+3)/(2g_mR-3)]^{\frac{1}{2}}, \quad (34)$$

and

$$C=\frac{\mp 2}{R\omega[4(g_mR)^2-9]^{\frac{1}{2}}}. \quad (35)$$

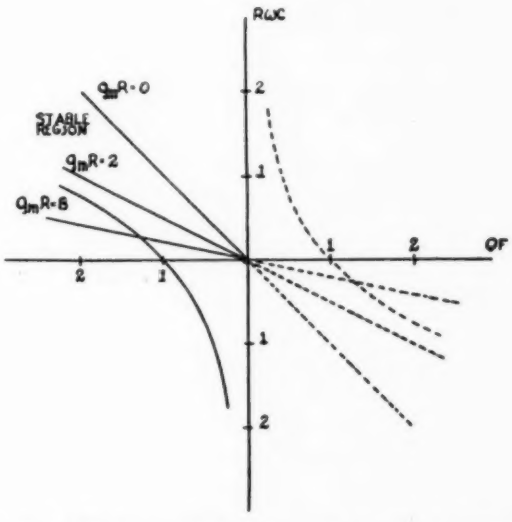

FIG. 3. Oscillation conditions for a single-tuned amplifier.

[3] B. J. Thompson, "Oscillation in tuned radio frequency amplifiers," Proc. I.R.E., 19, 421–437 (1931).

[4] J. R. Nelson, "Discussion of oscillation in tuned radio frequency amplifiers," Proc. I.R.E. 19, 1281 (1931).

It is necessary again to choose the negative sign of (QF) so that a positive value of C will result. As before, ω may be determined from (34), thus:

$$\omega^2-\omega_0^2=-\frac{\omega_0\omega}{Q}\left[\frac{3+2g_mR}{2g_mR-3}\right]^{\frac{1}{2}},$$

or

$$\omega=\frac{\omega_0}{2Q}\left\{-\left[\frac{2g_mR+3}{2g_mR-3}\right]^{\frac{1}{2}}+\left[4Q^2+\frac{2g_mR+3}{2g_mR-3}\right]^{\frac{1}{2}}\right\}, \quad (36)$$

wherein the positive sign of the radical has again been chosen to correspond with physical reality. Substitution of (36) in (35) then gives

$$C=\frac{4Q}{R\omega_0\{[(2g_mR+3)^2+4Q^2(4g_m{}^2R^2-9)]^{\frac{1}{2}}-(2g_mR+3)\}}. \quad (37)$$

Again it is seen that there is a critical value of g_mR below which it will be impossible to make the system oscillate. The critical value in this case is $g_mR=\frac{3}{2}$. For high stage gains and high Q's, C approaches $1/\omega_0 g_m R^2$, which is the approximate value found by previous investigators. The inherently stable region is illustrated in the curves of Fig. 4. Here the asymptote to the hyperbola corresponds to the straight line with $g_mR=\frac{3}{2}$ so that the stable region lies between $g_mR=0$ and $g_mR=\frac{3}{2}$.

The other part of the determining Eq. (31), $(Z_1+Z_2)=0$, produces no physically realizable conditions in this case and may, consequently, be neglected.

Three Stages

The definitive equation in this case is, from Table I,

$$Z_1{}^3+6Z_1{}^2Z_2+3g_mZ_1{}^2Z_2{}^2+10Z_1Z_2{}^2+8g_mZ_1Z_2{}^4 +g_m{}^2Z_1Z_2{}^4+4Z_2{}^3+3g_mZ_2{}^4=0, \quad (38)$$

which becomes, when separated into its real and imaginary parts,

$$(QF)^4+6R\omega C(QF)^3+[10(R\omega C)^2-6](QF)^2 +2R\omega C[2R\omega C-3g_mR-9](QF) +[1-10(R\omega C)^2-8g_mR(R\omega C)^2 -(g_mR)^2(R\omega C)^2]=0 \text{ (Real)}, \quad (39)$$

and

$$-4(QF)^3-3R\omega C[6+g_mR](QF)^2 +4[1-5(R\omega C)^2-2g_mR(R\omega C)^2]QF +(R\omega C)\{6-4(R\omega C)^2 +3g_mR[1-(R\omega C)^2]\}=0 \text{ (Imaginary)}. \quad (40)$$

Because an exact simultaneous solution of these equations is difficult to effect, an approximate solution is presented. If it is assumed that (g_mR) is very much greater than one and $(g_mR)(R\omega C)$ is of the order of unity, then Eqs. (39) and (40) become

$$(g_mR)^2(R\omega C)^2+6g_mR(R\omega C)QF +[6(QF)^2-(QF)^4-1]=0, \quad (41)$$

and

$$(1-Q^2F^2)[3g_mR+4QF]=0. \quad (42)$$

It is easy to show that the only value of (QF) which leads to a real simultaneous solution of (41) and (42) is $(QF)=-1$. The resulting values of C are then

$$C=\frac{0.764}{g_mR^2\omega}=\frac{1.526Q}{\omega_0 g_mR^2[(1+4Q^2)^{\frac{1}{2}}-1]}, \quad (43)$$

and

$$C\doteq\frac{5.236}{g_mR^2\omega}=\frac{10.472Q}{\omega_0 g_mR^2[(1+4Q^2)^{\frac{1}{2}}-1]}, \quad (44)$$

which are the results obtained by Thompson.

Because of the gross approximations involved in obtaining Eqs. (43) and (44), no region of intrinsic stability was found. By another method, it is possible to determine the stable region. If (QF) is eliminated between Eqs. (38) and (39), by some method such as Sylvester's, an equation of the twelfth degree in $(R\omega C)$ can be found. There is a theorem in algebra that states that the vanishing of the coefficient of the highest power term determines the infinite roots of the equation. From the previous discussion on one and two stages, it is apparent that this is just the condition that is desired. It can be shown that the coefficient of $(R\omega C)^{12}$ is $(3g_mR-4)(g_mR-4)(7g_m{}^2R^2+16g_mR-32)$, from which it follows that

$g_mR=1.28$ is the only root having physical significance. The inherently stable region of stage gain (g_mR), therefore, lies between $g_mR=0$ and $g_mR=1.28$.

Four Stages

Table I indicates that the conditions of oscillation are to be determined from

$$(Z_1^2+3Z_1Z_2+g_mZ_1Z_2^2+Z_2^2)(Z_1^2+5Z_1Z_2+3g_mZ_1Z_2^2+5Z_2^2+4g_mZ_2^3)=0. \quad (45)$$

The first quadratic on the left-hand side of (45), when separated into its real and imaginary parts, becomes

$$(QF)^2+3(R\omega C)(QF)+(R\omega C)^2-1=0 \text{ (Real part)}, \quad (46)$$

and

$$2(QF)+3(R\omega C)+(g_mR)(R\omega C)=0 \text{ (Imaginary part)}. \quad (47)$$

A simultaneous solution of these two equations yields

$$QF=\pm\frac{(3-2g_mR)}{[(g_mR)^2-5]^{\frac{1}{2}}}, \quad (48)$$

and

$$C=\frac{\mp 2}{R\omega[(g_mR)^2-5]^{\frac{1}{2}}}. \quad (49)$$

The angular velocity is found from Eq. (48) to be

$$\omega=\frac{\omega_0}{2Q}\left\{\pm\frac{(g_mR-3)}{[(g_mR)^2-5]^{\frac{1}{2}}}+\left[\frac{(g_mR-3)^2}{(g_mR)^2-5}+4Q^2\right]^{\frac{1}{2}}\right\}, \quad (50)$$

where again the positive sign of the radical resulting from the solution of the quadratic for ω must be chosen to correspond with physical reality. To produce a physically realizable value of C, it is necessary to choose the positive sign, which in turn requires that QF be negative; consequently the negative sign of the first quantity within the brackets of (50) must be used. Elimination of ω from (49) results in

$$C=\frac{4Q}{\omega_0R\{-(g_mR+3)+[(g_mR-3)^2+4Q^2((g_mR)^2-5)]^{\frac{1}{2}}\}}. \quad (51)$$

This value of C is then the only real value that produces oscillation, due to the vanishing of the first quadratic on the left of (45).

An exact solution of the second quadratic on the left-hand side of Eq. (45) is very difficult to obtain so only an approximate solution will be attempted. The real and imaginary parts of the quadratic in question are

$$3(QF)^2+(R\omega C)(10+3g_mR)(QF)+(R\omega C)^2(5+4g_mR)-1=0, \quad (52)$$

and

$$(QF)^3+5(R\omega C)(QF)^2+[5R\omega C-3](QF)-(R\omega C)(5-3g_mR)=0. \quad (53)$$

By Sylvester's method, it is possible to eliminate (QF) from these two equations and obtain

$$(R\omega C)^6(5+4g_mR)(g_m^2R^2+20g_mR-25)+(R\omega C)^4(81g_m^4R^4-432g_m^3R^3-2565g_m^2R^2-3140g_mR-400)+(R\omega C)^2(108g_m^2R^2-48g_mR-320)-64=0. \quad (54)$$

The first term of this expression is negligible, relative to the second since it is of the order of $(R\omega C)^6(g_mR)^3$, while the second is of order $(R\omega C)^4(g_mR)^4$. If the gain is high, then it is possible to neglect all the terms but those of highest degree in the coefficients of $(R\omega C)^4$ and $(R\omega C)^2$. Equation (54) then becomes

$$(R\omega C)^481g_m^4R^4+(R\omega C)^2108g_m^2R^2-64=0, \quad (55)$$

of which the only physically realizable solution is

$$C=2/3g_mR^2\omega. \quad (56)$$

It may be shown that corresponding to the above solution for C, $(QF)=-1$, so that

$$\omega=\omega_0\{-1+[1+4Q^2]^{\frac{1}{2}}\}. \quad (57)$$

Elimination of ω between Eqs. (56) and (57) produces

$$C=\frac{2}{3\omega_0[(1+4Q^2)^{\frac{1}{2}}-1]g_mR^2}. \quad (58)$$

Because of the rough approximations made in

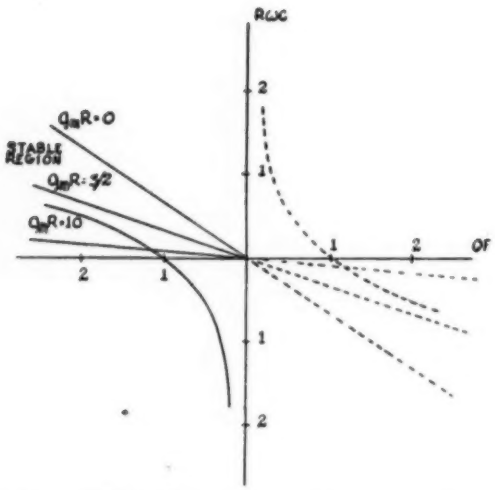

FIG. 4. Oscillation conditions for a two-stage single-tuned amplifier.

obtaining these results no stable region of gain is found; however, the infinite roots of $(R\omega C)$ are defined by the vanishing of the coefficient of the highest degree term in Eq. (54). The only physically realizable value of g_mR is found to be $g_mR=1.18$.

Five and Six Stages

Because of the complexity of these expressions, only partial solutions will be presented. Usually the least value of C that will cause oscillations is of the greatest interest so that only these results will be presented. By the use of approximations similar to those used for three stages it can be shown that for five stages

$$C=\frac{0.63}{g_mR^2\omega}=\frac{1.26Q}{\omega_0 g_mR^2[(4Q^2+1)^{\frac{1}{2}}-1]}, \qquad (59)$$

where (ω) is determined from the condition that $QF=-1$. The stable limits of gain lie between $g_mR=0$ and $g_mR=1.15$, approximately.

For six stages the corresponding value of C is

$$C=\frac{0.586}{\omega g_mR^2}=\frac{1.172Q}{g_mR[(4Q^2+1)^{\frac{1}{2}}-1]\omega_0}, \qquad (60)$$

in which ω is determined from $QF=-1$. The stable limits of gain are between $g_mR=0$ and $g_mR=1.12$, approximately.

6. CONCLUSIONS

The general expression for the voltage gain of an n-stage amplifier having identical but arbitrary plate impedances driven by a generator of any internal impedance has been obtained by the methods of the calculus of finite differences. The voltage gains, computed by this means reduce to the correct form as the grid-to-plate impedances of the tubes increase without limit.

An application of the general expression for the gain has been made in determining the criteria of oscillation in multi-stage, single-tuned amplifiers. These results check previous work for large values of Q, but also indicate a region of intrinsically stable stage gain wherein it is impossible to make the system oscillate even with a grid-to-plate capacitance arbitrarily large. The stable region of stage gain lies between zero and 2, 1.50, 1.28, 1.18, 1.15, and 1.12 for one, two, three, four, five, and six stages, respectively. An approximation, accurate within 10 percent of this sequence, is $(2)^{1/n}$ where n is the number of stages.

It is apparent from the discussion of oscillation conditions that if the actual inter-electrode capacity of the vacuum tubes in a cascaded amplifier is smaller than the least value calculated by the results derived above, the system can never oscillate because of feedback through the plate-to-grid capacitance and can be made to serve as a useful amplifier.

Calendar of Meetings

September

18–21 Illuminating Engineering Society, Quebec, Canada
19–21 American Physical Society, New York, New York
26–28 American Physical Society (Division of High Polymer Physics) and The Fiber Society (Charlottesville, Virginia) (Joint Meeting)
30–October 3 American Society of Mechanical Engineers, Boston, Massachusetts

October

3– 5 National Electronics Conference, Inc., Chicago, Illinois
3– 5 Optical Society of America, New York, New York
9–11 American Society of Civil Engineers, Kansas City, Missouri
25 American Mathematical Society, New York, New York

November

7– 9 Conference on Electrical Insulation, Division of Engineering and Industrial Research, National Research Council, Baltimore, Maryland
14–16 Acoustical Society of America, Chicago, Illinois
29–30 American Physical Society, Minneapolis, Minnesota

December

2– 6 American Society of Mechanical Engineers, New York, New York
5– 7 Electron Microscope Society of America and the American Society for X-Ray and Electron Diffraction, Pittsburgh, Pennsylvania (Joint Meeting)
17 Institute of Aeronautical Sciences, New York, New York
26–28 Geological Society of America, Chicago, Illinois

Letter to the Editor

The Evaporation of Antimony

LOUIS HARRIS
*Massachusetts Institute of Technology, Cambridge, Massachusetts**
June 19, 1946

THE aggregate formation observed in the evaporation of antimony has been found to have a counterpart in a simultaneous decrease in electrical resistivity of thin antimony deposits. The evaporation procedure has been modified as a result of these findings to produce films having lower electrical resistivity and higher thermal e.m.f. than obtained previously.

An unusual phenomenon was observed during studies on the evaporation of antimony. If the heating current was *discontinued* after the antimony was first observed to be condensing—as noted by an evaporation "meter" (see below)—the "meter" resistance continued to fall during a period of two to four minutes. For a number of runs (but not for every run) the decrease in resistance with time was found to follow the course of a first-order reaction. The phenomenon is not difficult to repeat, if the heating current is discontinued at a "meter" reading of about 5×10^{6} ohms (estimated antimony thickness $=5\times10^{-7}$ cm), the final reading of the "meter" will vary from 2000–10,000 ohms. (It will depend on the rate of heating before the heating current was discontinued.) The phenomenon has been observed for other types of meters than the one described here. It is best explained by assuming that the meter is recording a change to crystalline aggregates of antimony.[1]

The meter was directly (15 cm) above the evaporation boat (molybdenum). Two cellulose nitrate films, supported on mica frames, were disposed to either side of the meter. By looking down into the bell jar at the back of the cellulose nitrate films, during the supposed aggregation process, one can observe the growing areas of aggregates, as has already been reported.[2,3] (The growing areas may be observed also on the walls of the bell jar.)

We have modified the evaporating technique for antimony on the basis of these observations. We allow four minutes to elapse for the "crystallization" of the first deposit before proceeding further with the evaporation. The current through the boat is then increased gradually over a period of twenty minutes, until the boat is "red hot" and all the antimony has been evaporated. A vacuum of 10^{-4} mm Hg is maintained.

The progress of the evaporation was followed with the "meter" mentioned above.[4] The meter consists of a glass strip 5 cm$\times$0.35 cm. Chromium-silver is evaporated† at the ends and No. 22 copper wire leads are "soft" soldered to the chrome-silver. Leads from terminals are brought out of the bell jar to a "volt-ohmist." The electrical resistance of the meter serves as rough measure of the amount of metal deposit and of the resistivity of the metal deposit at the end of the evaporation process. Such a meter has been used for hundreds of evaporations and can be used for other metals besides antimony. The antimony is removed from the meter after the evaporation, by solution with concentrated hydrochloric acid or by rubbing with a damp cloth.

The antimony deposits are a brilliant steel-grey and show a pattern of tiny crystals to the unaided eye. The resistivity of the antimony deposits on cellulose nitrate films varies from 119×10^{-6} to 60×10^{-6} ohm-cm, for antimony thicknesses from 0.48 to 2.2×10^{-4} cm. The thicknesses were determined from weight measurements and assuming macroscopic density. The thermal e.m.f. *versus* copper of the antimony deposits varied from 33 to 38.6 microvolt per degree C.

If the initial rate of antimony deposition is too high, or if sufficient time is not allowed to elapse, then the final deposit does not show the crystalline pattern, though it will still have the brilliant steel-grey appearance. Such deposits have a more uniform appearance; however, the electrical resistivity of such films is usually greater than 120×10^{-6} ohm-cm and the thermal e.m.f. *versus* copper may fall to less than 30 microvolt per degree C.

* The work described here was carried out in whole or in part under contract OEMsr-1147 between the Office of Scientific Research and Development and the Massachusetts Institute of Technology.
[1] L. Marton and L. I. Schiff, J. App. Phys. **12**, 759 (1941).
[2] Hans Murmann, Zeits. f. Physik **54**, 755 (1929).
[3] R. Bowling Barnes and M. Czerny, Phys. Rev. **38**, 338 (1931).
[4] The meter used here is a modification of one used originally in this laboratory by A. Stockfleth (A. Stockfleth, Massachusetts Institute of Technology Ph.D. Thesis, November, 1942).
† I am indebted to Professor John D. Strong for evaporating the silver-chromium terminals for the meter.

Here and There

New "Microwave Tower"

Federal Telephone and Radio Corporation of Newark, New Jersey, is building a 300-foot "microwave tower" for Federal Telecommunication Laboratories at Nutley, New Jersey. It is believed that such towers will be headquarters in cities and towns for simultaneous use of many microwave radio functions, including f-m broadcasting, Pulse Time Modulation broadcasting, television, police radio networks, communication with mobile units, radar applications, aerial navigation, and the interception of illegal transmissions. At the ground-breaking ceremony Colonel Sosthenes Behn, President of International Telephone and Telegraph Corporation, stated, "Various broadcasting services in important communities will find it much more efficient to cooperate in building one great tower to be shared by all functions utilizing microwaves than for each service to build its own tower. Joint financing would make it possible to build a tower superior to any that could be afforded by individual services."

Federal's microwave tower will be an experimental laboratory, first of its kind ever to be built. Microwave experiments heretofore have been conducted in tall office buildings and other structures not well adapted to the purpose.

Ground has been broken also for the newest addition to Federal's existing Nutley laboratories, which will increase the present floor space of the laboratories by 65,000 square feet.

Meteorology Experts Available

The American Meteorological Society, through its president, Professor H. G. Houghton of Massachusetts Institute of Technology, wishes to call to the attention of American colleges the fact that a large number of carefully selected college students were given training in professional meteorology at a few selected universities in this country, preparatory to their employment by the Army and Navy Meteorological Services. A number of these men, before entering the meteorological field, had done a considerable amount of graduate work in physics and are now available for teaching and research in both these fields.

In most of our colleges which offer non-professional courses in meteorology to meet the needs of students in geography, geology, and agricultural subjects, it has been standard practice to have these non-professional courses taught by members of various departments. The return of many of the professionally trained service meteorologists offers an opportunity for our colleges to obtain the services of instructors who are capable of doing professional work in a physics department and at the same time are qualified as experienced and trained professional meteorologists to present stimulating non-professional courses in meteorology on a somewhat higher plane than may have been possible in the past.

The Society is anxious to cooperate with American colleges in providing information concerning these returning weather officers that might be helpful in placing them in suitable teaching positions. To that end, files have been kept which contain detailed information on the education and practical experience of these men. Inquiries may be directed to the Executive Secretary, American Meteorological Society, Five Joy Street, Boston 8, Massachusetts.

Books for Europe

The American Book Center for War Devastated Libraries, Inc., is collecting and shipping abroad scholarly books and periodicals which will be useful in research and necessary in the physical, economic, social, and industrial rehabilitation and reconstruction of Europe and the Far East. The Center cannot purchase books and periodicals; it must depend upon gifts from individuals, institutions, and organizations.

What is needed: Shipping facilities are precious and demand that all materials be carefully selected. Emphasis is placed upon publications issued during the past decade, scholarly books which are important contributions to their fields, periodicals (even incomplete volumes) of significance, fiction and non-fiction of distinction. All subjects—history, the social sciences, music, fine arts, literature, and especially the sciences and technologies—are wanted.

What is not needed: Textbooks, out-dated monographs, recreational reading, books for children and young people, light fiction, materials of purely local interest, popular magazines, popular non-fiction of little enduring significance, etc.

How to ship: All shipments should be sent prepaid via the cheapest means of transportation to The American Book Center, care of The Library of Congress, Washington 25, D. C. The Center cannot accept material which is sent collect. When possible, periodicals should be tied together by volume. It will be helpful if missing issues are noted on incomplete volumes.

New Section at Midwest Research Institute

The Midwest Research Institute, Kansas City, Missouri, recently announced the formation of its Engineering Mechanics Section. Previously, work in this field was done under the supervision of the Applied Physics Section. The new section is equipped with a large physical testing laboratory, machine shop, and electromechanical laboratory. Problems within the scope of the group include structural and mechanical design, vibrations, fluid flow, electron application in engineering, and servo-mechanisms.

Martin Goland, formerly of the Structures Department of the Curtiss-Wright Research Laboratory, Buffalo, New York, has been appointed chairman of the new section. Clayton O. Dohrenwend, formerly chairman of the Mechanics Departments at the Illinois Institute of Technology and the Armour Research Foundation, will serve as research consultant and senior scientist.

Food Packages for Europe

The Cooperative for American Remittances to Europe, Inc. (known as CARE) has announced a new service for sending food packages to Europe. CARE is a non-profit corporation organized by 24 relief agencies, with the support and approval of the President's War Relief Control Board.

CARE accepts orders for individuals, groups, or organizations in Austria, Czechoslovakia, Finland, France, Italy, Netherlands, Norway, and Poland, and recommends the purchase of a 10-in-1 package of Army rations for $15 each, with delivery overseas guaranteed. Orders when received here are rushed to Europe and filled overseas from a stockpile of CARE food packages already over there. When the food is delivered, CARE's overseas representative will get a signed receipt which will be sent to the donor. If a package cannot be delivered within a reasonable length of time, CARE will refund the full purchase price to the donor. A typical CARE package contains such products as Borden's butter, Nescafe, Swift's canned ham, Del Monte corn, Welch's jam, Hormel's sliced bacon, etc.

CARE's order blanks are available at banks and are also distributed by relief, fraternal, professional, and social organizations, but if you have difficulty in getting one, write to CARE, 50 Broad Street, New York 4, New York.

Annual Convention of I.E.S.

The Illuminating Engineering Society goes to Quebec September 18–20 for its Victory Convention, sharing with its Canadian membership this annual event which during the war years was limited to technical conferences.